Numerical Investigation into the Suppression Mechanism of Vortex-Induced Vibration for Box Girder in the Presence of Flap

フラップ設置による箱桁渦励振の制振メカニズムに関する数値解析検討

Dat Anh Tran

2014 September

YOKOHAMA NATIONAL UNIVERSITY

Urban Innovation Faculty

Numerical Investigation into the Suppression Mechanism of Vortex-Induced Vibration for Box Girder in the Presence of Flap

フラップ設置による箱桁渦励振の制振メカニズムに関する数値解析検討

A dissertation submitted in partial fulfillment of the requirements for the Degree of Doctor of Philosophy in Engineering

Dat Anh Tran

Graduate Student

11WA905

2014 September

Abstract

Aerodynamic countermeasures are concerned as effective control solutions to wind-induced vibrations mitigation in long span bridges. In order to decide a specific aerodynamic countermeasure, many experimental tests must be conducted case by case in wind tunnel, appearing some difficulties involved. Up to now, there has not yet been any common guideline in the selection of aerodynamic countermeasures. Hence, an effort of establishing the guideline is necessary in wind resistant design process.

This thesis focuses on the suppression mechanism of Vortex Induced Vibration (VIV) for box girder having a bluff-body shape in the presence of flap countermeasure. The effect of flap is investigated through Computational Fluid Dynamics (CFD) approach. In there, various geometric configurations of flap are examined thoroughly. The study is considered as a contribution of the fundamental guideline to flap application.

The Reynolds Averaged Navier-Stokes (RANS) method coupled with a new $k-\varepsilon$ eddy viscosity turbulent model is applied. The validation of numerical simulations is confirmed by means of the comparison with experimental results. The numerical investigation is carried out in two main parts comprising static and dynamic simulations. Particularly, the aerodynamic instability characteristics, together with the pattern of wind flow, are estimated by the results obtained from the static simulations. Then, the flutter derivative H_1^* calculated from the dynamic simulations is taken into account to assess the change of aerodynamic damping for each case of flap attached. In addition, some rectangular sections with flap installed are also inspected to reinforce the findings in the study. Finally, the conclusions outline the achievements and findings, as well as the direction of future research.

The thesis is arranged in seven chapters and the contents are sketched as follows:

- Chapter 1 introduces the general information regarding the impact of wind on long span bridges, especially on substructure. Then, the necessary of this research is presented. On the other hand, this chapter clearly defines the research aim, scope, objectives and methodology.

- Chapter 2 presents the theory of wind effects on bridge girder. Firstly, wind induced vibrations are clearly mentioned in company with estimation and calculation methods. Then, the theory of wind resistant design is carefully provided in case of long span bridge girder. Finally, the effect of aerodynamic countermeasures is given in some cases of real bridges. This chapter is concern as a fundamental theory part which is used to investigate the numerical results.

- Chapter 3 provides the theory of CFD with basic concepts such as the equations describing fluid flow, CFD application, discretization, finite volume method…In addition, turbulence models are systematically summarized. More particularly, the turbulence model used in this study is presented to make bases for the numerical simulations.

- Chapter 4 discusses about wind tunnel tests in general, the experimental data collection of a real bridge girder and several cases of rectangular cross-sections in some past researches. The data gathered in this chapter is vital basic to confirm the validation of all numerical simulations analyzed.

- Chapter 5 deals with the numerical investigation into static simulations. Numerical simulation properties are described in detail. The aerodynamic characteristics of the box section as well as some rectangular sections and the effect of flap with various geometry configurations are analyzed. The flow pattern is observed to clarify the suppression mechanism of VIV. On the other hand, a side effect to vehicle of flap is also discussed.

- Chapter 6 solves with the numerical investigation into dynamic simulations. Numerical simulation procedure is mentioned similarly as chapter 5. Flutter derivative H_1^* calculated from the results obtained in dynamic simulations is discussed to support more the confirmation for the effect of flap.

- Chapter 7 gives some conclusions basing the achieved results in flap application. The perspective of future researches is also recommended in this chapter.

Acknowledgements

Firstly, all the gratitude is directed to the Japanese people and the Government of Japan, gave the author an opportunity to study in Japan. The kindness, politeness and honesty of Japan are wonderful atmosphere for high quality scientific researches.

Honestly, the author would like to express the deepest appreciation to Professor Hiroshi Katsuchi, who has supported the author to accomplish the dissertation. The author enjoyed the interesting discussions with him, leading to good ideas in the manner to orient the research. It is obvious that the study cannot be finished without his guidance, advice and persistent instructions.

In addition, the author would like to thank Professor Hitoshi Yamada for his great help. Owning to his contribution, the thesis has been improved better. The author also gained a plenty of knowledge from the course he delivered. Besides, the author always is grateful for his efforts in training young scientists coming from Vietnam.

Next, the author would like to thank Associate Professor Mayuko Nishio for her comments and correction. The cooperation in the near future for developing some topics has been expected.

Then, the author wishes to thank Professor Tatsuya Tsubaki and Associate Professor Mamoru Kikumoto. Their comments helped to ameliorate the thesis.

For supporting the spiritual life and making the things going easier, the author would like to thank all the office mates for sharing the time together. Especially, the author would like to well appreciate Masuda, who helped a lot during these years.

Finally, the acknowledgments of the author are sent to his family and friends, who always encourage him to pass over difficult times.

Dat Anh Tran

List of contents

List of figures

List of tables

List of equations

1.1. General

One of the most important achievements in supporting infrastructure, to serve the development of world economy, is the great success of design and construction technology for long span bridges. Many kinds of long span bridges have been built since the previous century in a fast and worldwide advance, such as arch, truss, continuous girder, cable-stayed and suspension bridges. In terms of main span length, it has reached to a free span as long as 1991 m in case of suspension bridge named Akashi-Kaikyo Bridge in Japan as Figure 1.1, and 1104 m in case of cable-stayed bridge called Russky Bridge in Russia as Figure 1.2. In addition, it seems to indicate that long span bridges are often not only excellent remedy in respect of engineering, but also optimal solution with regard to construction cost according to the main span length expected. Figure 1.3 gives the economic main span range of various bridges, in the sense that using cable-stayed bridges will lead to high effect if it lies between 100 m with one tower and 1100 m with two towers. Because of the advantages of cable-stayed bridges, they have been chosen popularly with the main span increased ceaselessly as summarized in Figure 1.4 and Table 1.1.

Figure 1.1. The Akashi-Kaikyo Bridge [1]

Figure 1.2. The Russky Bridge [2]

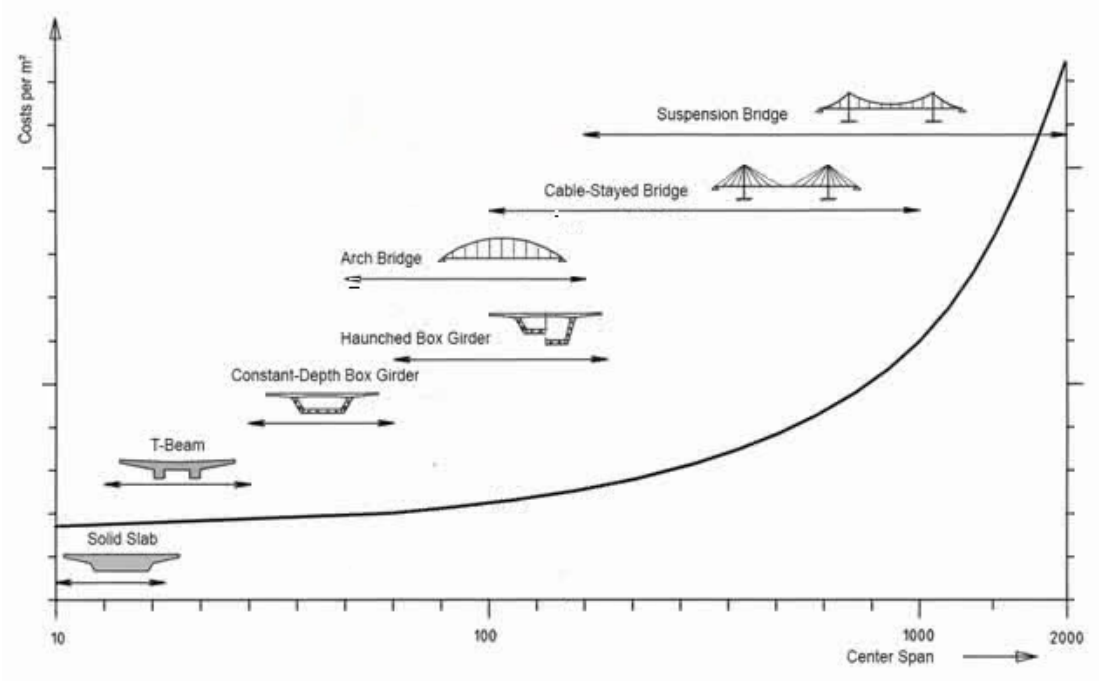

Figure 1.3. Relation between construction cost and main span lengths [3]

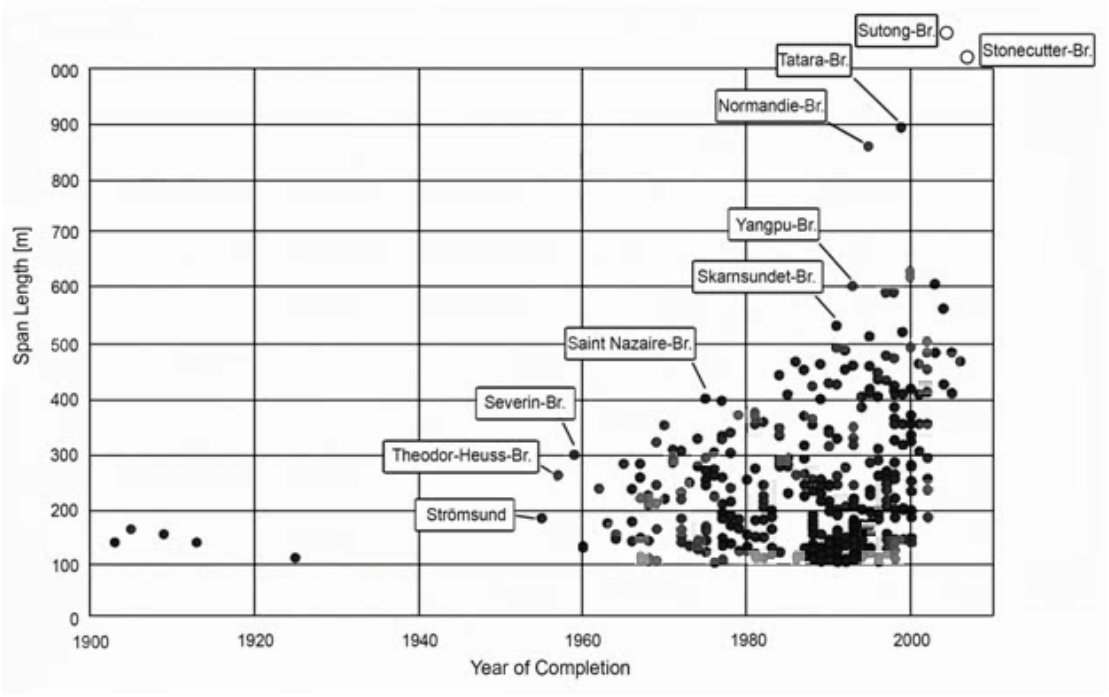

Figure 1.4. Relation between main span lengths and year of completion [3]

Table 1.1. Summary of the amount of cable-stayed bridges until 2000 [3]

Country	1900-1950	1960	1970	1980	1990	2000	Total
Japan				1	8	12	21
China						17	17
Germany		2	5	6	2		15
USA				2	7	4	13
Netherlands				2	1	2	5
France				2		2	4
USSR				1	1	2	4
Great Britain				1	1	2	4
Other				3	9	21	33
Total	0	2	5	18	29	62	116

In order to touch the largest long spans, it is necessary to utilize the light materials and delicate structures which cause the bridges become more flexible and sensitive with vibrations. This is a vital challenge which is inevitable for designers. When it comes to load consideration, wind- and earthquake excitations always are sophisticated issues that govern the design process for these kinds of bridges. Excitation by wind- and earthquake actions has distinct effects on structural characteristics. The stronger effect on low or short structures with high natural frequencies has been found in the earthquake action, whereas the more effect on tall or long ones with lower natural frequencies has been discovered in the wind action, Figure 1.5 [4]. As a result of that, wind load is needed to be concerned most in long span bridges plan. The importance has been proved by means of some disastrous accidents or dangerous oscillation measured in the past, including the well-known collapse of the Tacoma Narrow Bridge at USA in 1940 due to self-excited vibration named flutter phenomenon exceeded allowable limitation, as showed in Figure 1.6 and Figure 1.7 [5], the oscillation with large amplitude in vortex-induced phenomenon of the Trans-Tokyo Bay Highway Crossing Bridge at Japan in 1997, as given in Figure 1.8 [6], and large amplitude in vortex-induced oscillation of the Shin-minato Bridge at Japan in 2013, as presented in Figure 1.9 [7], [8]. Consequently, under the impact of wind load, the safety of long span bridges must be thoroughly investigated to not only satisfy ultimate limit state, but also meet fully requirements of serviceability state.

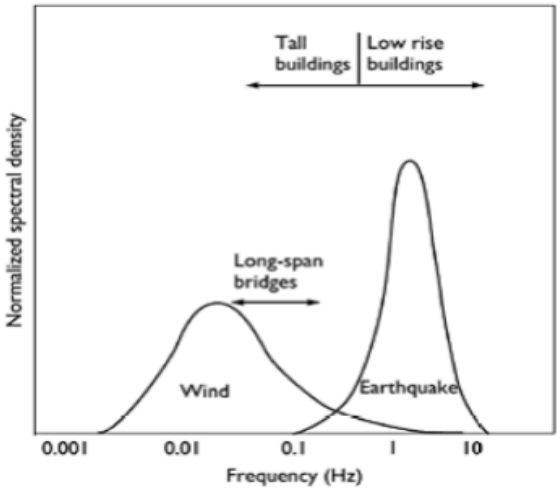

Figure 1.5. Relative effect of wind and earthquake loads to structures [4]

Figure 1.6. The Tacoma Narrow Bridge twisted and vibrated on the day of the collapse [5]

Figure 1.7. The Tacoma Narrow Bridge collapsing [5]

Figure 1.8. Large vortex-induced vibration at the Trans-Tokyo Bay Highway Bridge [6]

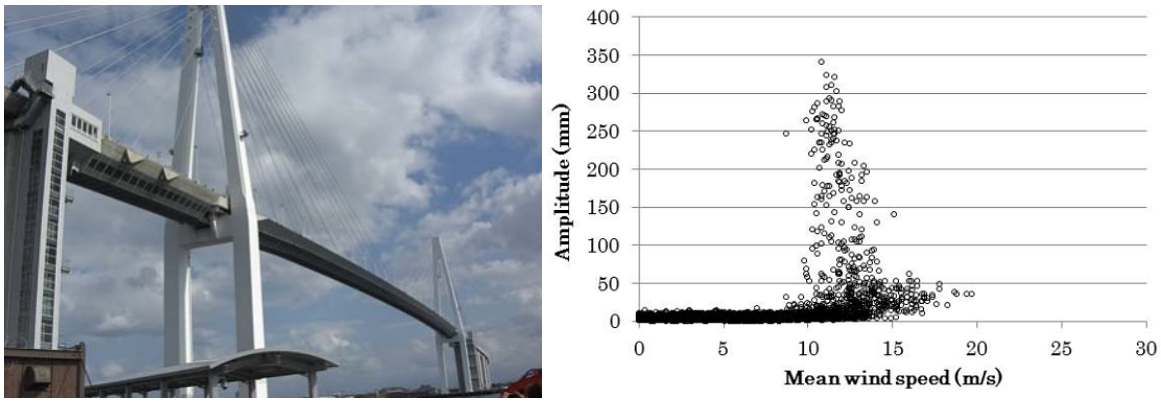

Figure 1.9. Large vortex-induced vibration at the Shin-minato Bridge in Japan [7], [8]

As the aftermath of the interaction between wind flow and bridge structure, the responses of structural members are extremely complicated. The aerodynamic forces on them chaotically vary case from case according to the geometries of structures, their movement under wind flows that are great nonlinear. Up to this time, a couple of researches and technical advances involved have been done in order to enlighten those complexities to wind resistant design of long span bridges. Normally, an experimental approach using a wind tunnel is indispensable to investigation into the stability of structure. Recently, thank to the robustness and efficiency of CFD, it has become a proficient tool to support more to wind tunnel tests for capturing the flow pattern and understanding the flow behavior.

1.2. Wind and long span bridges

As mentioned in Section 1.1, the effect of wind load on long span bridges is greatly momentous in the design phase, and each structural member such as girder, tower, pier, cable … must be carefully considered in the interaction. Basically, the impact of wind can be divided into two major ways which are known as static and dynamic actions. According to Wind Resistant Design Code (WRDC) for Honshu Shikoku Bridges (HSB) 2001 in Japan [9], which is a summary of experiences of actual wind resistant design for some last long span bridges in HSB project of Japan (Akashi-Kaikyo, Tatara, Kurushima-Kaikyo Bridges), the phenomena occurred by the interaction between structure and wind flow are classified as Table 1.2.

In terms of static actions, static deflection and stress are created by the static components of wind force which are independent of time and are calculated by basing on an average wind velocity with a particular time. In case of static instability, including two major forms are lateral buckling and torsion divergence, these phenomena often rapidly happen under the effect of steady force with a very high critical velocity.

Table 1.2. Wind impact classification

No	Actions	Phenomena	
1	Static actions	Static deflection and stress	
		Static instability	Lateral buckling
			Divergence
2	Dynamic actions	Limited vibration	Buffeting vibration
			Vortex-induced vibration
			Rain-wind-induced vibration
			Wake-induced vibration
		Divergent vibration (Self-excited vibration)	Galloping
			Flutter

As far as dynamic actions are concerned, limited vibration is the oscillation which has limited amplitude, not leading to the collapse of bridge structure momentarily during a short time. It, however, affects the fatigue of structure in the serviceability stage, or causes an unsecure sensation for traffic passengers. By various mechanisms, limited vibration can be found in buffeting vibration due to the random of wind flow, vortex-induced vibration due to the synchronization of the natural frequency of structure and the frequency of vortex

shedding generated at leeward region, rain-wind-induced vibration due to the geometric complexity of stayed cable section in rain-wind condition, and wake-induced vibration of leeward structure due to the interference of windward structure. All potential limited vibrations have to be taken into account so as to avoid the unfavorable influences in serviceability stage. When it comes to divergent vibration (self-excited vibration), this is the most dangerous oscillation mode whose amplitude is increased by adding force induced by motion of body in the air, such as flutter and galloping. Once these kinds of vibration occur, the vibration incessantly grows to an amplitude as large as resulting bridge destruction. Therefore, under the worst condition, self-excited vibrations are not allowed to appear.

The procedure of wind resistant design for bridges is normally considered in a way so that static and dynamic actions must be taken into account in sequence. In Japan, wind resistant design for highway bridges is conformed to the Specifications for Highway Bridges (SHB) [10]. This specification is only valid for the bridges with the span length of less than 200 m, in the sense that the examination of static actions is carefully conducted. In case of the bridges whose span length passing over 200 m, it can be applied with some modifications appropriate for each specific circumstance. Furthermore, if the wind-induced dynamic behavior of the bridge contains safety risk, Wind Resistant Design Manual for Highway Bridged (WRDM) [11], with a variety of supplementary information regarding dynamic issues, is used to verify the dynamic response of structures. The manual was composed basing upon the material obtained from the previously successful wind tunnel tests so that the wind resistant design could be implemented without carrying out experiments. In order to ensure the stringently safe requirements of the bridges with longer span lengths, special provisions are often established relying on the accumulated experiences of HSB projects and WRDC 2001 of HSB [9]. Figure 1.10 presents the procedure of wind resistant design for Akashi-Kaikyo, Tatara and Kurushima-Kaikyo Bridges. In accordance with WRDC, four main steps have to be examined as followings: cross-sections of structural members are selected depending on the static design procedure; wind tunnel tests must be carried out with sectional model to choose aerodynamically stable section for deck, and with aero-elastic model to make decision in selecting tower section; investigation into the static instability of the structure under wind action; wind induced phenomena, divergent oscillations, gust response and vortex-shedding excitations are examined by the aero-elastic full bridge model test and/or the dynamic analyses.

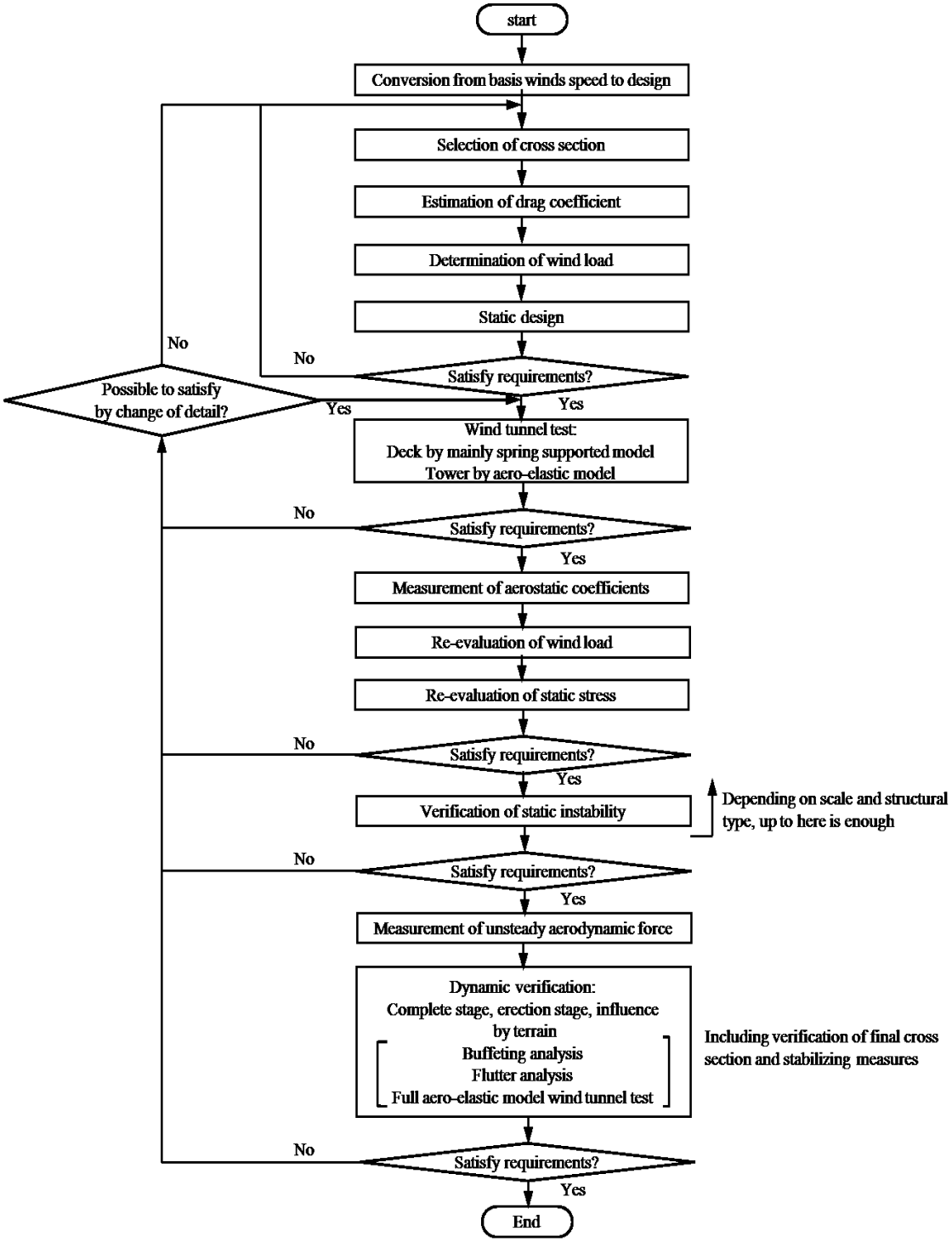

Figure 1.10. Wind resistant design for Akashi-Kaikyo, Tatara and Kurushima-Kaikyo Bridges [9]

1.3. Wind-induced vibration control for bridge girders

Wind resistant design for bridge girders in long span bridges plays a crucial role in the whole procedure. Depending on the width-to-depth ratio of the girder sections, the occurring possibility of wind-induced vibration types is diverse. There are three types of wind-induced vibration, which can be found, including [11]: Self-excited vibrations (SEV), such as galloping and flutter; Vortex-induced vibration (VIV); Buffeting vibration (BV). In WRDM [11], the wind-induced vibrations for superstructures are examined as the procedure showed in Figure 1.11.

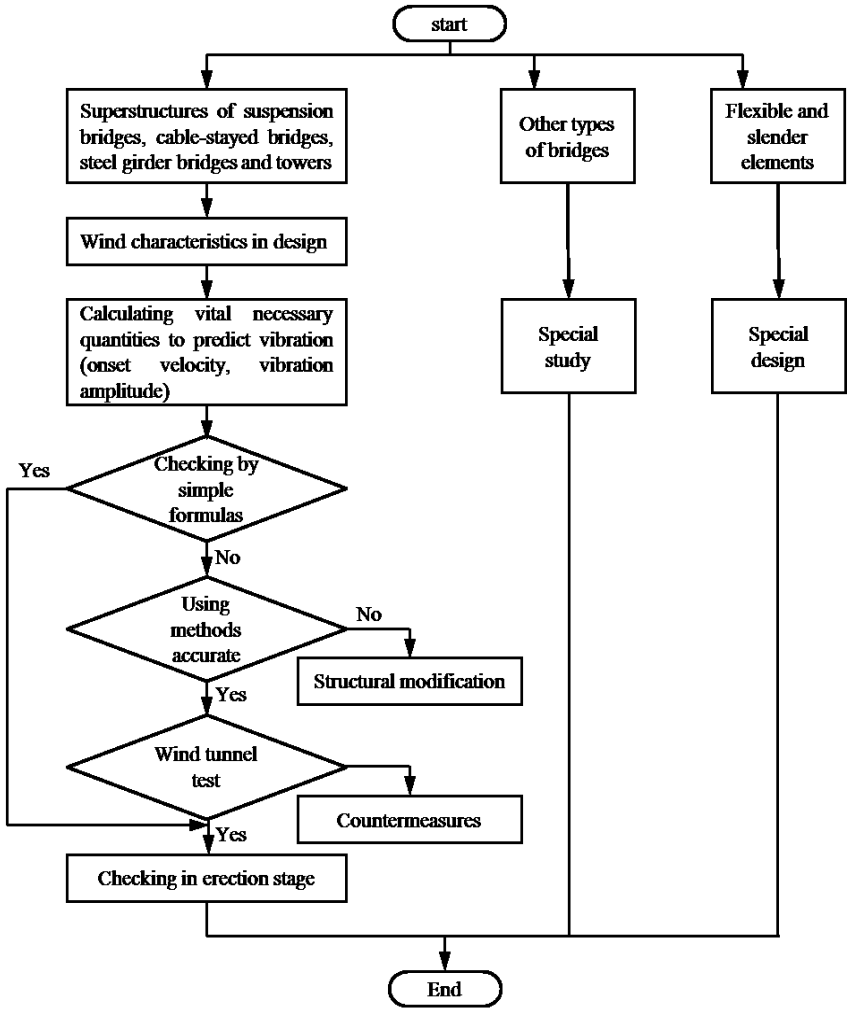

Figure 1.11. Procedures and methods in aerodynamic study for wind-induced vibration [11]

The fundamental principle of wind resistant design for girder can be sketched as followings:

- In cases of SEV, flutter and galloping must not be happened with any possibility. Because of its catastrophe, this requirement has to be seriously controlled. Under any worst conditions, it needs to be ensured that the reference wind speed, which is decided basing upon design wind speed and turbulence, is always less than the critical wind speed of bridge girder.
- In cases of VIV, it is satisfied if either the design wind speed does not exceed the critical wind speed for VIV of girder, or the amplitude of VIV is small enough in comparison with the allowed amplitude.
- In cases of BV, it is examined by means of the exaggeration of static wind load, instead of investigating dynamic responses. According to WRDM [11], in special cases, the buffeting amplitude should be verified against the amplitudes obtained in the requirement of serviceability stage.

Once potential wind-induced vibrations are anticipated in design process or are found in wind tunnel tests, control methods have to be carefully considered. There are various methods to control wind-induced vibrations for bridge girder. Generally, two essential methodology groups including aerodynamic countermeasures and structural countermeasures are often applied. The first group tends to improve cross-sectional shape towards aerodynamic geometry to smooth the flow pattern, diminishing the unfavorable aerodynamic forces. On the other hand, the second group attempts to interfere in the properties of structure in order to counteract the imposed forces.

Aerodynamic countermeasures have a variety of devices that associated with three different kinds of wind-induced vibration. Basically, Figure 1.12 presents the typical types of aerodynamic countermeasures.

Figure 1.12(a) shows the aerodynamic countermeasures against galloping vibration, in the sense that it is concentrated on adjust the flow pattern under the bridge deck. It is believed that the skirt at the lower corners of the girders with a certain angle and the horizontal plates at the lower side of girders can lessen the wind velocity at separation area from the leading edge, eliminating the divergent vibration.

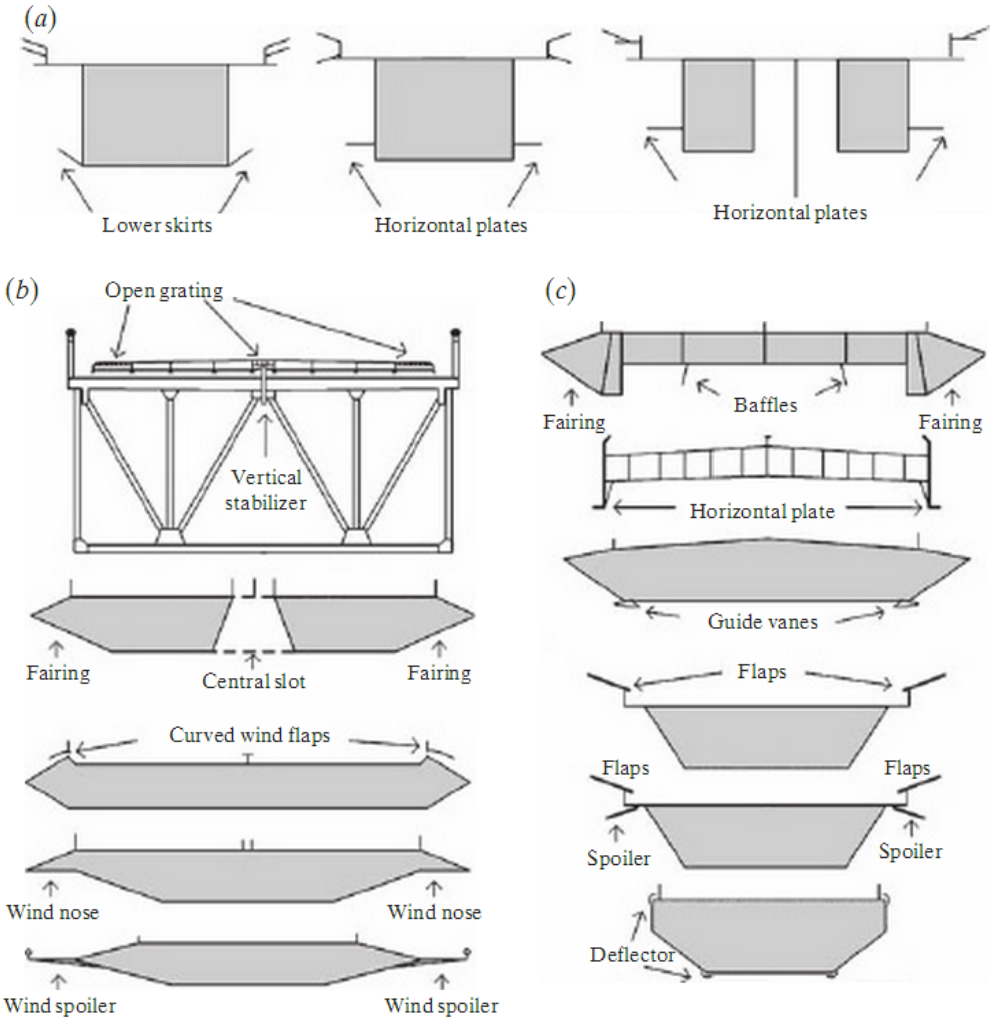

Figure 1.12. Aerodynamic countermeasures [12]: (a) for galloping, (b) for flutter, (c) for VIV

In cases of flutter vibration, the pressure difference between upper and lower surface of bridge girders is considered as the main reason causing vibration of bridge girders with a large width-to-depth ratio, and open grating is an effective remedy to decrease that difference, Figure 1.12(b). If flutter is found at the shallow box section with a small width-to-depth ratio, then the fairings, the wind noses, the deflectors and the spoilers are significant resorts through improving the flutter stability, Figure 1.12(b). In addition, with truss girders, it is thought that the gratings on the edge of deck, the vertical stabilizer and the center barrier can stabilize flutter instabilities in a common mechanism that control the flow pattern or weaken the separation bubbles from the leading edge, respectively, Figure 1.12(b).

When it comes to VIV, the effective solutions include the fairings promoting the reattachment of flow, the flaps and the horizontal plates suppressing the separation of flow,

the deflectors controlling the streamline of girder, the vertical and baffle plates preventing the formation of vortices, and the spoilers supporting the function of the flaps, Figure 1.12(c).

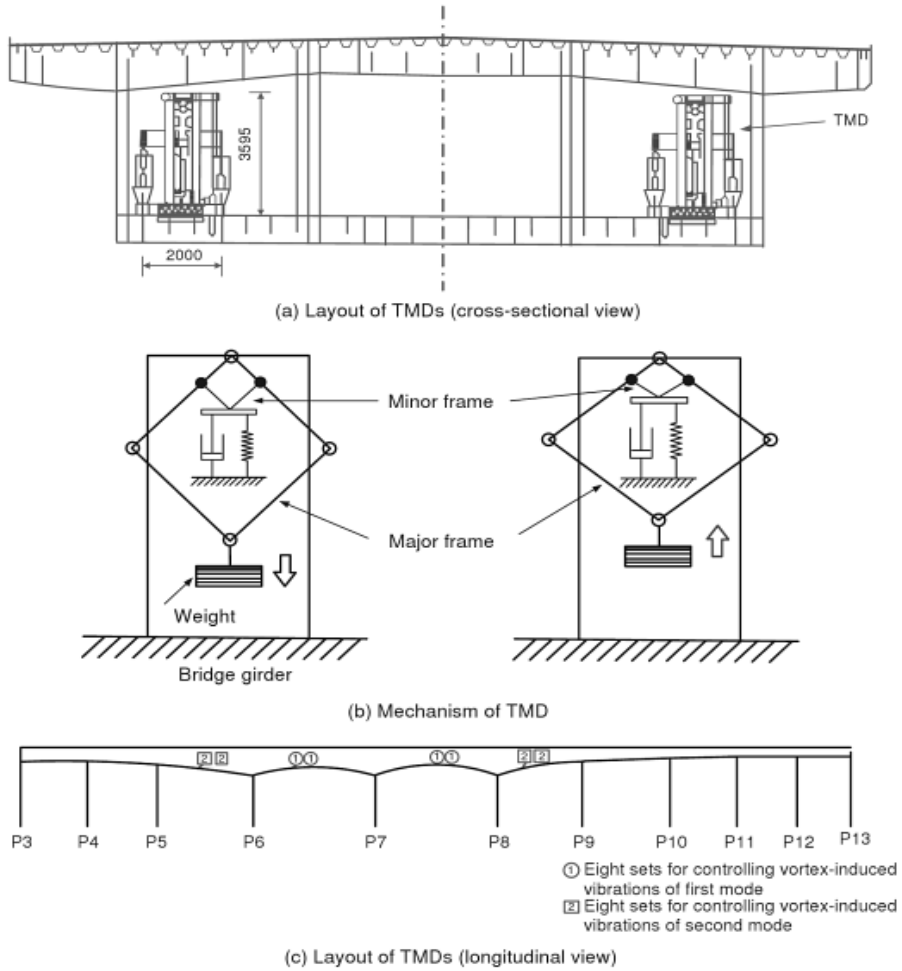

Figure 1.13. TMD system of the Trans-Tokyo Bridge [12]

Structural countermeasures can be classified into three methods involving enhancing the mass, intensifying the stiffness and increasing the structural damping of girder. Normally, the first method is rarely used because of its bulky form. The second one is often applied during the erection phase of structure, and the most popular system belonging to this kind is cable system. The purpose of intensifying the stiffness of girder is to change the onset velocity. In terms of the third one, with the strategy of trying to dissipate vibration energy, it is mostly received the priority of utilization in structural countermeasures selection. A tuned mass damper (TMD) is known as one of the most common devices artificial dampers in

suppression of VIV. Figure 1.13 illustrates a TMD system which operated in case of Trans-Tokyo Bridge to mitigate VIV [12].

1.4. Problem statement

In the design process of long span bridges, the decision of girder shape plays an important role so as to satisfy the structural safety under many circumstances. Box girders are known as section type having a number key of own advantages such as high stiffness, well resistant capability to torsion, lighter weight. The use of box girders is usually an effective deal to reach the longer span. Some aspects of box girders getting involved economic requirements, structural demands and safe issues, need to be carefully considered in the selection. In some cases, the selected configurations of box girder lead to aerodynamic instability vibration under the impact of wind. The vortex-induced oscillation of the Trans-Tokyo Bay Bridge [6] and the Shin-minato Bridge [7] detected, for instances, are typical cases. Normally, in order to optimize the aerodynamic load generated from fluid-structure interaction (FSI), aerodynamic countermeasures presented in section 1.3 are applied, instead of modifying the configurations of the original section. These include a variety of instruments such as flap, double flaps, faring, skirt, plate, et cetera. For example, in case of the Tozaki Viaduct, double flaps as countermeasure against the vortex-induced vibration and lower skirt against the galloping phenomenon were installed [13]. The effect of such countermeasures is distinct from case to case, because just a small modification in their geometry can cause a large change of flow [14]. Traditionally, wind tunnel tests are carried out to examine the aero-elastic response of long span bridges girders with many kinds of aerodynamic countermeasures, and the most effective one is selected from the experimental results. Wind tunnel tests are well evaluated and widely accepted. It is believed that the outcomes are the most reliable results for predicting flow characteristics. Yet, there are some disadvantages that emerge in this approach, such as time consuming, lacking information about the mechanism that controlling oscillation.

Recently, CFD study has become a useful tool in wind engineering. Thanks to the development of computer capacity, theory of discretization and turbulent models, the results obtained from CFD have got closer to the experimental investigations. Analysis CFD in bridge civil engineering is a young frontier, but the motivation of research is very exigent. Some typical researches using CFD in bridge are chronologically summarized in Table 1.3.

Table 1.3. Some typical researches using CFD approach in bridge civil engineering

N0	Authors	Research Topics	Year	Note
1	Santo, H. P. and Branco, F. B.	Wind forces on bridges numerical & experimental methods	1989	[15]
2	Tamura, T., Ohta, I. and Kuwahara, K.	On the reliability of two-dimensional simulation for unsteady flows around a cylinder-type structure	1990	[16]
3	Kuroda, S.	Numerical simulation of flow around a box girder of a long span suspension bridge	1997	[17]
4	Larsen, A. and Walther, J. H.	Aero-elastic analysis of bridge girder sections based on discrete vortex simulations	1997	[18]
5	Larsen, A.	Advances in aero-elastic analysis of suspension and cable-stayed bridges	1998	[19]
6	Buno, L., Khris, S. and Marcillat, J.	Contribution of numerical simulation to evaluating the effect of section details on the aerodynamic behavior of a long span bridge deck	1998	[20]
7	Shimada, K., Ishihara, T.	Applicability of modified k-ε model on the prediction of aerodynamic properties of rectangular cylinders with various elongated cross section	1998	[21]
8	Tamura Tetsuro	Reliability on CFD estimation for wind-structure interaction problems	1999	[22]
9	Frandsen, J. B.	Computational fluid-structure interaction applied to long span bridges	1999	[23]
10	Taylor, I., and Vezza, M.	Prediction of unsteady flow around square and rectangular cylinders using a discrete vortex method	1999	[24]
11	Taylor, I., and Vezza, M.	Analysis of wind loading on bridge deck sections using a discrete vortex method	1999	[25]
12	Morgentha, G.	Comparison of numerical methods for bridge deck aerodynamics	2000	[26]
13	Morgentha, G.	Aerodynamic analysis of structures using high resolution vortex particle methods	2002	[27]
14	Shimada, K., Ishihara, T. and Wakahara, T.	Prediction of flutter characteristics of rectangular cross-section by k-ε model	2002	[28]
15	Ishihara, T., Oka, S. and Fujino, Y.	Numerical prediction of aerodynamic characteristics of rectangular prism under uniform flow	2006	[29]
16	Sarwar, M. W. et al.	Prediction of aerodynamic characteristics of a box girder bridge section using the LES turbulence model	2008	[30]
17	Sarwar, M. W. and Ishihara, T.	Numerical study on suppression of vortex-induced vibrations of box girder bridge section by aerodynamic countermeasures	2010	[31]

The outcomes of these researches have well assisted scientists in comprehending the behaviors of bridge girder during the interaction with the wind flow, by means of steady aerodynamic coefficients, aerodynamic characteristics in wind-induced vibrations… which are captured from numerical analysis. However, most of these researches did not examine the presence of small attachments on bridge girder such as barriers, handrails and aerodynamic countermeasures which can dramatically change aerodynamic characteristics. Turning to details of aerodynamic countermeasures attached on bridge sections, CFD approach, with many kinds of robust turbulent model, triggers deep studies in order to understand the suppression mechanism of wind induced vibration in the presence of aerodynamic countermeasures. If this target is stimulated and successfully researched, then useful references or common guidelines in countermeasures lead to significant applications in design procedure, and wind tunnel tests are mostly reduced to save time and cost.

One of recent researches on aerodynamic countermeasures, basing on CFD simulation, is the numerical study on suppression of vortex-induced vibration of a box girder section by aerodynamic countermeasures reported by Sarwar, M. W. et al [31]. In the prediction of the vortex-induced vibration, Sarwar, M. W. et al showed the agreement between the results acquired from numerical simulations and from wind tunnel tests. In addition, the research concluded that double flaps can decrease the vortex formation, whereas fairings can result in a strong vortex formation on the upper surface of box girder section. However, there have been no any useful references recommended in selecting the geometric configurations of double flaps or fairings. Anyway, the success of this study in finding the functions of double flaps and fairings attached on the box girder section through CFD has motivated using CFD to research aerodynamic countermeasures moved forward.

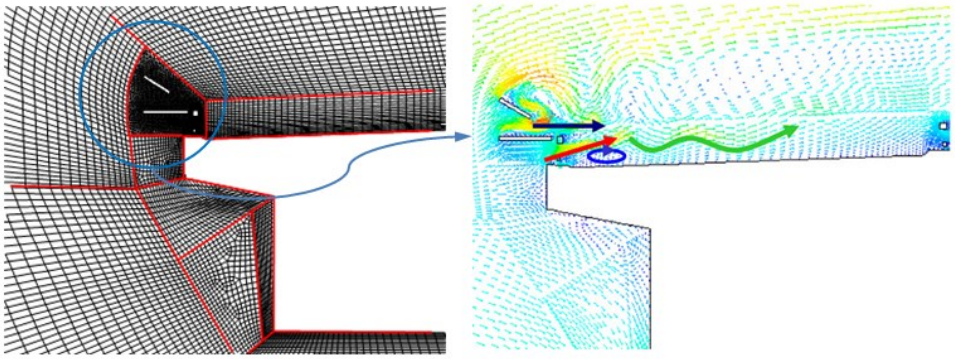

Figure 1.14. Numerical study on aerodynamic countermeasure of Sarwar, M. M. et al [31]

In fact, VIV has been detected in many cases of long span bridges with their substructures using box girder sections [6], [7], [8]. Flap countermeasure has been found that it can control the wind flow around the box section to effectively reducing the VIV. In case of the Shin-minato Bridge, a flap countermeasure was decided by wind tunnel tests to suppress the VIV [7]. Nevertheless, how to choose a relevant flap with specific geometric configurations to install on box girder sections is still an open question left without any recommendation. Wind tunnel tests implemented can provide the best solution, but accompanying the disadvantages mentioned above. The success of recent studies using CFD in countermeasures leads to a promising track in figuring out the unknown mechanisms. In order to contribute to the efforts in commonly reference establishment for aerodynamic countermeasure application, a numerical study on the wind flow around box girder section in the presence of flap countermeasure is quite necessary, feasible and expected. It is not only meaningful in practical engineering aspect, but also in scientific one. In terms of the practical engineering, it is expected to decrease the number of wind tunnel tests needing to be conducted, lessening budget and saving time in the early wind resistant design process. In scientific aspect, it is believed that the behavior of the wind flow in the presence of countermeasure is figured out.

1.5. Research aim, scope, objectives and methodology

The aim of this study is to gain better understanding of the suppression mechanism of wind induced vibrations and the behaviors of box bridge girder under the impact of wind load, in the context of considering the presence of flap countermeasure, by means of CFD technology approach. Consequently, a useful reference in flap countermeasure application is recommended in case of box girder. This one is concerned as an effort in promoting the establishment of common guideline for aerodynamic countermeasures to gradually reduce the numbers of experimental works in wind tunnel. On the other hand, the study is able to motivate the CFD approach in the field of bridge engineering in general and aerodynamic countermeasures in particular, as well as to support the information which wind tunnel tests cannot afford to provide.

The scope of this study is concentrated on the effect of flap countermeasure attached on box girder and some rectangular cross-sections having different width-to-depth ratios in VIV, which is often accepted widely to suppress the VIV.

By the range of the aim mentioned above, the major objectives of present thesis are determined as follows:

- To reasonably simulate a real bridge girder section, small attachment members on the girder, boundary conditions, mesh size, turbulence model… in numerical analyses.

- To examine the aerodynamic behavior of the wind flow around the box girder and the rectangular cross-sections having different width-to-depth ratios, in the presence of flap.

- To investigate the suppression mechanism of VIV of the box girder and the rectangular cross-sections having various width-to depth ratios, in the context of the presence of flap with diverse geometric configurations.

- To clarify the effect of flap in suppression VIV. Since then, some optimum configurations of flap are recommended as a useful reference or a common guideline in applying flap.

- To examine the influence of flap on the wind profile above the section as a side effect to vehicles, capturing how the flap disturbs the profile.

This research is a case study based on numerical analyses of aerodynamic characteristics, experimental data collected in wind tunnel tests and finite volume method. Numerical simulations are carried out into two parts including static and dynamic simulation, in the sense that the investigation is implemented through the steady force coefficients impacting on objects, the power spectrum density (PSD) of aerodynamic forces, root mean square (RMS) of surface pressure coefficient and aerodynamic forces, the wind flow pattern around objects, the turbulence intensity of wind flow above the sections and the flutter characteristic of objects. The numerical results obtained are compared with the collected experimental data in wind tunnel tests at Yokohama National University (YNU) [7], [8] of a real bridge girder and some previous researches on rectangular cross-sections [32], [33] to confirm the validation of simulations. The finite volume method is utilized in this study by means of the computer software STAR-CCM+ and all other calculations are done by using the computer software Microsoft Excel.

1.6. Outline of the thesis

The present thesis is arranged in seven chapters indicated in Figure 1.15 and the addition of all references is listed in the end. The contents of seven chapters are sketched as follows:

- Chapter 1 introduces the general information regarding the impact of wind on long span bridges, especially substructure. Then, the necessary of this research is presented. On the other hand, this chapter clearly defines the research aim, scope, objectives and methodology.

- Chapter 2 presents the theory of wind effects on bridge girder. Firstly, wind induced vibrations are clearly mentioned in company with estimation and calculation methods. Then, the theory of wind resistant design is carefully provided in case of long span bridge girder. Finally, the effect of aerodynamic countermeasures is given in some cases of real bridges. This chapter is concern as a fundamental theory part which is used to investigate the numerical results of later chapters.

- Chapter 3 provides the theory of CFD with basic concepts such as the equations describing fluid flow, CFD application, discretization, finite volume method…In addition, turbulence models are systematically summarized. More particularly, the turbulence model used in this study is presented to make bases for the later numerical simulations.

- Chapter 4 discusses about wind tunnel tests in general, the experimental data collection of a real bridge girder and several cases of rectangular cross-sections in some past researches. The data gathered in this chapter is vital basic to confirm the validation of all numerical simulations analyzed in this study.

- Chapter 5 deals with the numerical investigation into static simulation. Numerical simulation properties are described in detail. The aerodynamic characteristics of the box section and some rectangular cross-sections and the effect of flap countermeasure with various geometry configurations are analyzed. The flow pattern is observed to classify the suppression mechanism of VIV. On the other hand, a side effect to vehicle of flap is also discussed.

- Chapter 6 solves with the numerical investigation into dynamic simulation. Numerical simulation procedure is mentioned similarly as chapter 5. Flutter derivative H_1^* calculated from the results obtained in dynamic simulation is discussed to support more the confirmation for the effect of flap.

- Chapter 7 gives some conclusions basing the achieved results in flap application. The perspective of future researches is also recommended in this chapter.

The main contents of each chapter are summarized in the end of each one in order to make readers systematize the thesis easily.

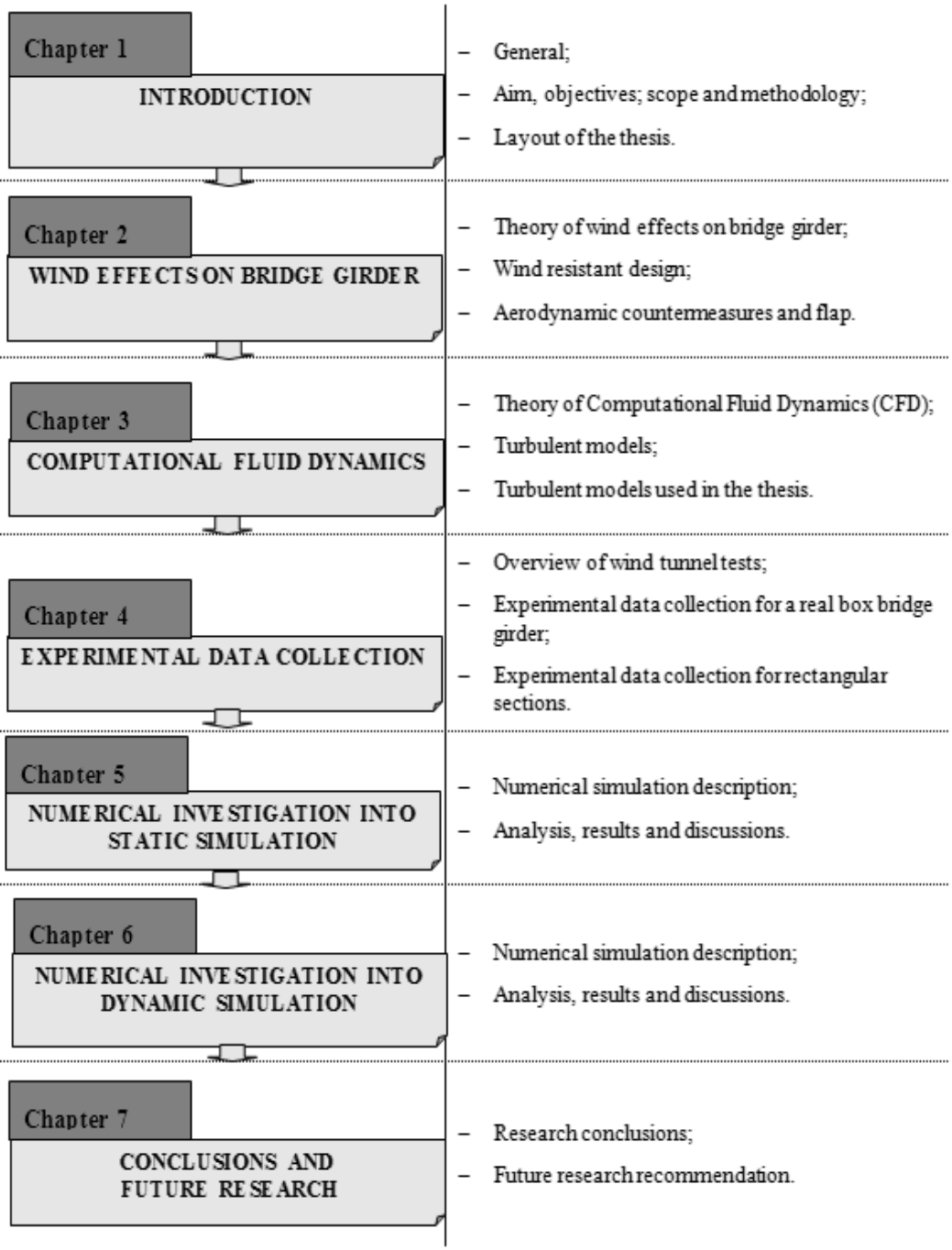

Figure 1.15. Layout of the thesis

1.7. Summary of Chapter 1

It has been expected that the introduction of the thesis is logically made in this chapter. Following this target, it is necessary to firstly remind the relationship between long span bridges and wind load (Section 1.1), the crucial role of wind resistant design (Section 1.2) and the controlling methods of wind-induced vibrations (Section 1.3). The existing issues of aerodynamic countermeasures application, the previously involved researches of two approaches including wind tunnel tests and numerical analyses, and the prospects of developing CFD technology in investigation into the wind flow with the presence of aerodynamic countermeasures are then discussed so as to arouse the problem statement (Section 1.4). By basic sections above, the aim, objectives, scope and methodology of the thesis are next particularly proclaimed (Section 1.5). At this stage, the outline of entire thesis is finally worked out in the end of the chapter (Section 1.6), presenting the main contents of each chapter intended.

2.1. Wind-induced vibrations on bridge girder

In wind environment, a bridge girder is subjected to surface pressures generated by the interaction of wind flow and that girder. The surface pressures can be caused by many sources taken into account, such as the turbulence of incident flow, the movement or deformation of bridge girder… Aerodynamic and aeroelastic instabilities can be found under the impact of those pressures. Therefore, wind-induced vibration of bridge girders needs to be investigated carefully. In case of bridge girders, there are three types of oscillation which are necessary to be considered: Self-excited vibrations (SEV), Vortex-induced vibration (VIV) and buffeting vibration (BV). A vast research on this field has been devoted towards theoretical formulations and experimental tests since the past decades. The fundamental aspects of aeroelastic phenomena are discussed in this section in order to provide the basics involved.

2.1.1. Self-excited vibrations (SEV)

SEV is a vibration whose amplitude ceaselessly increases by induced forces due to the motion of body in the air. For this reason, once SEV appears, the destruction of structures is inevitable. The mechanism of SEV occurrence can be explained through the simple vibration system as following. By the quantities of system are termed as: m is mass of system, c is structural damping constant, k is spring constant, y is displacement, F_0 is amplitude of aeroelastic force, ω is frequency of aeroelastic force and β is the lag phase between aeroelastic force and displacement, the equation of motion can be written as (2.1) or (2.2).

$$m\ddot{y} + c\dot{y} + ky = F_0 \sin(\omega t + \beta) \tag{2.1}$$

$$\mathrm{m\ddot{y} + c\dot{y} + ky = F_0 \cos\beta \sin\omega t + F_0 \sin\beta \cos\omega t} \tag{2.2}$$

If $y = y_0 sin\omega t$ and $\dot{y} = \omega cos\omega t$ are set to (2.2), then the motion equation will become (2.3).

$$m\ddot{y} + \left(c - \frac{F_0 sin\beta}{\omega y_0}\right)\dot{y} + \left(k - \frac{F_0 cos\beta}{y_0}\right)y = 0 \tag{2.3}$$

The condition for occurrence of SEV is damping term in (2.3) equal/less than 0, also meaning that $c = 0, sin\beta \geq 0 \; or \; \beta \geq 0$ is satisfied.

$$\left(c - \frac{F_0 sin\beta}{\omega y_0}\right) \leq 0 \tag{2.4}$$

On the other hand, if the relationship of oncoming velocity is used to explain SEV, then it is known that SEV only occurs when the oncoming velocity is higher than the critical wind speed selected through wind tunnel tests.

Flutter and galloping are two phenomena that mostly known in SEV of bridge girders. If flutter occurs in bridge girders with relatively large width-to-depth ratio, then galloping is often found in bridge girders with relatively small width-to-depth ratio. These phenomena are presented in sequence as followings.

a) Flutter

As mentioned in Simiu and Scanlan's book "Wind effects on structures" [34], three are four kinds of name including classical flutter, stall flutter, single-degree-of-freedom flutter and panel flutter to describe flutter phenomenon. All of them were originally used in aerospace application and then gradually encroached on wind civil engineering. In the treatment of flutter for bridge girder, classical flutter (two degrees of freedom heaving and torsional oscillations coupled together) and stall flutter (a single-degree-of-freedom oscillation in torsional mode) has been interested in researches. Flutter occurs when the magnitudes of torsional and heaving stiffness are close together. In fact of bridge girder situations, flutter tends to be dominated by two modes and the lowest solutions for natural frequency often lead to the critical condition. Figure 2.1 shows the flutter phenomenon occurred at the Tacoma Narrow Bridge [35], [36], [37].

(a)

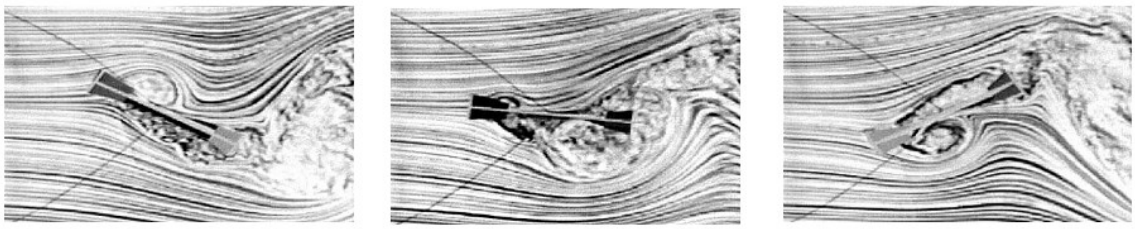

(b)

Figure 2.1. Flutter at the Tacoma Narrow Bridge [35], [36], [37]

The equations of motion of a symmetrical bridge deck immersed in a 2D wind flow, without considering drag force and assumed to be vibrated with two degrees of freedom (bending displacement *h* and torsion angle *a*), can be written by (2.5) [34].

$$\begin{aligned} m\left(\ddot{h} + 2\zeta_h \omega_h \dot{h} + {\omega_h}^2 h\right) &= L_h \\ I(\ddot{\alpha} + 2\zeta_\alpha \omega_\alpha \dot{\alpha} + {\omega_\alpha}^2 \alpha) &= M_\alpha \end{aligned} \tag{2.5}$$

where m, I are mass and moment of inertia of the bridge deck, ζ_h, ζ_α are damping factors in two modes, ω_h, ω_α are natural circular frequencies in *h* and *a* degrees of freedom, L_h and M_α are lift force and pitching moment per unit span.

Scanlan and Simiu proposed that the linear forms of L_h and $M_\alpha$can be described in the real field as ((2.6) [34]

$$\begin{aligned} L_h &= \frac{1}{2}\rho U^2 B\left[KH_1^*(K)\frac{\dot{h}}{U} + KH_2^*(K)\frac{B\dot{\alpha}}{U} + K^2H_3^*(K)\alpha + K^2H_4^*\frac{h}{B}\right] \\ M_\alpha &= \frac{1}{2}\rho U^2 B^2\left[KA_1^*(K)\frac{\dot{h}}{U} + KA_2^*(K)\frac{B\dot{\alpha}}{U} + K^2A_3^*(K)\alpha + K^2A_4^*\frac{h}{B}\right] \end{aligned} \tag{2.6}$$

where ρ is air density, U is oncoming wind velocity, B is deck width, $K = B\Omega/U = B(2\pi n)/U$ is reduced frequency (n is the frequency of oscillation), and H_i^*, A_i^* $(i = 1, 2, 3, 4)$ are flutter derivatives as dimensionless functions of K.

Flutter derivatives are importantly aerodynamic coefficients to judge the oscillatory tendency of bridge decks. These coefficients are dependent upon the reduced frequency K and dimensionless functions. Hence, the analytical methods of the flutter are very complicated. One of these methods is setting a certain value K considered as an initial value. Then, the flutter derivatives corresponding to that value can be obtained from the experimental functions. By assuming *h* and *a* under $e^{i\omega t}$ form, the stability condition is established by using the zero determinant of coefficients of *h* and *a*. The final stage of this step is getting the $\omega = \omega_1 + i\omega_2, \omega_2 \neq 0$ solution. There are two cases possible, the first one is corresponding to a decaying oscillation with the $\omega_2 > 0$ condition and the second one is regarding to a divergent oscillation with the $\omega_2 < 0$ condition. This procedure is repeated with the different values of K to receive $\omega \approx \omega_1$, in the sense that the solution of flutter corresponds the flutter condition through the critical velocity .

$$U_c = \frac{B\omega_1}{K_c}, K_c = K \; at \; \omega \approx \omega_1 \tag{2.7}$$

In addition, flutter derivatives should be used to estimate the aerodynamic oscillation properties of bridge deck under flow action. In quantitative analysis, these ones are parameters that can be calculated from the results measured in wind tunnel or the results obtained in numerical study. Figure 2.2 below presents the flutter derivatives of the Great Belt East Bridge cross-section obtained by experimental tests and numerical analysis [38].

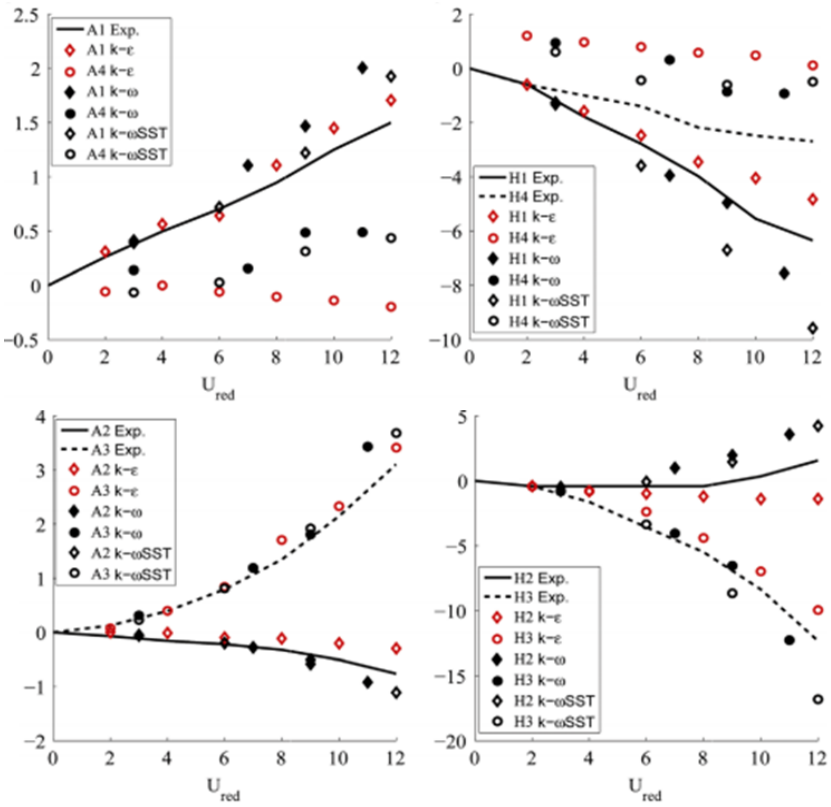

Figure 2.2. Flutter derivatives of the Great Belt East Bridge cross-section [38]

b) Galloping

There are two kinds of galloping including across-wind galloping and wake galloping. The first one is aerodynamic instability phenomenon discovered in cases of slender structures like bridge girder sections with the range of width-to-depth ratio 0.7-3.0, but the later one often occurs in case of two cylinders whose one is located upstream of the other. In terms of bridge girder sections, across-wind galloping can be defined as an aerodynamic instability involved in very high amplitude oscillation in the direction perpendicular to the oncoming wind flow (heaving mode). It is known as the instability vibration having lower frequencies in comparison with the vortex shedding from the same section, and the amplitude develops ceaselessly until the structure will be destroyed.

The mechanism of galloping in bridge girders with ratio of 0.7-3.0 can be explained by means of the behaviors of separation or reattachment in the wind flow around the sections. It is believed that galloping will not be found in the long cross-sections having a large width-to-depth ratio due to the phenomenon of reattachment becomes dominated, as Figure 2.3.

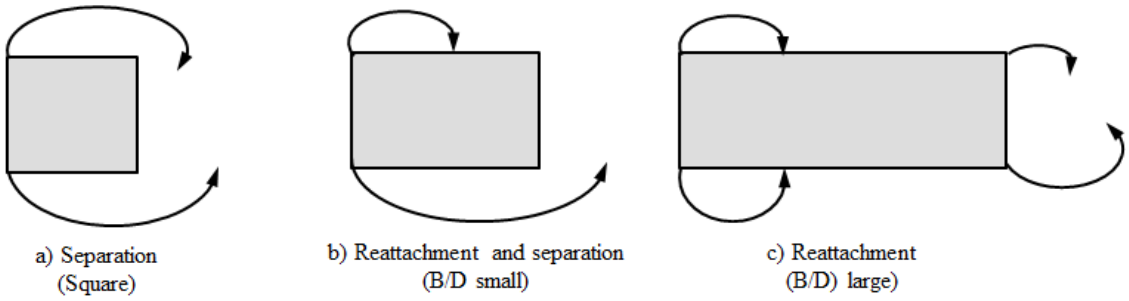

Figure 2.3. Separation and reattachment of the wind flow around the sections

Similarly to equation (2.1), assuming that the object has mass per m unit length, is set up with a spring having stiffness k, has a linear damping with ratio ζ and a natural circular frequency ω_1, the equation of motion of the object subject to wind load can be expressed as (2.8). The F_y in this equation is the aerodynamic force impaction on the object.

$$m(\ddot{y} + 2\zeta\omega_1\dot{y} + \omega_1^2 y) = F_y \tag{2.8}$$

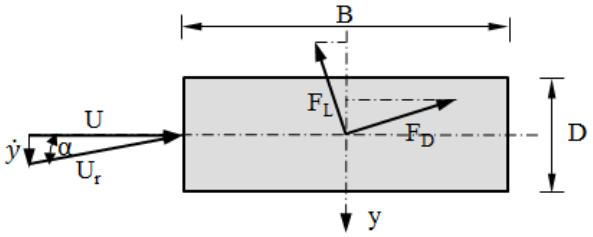

Figure 2.4. Lift and drag forces on an object subjected to wind load

Figure 2.4 describes a certain object fixed and subjected to wind load to clarify the formulations. Using quasi-steady theory with assumption that the motion is very slow, the force F_y can be normalized as the aerodynamic force $F_y(\alpha)$ acting on the fixed object [34]. The formulations, from (2.9) to (2.13), are used to determine the value of $F_y(\alpha)$.

$$D(\alpha) = \frac{1}{2}\rho U_r^2 D C_D(\alpha) \tag{2.9}$$

$$L(\alpha) = \frac{1}{2}\rho U_r^2 D C_L(\alpha) \tag{2.10}$$

$$F_y(\alpha) = -D(\alpha)sin\alpha - L(\alpha)cos\alpha \tag{2.11}$$

$$F_y(\alpha) = \frac{1}{2}\rho U^2 D C_F(\alpha) \tag{2.12}$$

$$C_F(\alpha) = -\frac{1}{cos\alpha}[C_L(\alpha) + C_D(\alpha)tan\alpha] \tag{2.13}$$

where:

$D(\alpha)$is the component of the mean drag force F_D and $C_D(\alpha)$ is its coefficient;

$L(\alpha)$is the component of the mean lift force F_L and $C_L(\alpha)$ is its coefficient;

α is the angle of attack of wind flow;

U_r is the relative velocity of flow with the moving object;

U is the wind flow velocity.

In case of small motion, the conditions (2.14) and (2.15) can be come up and the equation of motion can be written under the other form like the equation (2.16).

$$F_y \cong \left.\frac{\partial F_y(\alpha)}{\partial \alpha}\right|_{\alpha=0} \alpha;\ \alpha \cong \frac{\dot{y}}{U} \cong 0 \tag{2.14}$$

$$\left.\frac{dC_{F_y}(\alpha)}{d\alpha}\right|_{\alpha=0} = -\left(\frac{dC_L}{d\alpha} + C_D\right)_0 \tag{2.15}$$

$$m(\ddot{y} + 2\zeta\omega_1\dot{y} + \omega_1^2 y) = -\frac{1}{2}\rho U^2 D\left(\frac{dC_L}{d\alpha} + C_D\right)_0 \frac{\dot{y}}{U} \tag{2.16}$$

In the equation (2.16), the damping coefficient of system can be divided into two parts: the mechanical damping coefficient $2m\zeta\omega_1 \geq 0$ and the aerodynamic damping coefficient $\frac{1}{2}\rho UD\left(\frac{dC_L}{d\alpha} + C_D\right)_0$. Hence, the condition for instability phenomenon can be expressed as (2.17) and is known as the Glauert-Den Hartog criterion in case of incipient galloping instability.

$$\left(\frac{dC_L}{d\alpha} + C_D\right)_0 < 0 \tag{2.17}$$

2.1.2. Vortex-induced vibration (VIV)

VIV can be known as the aerodynamic vibration which is caused by the alternate vortices generated from the interaction between the objects and wind flow. VIV cannot lead to the collapse of structure immediately because it has the limited amplitude. However, it is of interest to control VIV due to the other reasons related to structural fatigue and passenger feeling. Particularly, VIV is classified into two kinds: VIV due to Karman vortices and VIV due to the vortices generated along the deck section in consideration of the movement of the deck [12]. The latter one is usually discovered in most cases of the flat box girder in cable-supported bridges [39].

Normally, the dimensionless constant called Strouhal number is used to evaluate the characteristic property of each bluff-body in wind flow by means of the vortex shedding behind the object, as Figure 2.5. It is defined in the equation (2.18).

$$S_t = \frac{N_s D}{U} \tag{2.18}$$

where:

N_s is the primary frequency of vortex shedding, as ;

D is the across-wind dimension or the representative length of the object;

U is the mean velocity of wind flow in which the object is subjected.

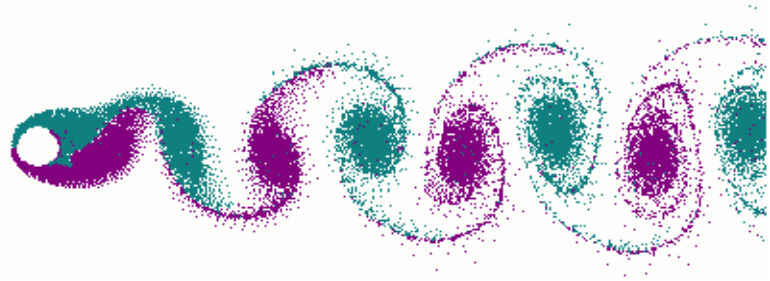

Figure 2.5. Vortex shedding behind a cylinder [40]

The primary frequency of alternate vortices increases proportionally to the velocity of wind flow. If the object is elastically supported in a spring, it has a natural frequency in motion which effects to the flow around. The VIV occurs at a region in which the frequency of vortices equals to the natural frequency. This is called "lock-in" region and is considered as the synchronization between the vortices with vibration system, Figure 2.6. Therefore, once

the frequency of vortices corresponding to a certain oncoming velocity reaches the natural frequency of the object, the vortex shedding will be controlled by structure at that natural frequency. This leads to a resonant vibration with maximum amplitude. Since the range of velocity to this phenomenon is limited, the amplitude of VIV has a limitation. Hence, VIV is classified as a limitation oscillation.

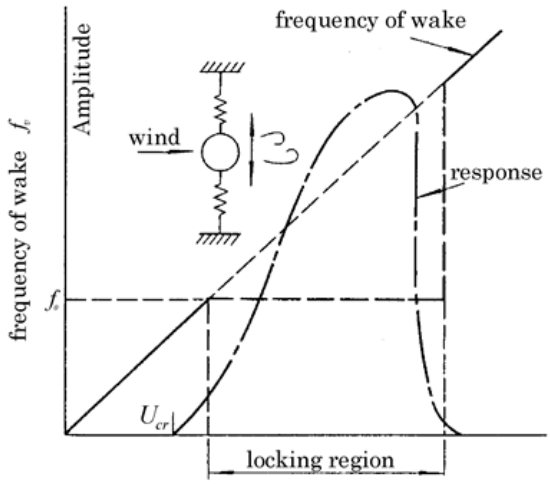

Figure 2.6. Lock-in region in VIV

In addition, the Strouhal number can be used to estimate the onset velocity of VIV through its principle. Assuming that N_0 is the natural frequency of the object, the onset velocity $U_{cr(VIV)}$ is expressed by (2.19). Then, by applying the equation (2.18) the reduced velocity of $U_{cr(VIV)}$ is $U_{Re,cr(VIV)}$ which is written in the equation (2.20). Therefore, the critical velocity of VIV can be judged by the direct relationship with the Strouhal number of the object.

$$U_{cr(VIV)} = \frac{N_0 D}{S_t} \tag{2.19}$$

$$U_{Re,cr(VIV)} = \frac{U_{cr(VIV)}}{N_0 D} = \frac{1}{S_t} \tag{2.20}$$

In wind engineering for long span bridges, VIV due to the separated vortices from leading edge and the secondary vortices at trailing edge is well-known as motion-induced

vortices vibration (MIV). The classification of VIV can be illustrated through Figure 2.7 [39]. The MIV onset reduced velocity is predicted at (B/D)/0.6, not 1/St, with the range of side ratios lying between 2 and 7.5. In addition, the MIV can be also found at onset reduced velocity at 0.5(B/D)/0.6 with a smaller amplitude. In other words, the shapes of box girder could play a major role in generating the vortices. It was confirmed that the combination between the vortices at leading and trailing edges dominate the oscillation.

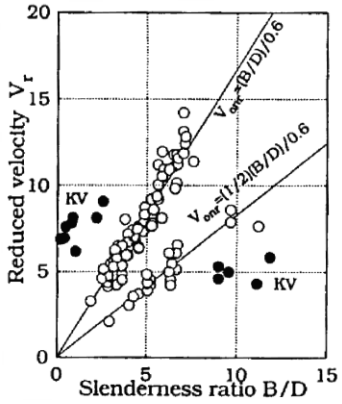

Figure 2.7. Classification of VIV [39]

In order to examine the vortex-induced response, one of the approximations to the across-wind force per unit span F can be set as the equation (2.21) [34], where $\omega_s = 2\pi N_s$ and C_{LS} is the lift force coefficient. Yet, this approximation is inadequate for the correlation along the span dimension.

$$F = \frac{1}{2}\rho U^2 D C_{LS} sin\omega_s t \tag{2.21}$$

On the other hand, the equation of motion of the object in vortex-induced response can be written as (2.22). The lift force F depends on displacement y, the derivatives $\dot{y}, \ddot{y}$ and time. A variety of experimental means have been carried out to fit the lift force F. In VIV, it is illustrated that the close-sinusoidal response of the object is found in two prominent frequencies which are the Strouhal and the natural one.

$$m\ddot{y} + c\dot{y} + ky = F(y, \dot{y}, \ddot{y}, t) \tag{2.22}$$

Otherwise, the characteristic of VIV can be evaluated through the flutter derivative $H_1^*(K)$ extracted from the experimental tests in wind tunnel or the numerical simulations in CFD technology. The forced method with a harmonic excitation impacting on the object is usually applied to derive $H_1^*(K)$ by means of the time history of unsteady forces obtained from the outcomes of wind tunnel tests or numerical simulations. According to $H_1^*(K)$ or the imaginary component of unsteady force, it can be judge the range of critical velocity in VIV. The positive value of $H_1^*(K)$ or the positive value of imaginary component has resulted in a negative aerodynamic damping in vibration system in which the VIV occurs. Figure 2.8 presents an example of using $H_1^*(K)$ (calculated from CFD results and compared with experimental ones) to assess the VIV in a box bridge girder [31].

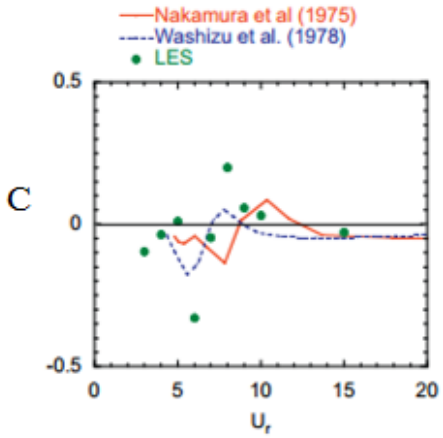

Figure 2.8. Positive imaginary component of unsteady life force found in VIV [31]

2.1.3. Buffeting vibration (BV)

BV is defined as the vibration of an object generated by the random fluctuation of the unsteady loading. There are two types of BV: wake buffeting induced in the turbulent zone of an upstream object and incident turbulence buffeting created in an atmospheric flow at a certain terrain. The first one is beyond in bridge wind effects, but the latter is prominent in slender structures like the bridge girder of long span bridges. Normally, the combination between the turbulence of oncoming velocity and the wind-induced vibration of the object decides the response of bridge deck in BV. In long span bridges, the longer main span is, the more BV response increases.

A bridge girder subjected to wind loading can be considered as a line-like structure. In terms of BV examination in atmospheric turbulence, the aerodynamic forces can be superposed by self-excited forces and buffeting forces. The self excited forces were presented in section 2.1.1, in the sense that those ones may be expressed in equation ((2.6). The calculated formulation of the buffeting forces can be written down by using quasi-steady theory [34] as equations (2.23).

$$\frac{D(t)}{\frac{1}{2}\rho U^2 B} = C_D(\alpha_0)\frac{A}{B}\left[1 + 2\frac{u(x,t)}{U}\right]$$

$$\frac{-L(t)}{\frac{1}{2}\rho U^2 B} = C_L(\alpha_0)\left[1 + 2\frac{u(x,t)}{U}\right] + \left[\left.\frac{dC_L}{d\alpha}\right|_{\alpha=\alpha_0} + \frac{A}{B}C_D(\alpha_0)\right]\frac{w(x,t)}{U} \tag{2.23}$$

$$\frac{M(t)}{\frac{1}{2}\rho U^2 B^2} = \left[C_M(\alpha_0) + C_D(\alpha_0)\frac{A_r}{B^2}\right]\left[1 + 2\frac{u(x,t)}{U}\right] + \left.\frac{dC_L}{d\alpha}\right|_{\alpha=\alpha_0}\frac{w(x,t)}{U}$$

where:

$D(t), L(t), M(t)$ are the buffeting drag, lift and aerodynamic moment;

C_D, C_L, C_M are the force coefficients of the above forces;

u, v, w are the components of velocity fluctuations;

B is the representative dimension of the object;

A is the across-wind area per unit length projected on the plane perpendicular to the mean velocity;

r is the distance between the mass center of the object and rotation axis.

The superposition principle can be applied to evaluate the effect of BV by means of considering the buffeting load as an accumulating set of a variety of individual harmonic loads. Hence, the BV can be viewed as a superposition of harmonic responses generated by the relevant loads.

2.2. Wind resistant design

The wind-induced vibrations of long-span bridges are indicated in Figure 2.9. The VIV occurs in a range of small wind velocity and it has the limited amplitude. On the contrary, the SEVs only come up at a certain high wind velocity and the vibration amplitude ceaselessly develops. In addition, the BV can appear at the wind velocity less than the critical wind velocity of SEVs, and it can lead to a gradual transition to large vibration amplitude. Depending on type of vibration, the remedy of wind resistant design in long-span bridges is different. The fundamental design principles and the dynamic wind design procedure in Japan were generally presented in Section 1.3 and Figure 1.11.

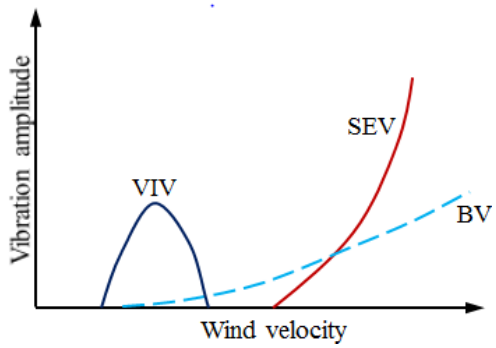

Figure 2.9. Wind-induced vibrations in long-span bridges

More particularly, SEVs such as flutter and galloping have to be carefully inspected during the design process of the bridges. It is very dangerous once these vibrations occur, because the bridges will be collapsed due to the development of the oscillation amplitude. In Japan, wind tunnel tests are always required to examine those ones. If the SEVs are found in experimental results, then the controlling methods have to be applied to eliminate those vibrations. The reference velocity must, which is determined from the design wind velocity and wind turbulence, be smaller than the critical wind velocity of SEVs. This is compulsory condition which is ensured under any stage.

In spite of not causing the damage of structures instantaneously, VIV has to be adequately investigated during the design process of long-span bridges. The feeling of passengers, the fatigue damages of structures…, due to VIV, need to be considered in the serviceability of the bridges. There are two either conditions to be required to satisfy in VIV:

the amplitude of VIV has to be smaller than the allowable amplitude determined from the serviceability state (the amplitude corresponding to the acceleration of 1.00 m/s^2 is accepted in the Wind Resistant Design Manual for Highway Bridges in Japan [11]), or the critical velocity of VIV has to be higher than the design velocity [12]. Aerodynamic and structural countermeasures often exhibit their significant effect in controlling VIV. The suppressing solutions can be decided after the VIV discovered during the bridge construction or after the vibration observation in the period of completion. Wind tunnel tests are carried out to examine the behavior of VIV.

In order to avoid the complex in analysis of dynamic response due to the random of buffeting load, the BV is often dealt with the increase of static wind load. In some cases, the BV can be concerned in the same way with the VIV, because it also has limitation in oscillation amplitude. The serviceability standards have to be taken into account. Hence, it is necessary to verify the BV amplitude and ensure that this amplitude have to be less than the allowable amplitude obtained in a similar manner for VIV state (the amplitude corresponding to the acceleration 1.00 m/s^2 is accepted in the Wind Resistant Design Manual for Highway Bridges in Japan [11]). Enhancing the stiffness of structure or diminishing the drag force is usually chosen as a counter to reducing the BV of the bridges.

2.3. Aerodynamic countermeasures

Aerodynamic countermeasures and structural countermeasures are two main solutions in suppressing wind-induced vibrations of long-span bridges. In section **Error! Reference source not found.**, the concepts of those ones were presented. The shapes of various aerodynamic countermeasures were also mentioned in Figure 1.12. This section discussed more detail about the working principles of aerodynamic countermeasures.

According to Wind Resistant Design of Bridges in Japan [12], the working principles of some normally aerodynamic countermeasure are summarized in Table 2.1.

Table 2.1. Summary of aerodynamic countermeasures [12]

N0	Wind-induced Vibration		Subject	Aerodynamic Countermeasures		Working Principle	Note
1	Self-excited Vibrations	Flutter	Bridge girders with the large ratio (B/D)	Open grating	Figure 1.12 b)	Decreasing the pressure difference between the upper and lower side surface of the girder	Mechanical devices can be applied to mitigate the aerodynamic forces in cases of keeping the original girder section: - Movable wings at the edge of the girders can eliminate the aerodynamic forces on the girder. - Movable flaps or fairings having the different phase with the deck motion can reduce the wind-induced vibration.
			Shallow box girders with the small (B/D)	Fairings		Improving the flutter stability by means of controlling the flow at the leading edge of the girders	
				Wind noses			
				Deflectors			
				Spoilers			
			Truss girder	Open grating		Stabilizing the flutter instabilities through the changing flow pattern around the deck and the upper chord	
				Center barrier		Reducing the flutter instabilities because of weakening the action of the separation bubbles from the leading edge	
				Vertical stabilizer			
		Galloping	Bridge girders (box girder shape) with the small ratio (B/D)	Skirt	Figure 1.12 a)	Controlling the wind flow under the bridge deck to reduce the wind velocity of the separated flow from the leading edge	Using mechanical approach can control the boundary layer separation
				Horizontal plates			

2	Vortex-induced Vibration	Bridge girders (usually box girder shape) with the small width-to-depth ratio (B/D)	Fairings	Figure 1.12 c)	Promoting the reattachment of the separated flow from the leading edge	- Open grating sometimes is used to constrain VIV. - Mechanical approaches can be applied to control the boundary separation: a rotor installed at the corner of the sections, an artificial flow supplied to the inner side of the boundary layer.
			Flaps		Suppressing the flow separation from the upper edge	
			Deflectors		Controlling the flow separation from the leading edge by streamlining the overall girder shape	
			Horizontal plates		Similar to deflectors but from the bottom of the section	
			Vertical plate		Preventing the generation of vortices around the girder	
			Baffle plate			
3	Buffeting Vibration	Bridge girders			Reducing the drag coefficient or increasing the stiffness is known as a main solution. In some special cases, aerodynamic appendages are considered to mitigate the static wind loads	

Comprehending the mechanism of wind flow in the presence of aerodynamic countermeasures has issued a challenge in wind civil engineering so far. It is very difficult to recommend a specific countermeasure to each particular wind-induced vibration. The general discussion in Table 2.1 can orient in selection. In some cases, a countermeasure is good on a certain vibration, but it can cause adverse effects to a different oscillation. If that is the case, the combination between them can be applied to achieve the best solution.

It is very necessary to build up a common guideline in aerodynamic countermeasure application. CFD has emerged as prospects in supporting to the information obtained from wind tunnel tests to realize the answer. Hence, this is one of the major research trends in wind-bridge engineering and is also the motivation of the thesis. The wind flow around a box girder section in the presence of flap with various geometric configurations is investigated by numerical simulations to contribute for that mission.

2.4. Vortex induced vibration in some real cases

VIV has been discovered in many long-span bridges. VIV observed during the final construction stage of Great Belt Bridge in Denmark is one of interesting circumstances. Aerodynamic countermeasure called guide vanes were utilized, and it brought in the significant effect [41]. In Japan, Tozaki Bridge, Trans-Tokyo Bridge and Shin-minato Bridge are some typical instances where VIVs were revealed. In case of Trans-Tokyo Bridge, a TMD system was installed to control the oscillation [6]. When it turns to Tozaki Bridge [42] and Shin-minato Bridge [7], double flaps and flap have effectively exhibited the role in vibration reduction, respectively. Table 2.2 summarizes the major information of the above mentioned bridges.

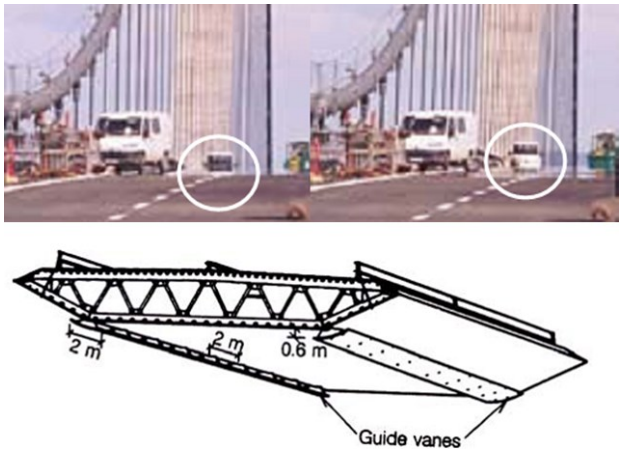

Figure 2.10. VIV found in Great Belt Bridge and guide vanes countermeasure [41]

In terms of Shin-minato Bridge [7], the various shapes of flap were examined in wind tunnel tests to optimize the solution. This research uses the girder section of Shin-minato Bridge as a primary object to investigate the role of flap. The wind flow around the section in

the presence of flap is explained by means of numerical simulations. The results obtained from experimental works are precious material to confirm the validation of numerical simulations.

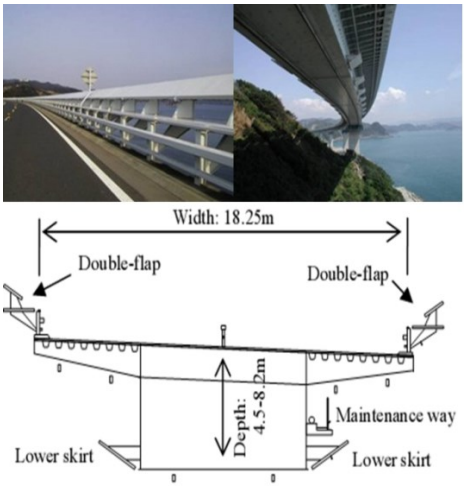

Figure 2.11. Double flaps and lower skirt installed in Tozaki Bridge [42]

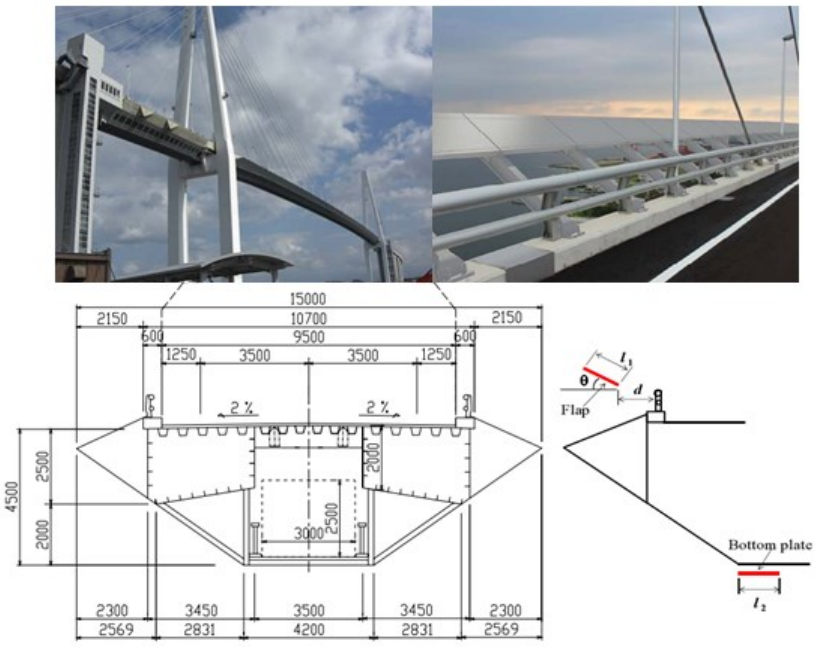

Figure 2.12. Flap attached on the section of Shin-minato Bridge [7]

Table 2.2. VIV found in some real cases

N0	Bridge	Main Parameters	Vibration	Solution	Note
1	Great Belt	- Suspension bridge - In Denmark - 3 spans: 535 m+1624 m+535 m - Box girder section	- VIV occurred in heaving mode - The velocity range of VIV: 5 m/s - 10m/s	Guide Vanes were attached to the bridge deck in order to reduce the amplitude vibration	
2	Tozaki	- Multi-span bridge - In Japan - The maximum span length: 190.4 m - Box girder section: The deck width 18.25 m, the deck height from 4.5 m to 8.2 m	- VIV occurred in heaving mode - The velocity range of VIV: 15 m/s - 20 m/s - The amplitude oscillation is 350 mm at the 0^o angle of attack, 410 mm at 3^o, 340 mm at 5^o and 680 mm at 10^o - Galloping occurred at the onset wind velocity 70 m/s at the 0^o angle of attack, 30 m/s at the angles of attack 3^o-10^o	- Lower skirts to suppress the galloping vibration, but enhancing the amplitude of VIV - Double flaps exhibited the significant effect on depressing VIV, but insufficient for suppressing the galloping - Both Lower skirts and Double flaps eventually were used	
3	Trans-Tokyo	- 10 steel span continuous bridge - In Japan - 2 longest spans: 240 m - Box girder section	- VIV occurred in heaving mode - The velocity range of VIV: 16 m/s - 17 m/s - The maximum amplitude of VIV: 500 mm	TMD system was used to reduce the amplitude oscillation	
4	Shin-minato	- Cable-stayed bridge - In Japan - 3 spans: 120 m+360 m+120 m - Steel box girder section	- VIV occurred in heaving mode - The velocity range of VIV: 12 m/s - 14 m/s - The maximum amplitude of VIV: 350 mm	Flap was installed on the bridge deck to control the vibration	

2.5. Summary of Chapter 2

Chapter 2 contains the main contents related to the theory of the wind effects on bridge girders and wind resistant design. Firstly, the essence of wind-induced vibrations and how to estimate those effects are presented in Section 2.1. Then, the requirements of wind resistant design for long-span bridges are mentioned in Section 2.2. As part of this discussion, the specific standards ruled over each type of wind-induced vibrations are systematized. Next, moving to Section 2.3, the commonly working principles of aerodynamic countermeasures are summarized particularly. The effort needed to be contributed to comprehend the performance of aerodynamic countermeasures can be found in this section, and it is regarded as the motivation of this research. Finally, some VIVs of real bridges and the applied methods to suppress the oscillation are introduced in Section 2.4. This section is concerned as one of real data source to serve the next chapters of which the main target is to clarify the role of flap countermeasure.

3.1. Governing equations of fluid flow

3.1.1. Fundamental physical principles

Mathematically, the state and motion of fluid flow can be expressed by a basic equation system called the governing equations of fluid flow. Those ones were derived from the fundamental physical principles including mass conservation law, Newton's second law and energy conservation law. Consequently, the governing equations of fluid flow comprise the continuity equation, the momentum equation and the energy equation respectively.

3.1.2. Governing equations

a) The continuity equation

The mass conservation law makes a statement that the mass of a control volume will be kept constant over time. Hence, the value of mass does not change and it is conserved in a close system. By this concept, the net mass flow out of the control volume is equal to the time rate of decrease mass inside.

The continuity equation can be written as follow [43], [44], [45]:

$$\frac{\partial \rho}{\partial t} + \frac{\partial(\rho u)}{\partial x} + \frac{\partial(\rho v)}{\partial y} + \frac{\partial(\rho w)}{\partial z} = S_m, or \qquad (3.1)$$

$$\frac{\partial \rho}{\partial t} + div(\rho \boldsymbol{u}) = S_m$$

where:

$\boldsymbol{u}$ is the velocity of fluid flow with 3 components u, v, w in x, y, z directions of Cartesian coordinate system;

ρ is the density of fluid flow;

S_m is the mass source added to the system.

b) The momentum equation

Applying the Newton's second law of motion, the momentum equation of fluid flow will be derived. It is stated that the time rate of momentum change equals to the sum of the

forces imposing on a particle. Normally, the momentum equation is described through the pressure and viscous stresses acting on the particle. The forces include body forces (gravitational, electric and magnetic forces) and surface forces (the pressure distribution on the surface due to the surrounding fluid, the shear and normal stress distribution from friction). In Cartesian coordinate, these equations can be expressed as follows [43], [44], [45]:

$$\begin{aligned}
\frac{\partial \rho u}{\partial t} + div(\rho u \boldsymbol{u}) &= -\frac{\partial p}{\partial x} + \frac{\partial \tau_{xx}}{\partial x} + \frac{\partial \tau_{xy}}{\partial y} + \frac{\partial \tau_{xz}}{\partial z} + S_{mx} \\
\frac{\partial \rho v}{\partial t} + div(\rho v \boldsymbol{u}) &= -\frac{\partial p}{\partial y} + \frac{\partial \tau_{xy}}{\partial x} + \frac{\partial \tau_{yy}}{\partial y} + \frac{\partial \tau_{zy}}{\partial z} + S_{my} \\
\frac{\partial \rho w}{\partial t} + div(\rho w \boldsymbol{u}) &= -\frac{\partial p}{\partial z} + \frac{\partial \tau_{xz}}{\partial x} + \frac{\partial \tau_{yz}}{\partial y} + \frac{\partial \tau_{zz}}{\partial z} + S_{mz}
\end{aligned} \tag{3.2}$$

where:

p is the pressure;

τ are the viscous stresses;

S_{mx}, S_{my}, S_{mz} are the body forces per unit volume on the fluid in x, y, z directions of Cartesian coordinate system .

c) The energy equation

The third fundamental physical principle used to derive the energy equation is the first law of thermodynamics or the energy conservation law. According to this law, the rate of energy change inside the fluid element (the internal energy generated from the random molecular motion e and the kinetic energy induced from the translational motion $|\boldsymbol{u}|^2/2$) equals to the net flux of heat into the element (the volume heating of element such as absorption or emission of radiation, the heat transfer across the surface due to temperature gradients, and thermal conduction,…) and the rate of work done on the element due to the body and surface forces [43]. In terms of thermodynamics, the energy equation is known as the transport of head energy through a fluid and its effects.

$$\frac{\partial\left[\rho(e+\frac{|\boldsymbol{u}|^2}{2})\right]}{\partial t}+div\left[\rho(e+\frac{|\boldsymbol{u}|^2}{2})\boldsymbol{u}\right]$$
$$=S_E-div(p\boldsymbol{u})+div(kgradT)$$
$$+\left[\frac{\partial(u\tau_{xx})}{\partial x}+\frac{\partial(u\tau_{xy})}{\partial y}+\frac{\partial(u\tau_{xz})}{\partial z}\right] \quad (3.3)$$
$$+\left[\frac{\partial(v\tau_{xy})}{\partial x}+\frac{\partial(v\tau_{yy})}{\partial y}+\frac{\partial(v\tau_{yz})}{\partial z}\right]$$
$$+\left[\frac{\partial(w\tau_{xz})}{\partial x}+\frac{\partial(w\tau_{yz})}{\partial y}+\frac{\partial(w\tau_{zz})}{\partial z}\right]$$

where:

T is the temperature;

k is thermal conductivity;

S_E is the source of energy per unit volume and time.

d) The Navier-Stokes and Euler equations

The governing equations obtained above can be applied to a viscous flow in which the transport phenomena of friction, thermal conduction and mass diffusion can be taken place. Such whole governing equations are called the Navier-Stokes equations. In case of inviscid flow in which the transport phenomena of viscosity, thermal conductivity and mass diffusion are ignored, the resulting equations after cancelling the terms related to friction, thermal conduction are named by the Euler equations. Respectively, Table 3.1 and Table 3.2 summarize the Navier-Stokes and Euler equations for an unsteady, three-dimensional, compressible flow.

Table 3.1. Summary of the Navier-Stokes equations – Conservation form

N0	Equation Name	Description	Note
1	Continuity	$$\frac{\partial \rho}{\partial t} + div(\rho \boldsymbol{u}) = S_m$$	(3.1a)
2	Momentum	$$\frac{\partial \rho u}{\partial t} + div(\rho u \boldsymbol{u}) = -\frac{\partial p}{\partial x} + \frac{\partial \tau_{xx}}{\partial x} + \frac{\partial \tau_{xy}}{\partial y} + \frac{\partial \tau_{xz}}{\partial z} + S_{mx}$$ $$\frac{\partial \rho v}{\partial t} + div(\rho v \boldsymbol{u}) = -\frac{\partial p}{\partial y} + \frac{\partial \tau_{xy}}{\partial x} + \frac{\partial \tau_{yy}}{\partial y} + \frac{\partial \tau_{zy}}{\partial z} + S_{my}$$ $$\frac{\partial \rho w}{\partial t} + div(\rho w \boldsymbol{u}) = -\frac{\partial p}{\partial z} + \frac{\partial \tau_{xz}}{\partial x} + \frac{\partial \tau_{yz}}{\partial y} + \frac{\partial \tau_{zz}}{\partial z} + S_{mz}$$	(3.2)
3	Energy	$$\frac{\partial \left[\rho\left(e + \frac{\lvert \boldsymbol{u} \rvert^2}{2}\right)\right]}{\partial t} + div\left[\rho\left(e + \frac{\lvert \boldsymbol{u} \rvert^2}{2}\right)\boldsymbol{u}\right] = S_E - div(p\boldsymbol{u}) + div(kgradT) + \left[\frac{\partial (u\tau_{xx})}{\partial x} + \frac{\partial (u\tau_{xy})}{\partial y} + \frac{\partial (u\tau_{xz})}{\partial z}\right] + \left[\frac{\partial (v\tau_{xy})}{\partial x} + \frac{\partial (v\tau_{yy})}{\partial y} + \frac{\partial (v\tau_{yz})}{\partial z}\right] + \left[\frac{\partial (w\tau_{xz})}{\partial x} + \frac{\partial (w\tau_{yz})}{\partial y} + \frac{\partial (w\tau_{zz})}{\partial z}\right]$$	(3.3)

Table 3.2. Summary of the Euler equations – Conservation form

N0	Equation Name	Description	Note
1	Continuity	$\frac{\partial \rho}{\partial t} + div(\rho \boldsymbol{u}) = S_m$	(3.1b)
2	Momentum	$\frac{\partial \rho u}{\partial t} + div(\rho u \boldsymbol{u}) = -\frac{\partial p}{\partial x} + S_{mx}$ $\frac{\partial \rho v}{\partial t} + div(\rho v \boldsymbol{u}) = -\frac{\partial p}{\partial y} + S_{my}$ $\frac{\partial \rho w}{\partial t} + div(\rho w \boldsymbol{u}) = -\frac{\partial p}{\partial z} + S_{mz}$	(3.2)
3	Energy	$\frac{\partial \left[\rho\left(e + \frac{\lvert\boldsymbol{u}\rvert^2}{2}\right)\right]}{\partial t} + div\left[\rho\left(e + \frac{\lvert\boldsymbol{u}\rvert^2}{2}\right)\boldsymbol{u}\right] = S_E - div(p\boldsymbol{u}) + div(kgradT)$	(3.3)

The shear stresses involved Newtonian fluid, in which the shear stress is proportional to the time rate of strain, velocity gradients, can be calculated as follows:

$$\tau_{xx} = 2\mu\frac{\partial u}{\partial x} + \lambda div\boldsymbol{u};\ \tau_{yy} = 2\mu\frac{\partial v}{\partial y} + \lambda div\boldsymbol{u};$$
$$\tau_{zz} = 2\mu\frac{\partial w}{\partial z} + \lambda div\boldsymbol{u};$$
$$\tau_{xy} = \tau_{yx} = \mu\left(\frac{\partial u}{\partial y} + \frac{\partial v}{\partial x}\right);\ \tau_{xz} = \tau_{zx} = \mu\left(\frac{\partial u}{\partial z} + \frac{\partial w}{\partial x}\right);$$
$$\tau_{yz} = \tau_{zy} = \mu\left(\frac{\partial v}{\partial z} + \frac{\partial w}{\partial y}\right) \quad (3.4)$$

Gases and liquids with low velocity can be considered as incompressible fluid. The above equations will become simpler when the density of fluid ρ remained constant.

3.2. Computational fluid dynamics

3.2.1. General

The essence of CFD is the digitization process of the governing equations discussed above. Recently, thank to the advance of computer technology, CFD can solve a variety of sophisticated issues in fluid dynamic, especially in wind civil engineering. The main paces of CFD procedure are often coded in 3 parts named: Pre-processor, solver and post-processor.

a) Pre-processor

The necessary parameters of numerical solution are fully set up in this stage in order to serve for the next part - solver. The parameters include computational domain, mesh generation, physical model characteristics, fluid properties and boundary conditions. Each one plays an important role in getting the best solution with respect to the accuracy of simulation.

- Computational domain is the region of fluid to be modeled in numerical simulation to capture the properties of flow. Depending on each specific case, the shape and size of computational domain are rationally decided to ensure the accuracy of the outcomes. The small size one can save the cost of computational time and vice versa. The experiences of previous researches in domain selection should be carefully referenced to have suitable decision.

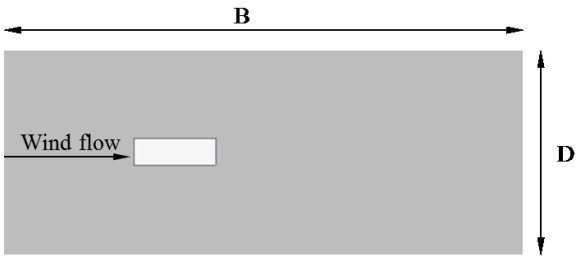

Figure 3.1. Computational domain with rectangular shape

- Mesh system is the network of discrete elements assigned into the computational domain to discretize the governing equations. The mesh or gridlines is defined as the discrete locations at which the unknown variables are determined. Mesh generation can mostly dominate the reliability of numerical simulation in CFD. There are 3 kinds of mesh [44]: Structured mesh, block-structured mesh and unstructured mesh, as Figure 3.2. The structured mesh is the simplest one and it

suits to the bodies having the simple shape and sharp edges. The unstructured mesh is used in case of the bodies with complex geometries, and it is suitable to the finite volume method.

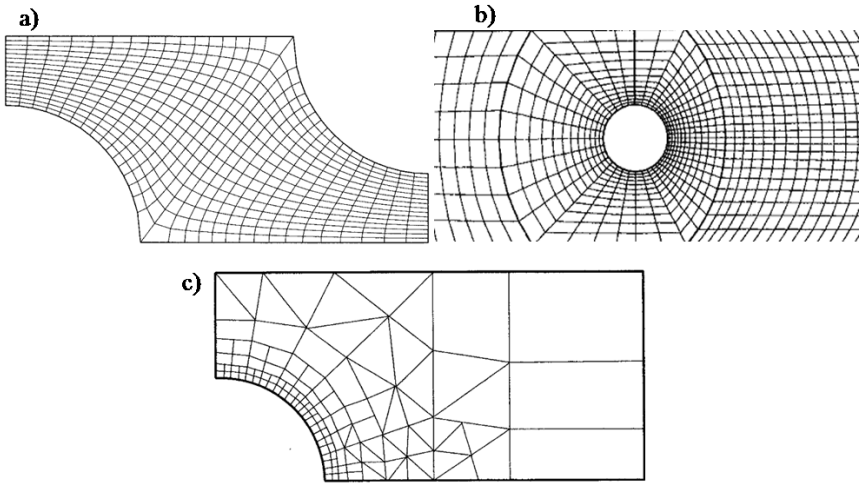

Figure 3.2. Typical mesh: a) Structured, b) Block-Structured, c) Unstructured [44]

- Physical models and fluid properties need to be assigned in the computational domain, because these ones are mathematical and physical basics used to compute the characteristic of fluid flow over space and time. Physical models should be carefully considered in order to correctly simulate the behavior of fluid flow, especially in the turbulent areas.
- Boundary conditions are the known variable values of some boundary points at initial time. The solution of numerical simulations will not be found without the boundary conditions which are given in advance. Several boundary conditions for the discretization equations should be paid attention: Inlet and outlet boundary conditions (stipulating the entering and exiting characteristics of flow: velocity, pressure or mass), wall boundary condition (set up at the interface of flow and bodies), pressure boundary condition (used in case of external flows around objects, free surface flows, or internal flows with multiple outlets), symmetry boundary condition (no flow across the boundary), and periodic boundary condition (applied as the physical geometry and the pattern of flow repeat periodically).

b) Solver

This is a crucial part in CFD procedure. All properties of fluid flow are calculated in solver through the translation of the governing equations into a numerical analogue. The finite difference, finite element and finite volume methods are major approaches to iteratively compute the flow parameters. In solver, the requirement of convergence in numerical simulation must be ensured.

c) Post-processor

The results obtained from solver will be systematically organized in this part. In post-processor, numerical outcomes and flow visualization are available. The quantitative estimation of flow properties can be easily reckoned. In current CFD technology, it is not hard to make vector or contour plots to describe the behavior of velocity field, pressure, energy…

3.2.2. Discretization

Discretization can be defined as the process of transforming the continuous fluid flow into discrete numerical data. In essence of discretization, the closed-form mathematical expression (function, differential and integral equations) of continuous fluid flow will be approximated by analogous expression under a finite number of discrete points or volumes in the computational domain. Normally, discretization is carried out in solving fluid flow problems with three parts including equation, space and time.

In spatial discretization, the computational domain is split sub-parts which are composed from the mesh. All meshes in numerical simulation contain a variety of nodes at which the parameters of flow are resolved. The category of mesh system was mentioned above in pre-processor part.

In time discretization, the time steps are decided to divide the temporal process during solving the fluid flow. In the time-dependent governing equations, discretization progression leads to an equation system comprising unknown variables at a given time as a function of the variables of the previous time step. Explicit and implicit approaches are applied to calculate the unsteady time-dependent equations [43]. An explicit way will solve each equation containing only one unknown at a certain time from the previous known time straightforwardly, Figure 3.3a. An implicit one will solve a equation system simultaneously at

all the grid points arrayed at a given time level, Figure 3.3b. Hence, the implicit approach involves a more complex set of calculations than the explicit approach.

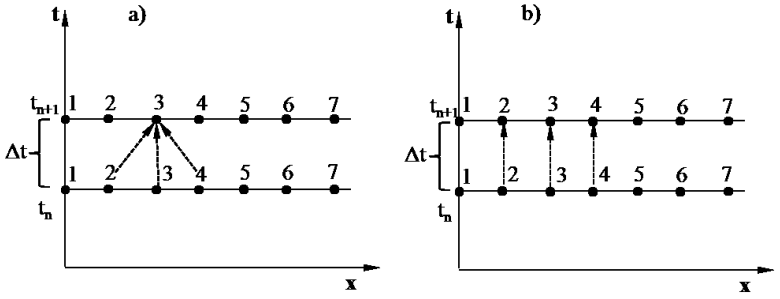

Figure 3.3. Explicit (a) and implicit (b) approaches [43]

In terms of equation discretization, there are three main techniques can be used: the finite difference method (FDM), the finite element method (FEM) and the finite volume method (FVM).

- FDM: It is believed that FDM has been introduced in the 18th century by Euler and it is also considered as the oldest method for numerical solution of partial differential equations [44]. The FDM uses Taylor series expansion and polynomial fitting to solve the first and second derivatives of the variables in the governing equations of fluid flow. At each grid point in the computational domain, the governing equations under the conservation differential form are approximated by a simultaneous algebraic equations system. It is estimated that the FDM leads to the high effective on structured grids, but not appropriate to the complex geometry.
- FEM: on the contrary to FDM, the FEM uses the starting point with conservation form in an integral formulation, instead of basing on the differential one. The computational domain is broken into a finite number of elements, and each element contains a certain number of nodes where the numerical values of variables are resolved. It seems to be suitable to unstructured grid system. The FEM has a distinguishing feature needed to be considered that a weight function multiplied to the equations before integrating over the entire domain. It is believed that arbitrary geometries cannot cause any difficulty for FEM. However, it requires a higher capacity of computer to deal with the problems rather than FDM.

- FVM: The FVM and FEM have the same strategy of discretization. The computational domain is discretized into a finite number of contiguous control volumes. Then, the governing equations are iteratively solved on each control volume by means of the integral formulations. The value of variables will be computed at the center of the control volumes which is known as computational nodes. In addition, the value of variables at the control volume surface will be interpolated through the values at the center. The FVM can be applied to the structured mesh system or unstructured mesh system, especially in case of complex geometries. Because of taking direct integration, it tends to be easier to code the program in CFD procedure. Hence, the FVM has been recently developed in CFD technology. Yet, the order higher than second in the equations causes the difficulty for applying in three dimension simulations.

3.3. Turbulence models

Depending on the Reynolds number, the flow can be classified into two types: the laminar flow with the low Reynolds number and the turbulent flow with the high Reynolds number. In engineering practice, the turbulent flow often attracts the scientist's attention to study and manage, because most of flows are turbulent in nature. The complication of turbulence can be observed through the random variation in space and time, in the sense that the appearance of various eddies with a large range of length and time scales. Irregularity, three dimensionality and sophisticated dissipation are typical characteristics that found in the turbulent flow. Generally, the exchange process of energy and the transfer of momentum in the flow are implemented by means of large scale eddies. Meanwhile, the energy is dissipated at smaller scale eddies through the viscosity of flow.

Normally, the primary examination of turbulence has been conducted in experiments. On the other hand, numerical methods have been recently used to support to the sophisticated experiment. In order to numerically deal with the turbulence of flow, there are some different approaches corresponding to the complex of issue and the required accuracy. The followings introduce three categories in turn of reducing the cost of computational time as well as the accuracy of numerical results: Direct Numerical Simulation (DNS), Large Eddy Simulation (LES) and Reynolds Averaged Navier-Stokes (RANS). In there, the RANS

approach is presented in more detail than the others, because it will be applied to solve all the problems related to this thesis.

3.3.1. Direct Numerical Simulation (DNS)

As mentioned by Ferziger H. and Peric M. [44], DNS is the most accurate and simplest method to deal with the turbulence of flow. In DNS approach, the Navier-Stokes equations are solved without taking the average or approximation. It can compute all the significant scales of motion in the flow until the Kolmogorov scales where the energy dissipation occurs. To capture all of the significant structures of the turbulence, the computational domain must be at least equals to the physical domain or the largest turbulent eddy.

DNS has resulted in the very high accuracy. Hence, it has been often applied in cases of the severe requirement in numerical simulations, such as fundamental researches in the turbulence of flow. However, it showed that the computational time cost is the largest disadvantage of DNS and the application seems to be not feasible with the high Reynolds number.

3.3.2. Large Eddy Simulation (LES)

LES approach accepts the concept that settling the large eddies of turbulent flow is more exactly than solving the small ones. It takes into account the vital role of the large eddies in transferring energy and momentum in the flow. The LES is much less expensive than the DNS mentioned above, even though it is three dimensional, time dependent. The priority of using LES rather than DNS can be found in the flows in which the Reynolds number is very high or the geometry is too complex.

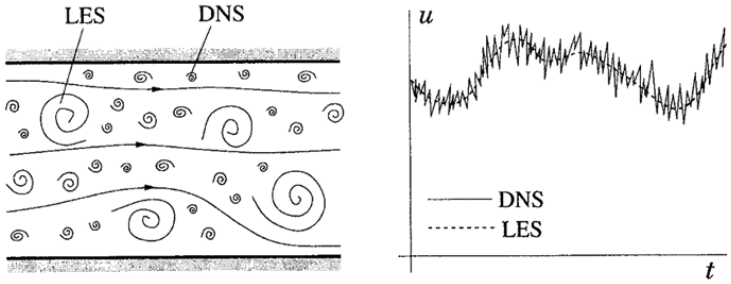

Figure 3.4. Model of turbulence motion and time dependence of a velocity [44]

A filter function is proposed to classify the large eddy scale and the small eddy scale in simulations. In there, all eddies larger than the filter width which is introduced by a length scale Δ are resolved directly. Then, the other smaller eddies are modeled approximately. After filtering the Navier-Stokes equations, a set of equations, having the terms of the subgrid-scale (SGS) Reynolds stresses τ_{ij}, will be obtained. Ordinarily, Smagorinsky model (through the eddy viscosity basing on the well-known Boussinesq hypothesis) is used to estimate SGS stresses.

3.3.3. Reynolds Averaged Navier-Stokes (RANS)

RANS has been usually applied in practical engineering because it can reduce a vast of time for calculation. This advantage is achieved from the simple approach to cope with the turbulence that all of the unsteadiness is averaged out. Substituting the averaged quantities into the Navier-Stokes equations leads to the RANS equations. Some new terms arising in the equations cause an unclosed form. These ones must be modeled to find out the solution.

Mathematically, every variable in the flow can be separated into two parts including an averaged value and a fluctuation value [44]:

$$\emptyset(x_i, t) = \overline{\emptyset}(x_i) + \emptyset'(x_i, t) \tag{3.5}$$

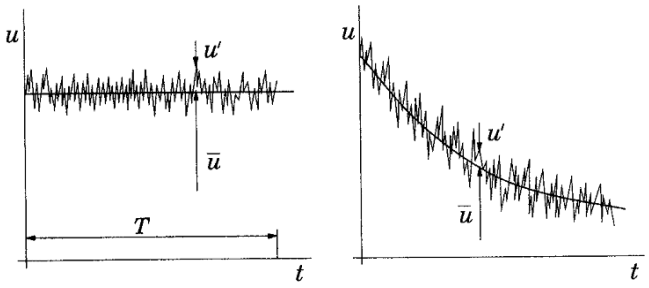

Figure 3.5. Time average in cases of steady and unsteady flow [44]

Depending upon whether a statistically steady flow or unsteady flow, the averaged value can be expressed as the time-average quantity (3.6) or the ensemble quantity (3.7):

$$\overline{\emptyset}(x_i) = \lim_{T\to\infty} \frac{1}{T} \int_0^T \emptyset(x_i, t)dt \tag{3.6}$$

$$\overline{\emptyset}(x_i) = \lim_{N\to\infty} \frac{1}{N} \sum_{n=1}^{N} \emptyset(x_i, t) \tag{3.7}$$

where:

T is the averaging interval;

N is the number of elements of the ensemble.

The value of T has to be large enough in comparison to the typical time scale of the fluctuations. The values of N must be large enough to get rid of the effects of the fluctuations.

In terms of incompressible flows without any body forces, the RANS equations can be written in Cartesian coordinates as follows:

$$\frac{\partial(\rho\bar{u}_i)}{\partial x_i} = 0 \tag{3.8}$$

$$\frac{\partial(\rho\bar{u}_i)}{\partial t} + \frac{\partial}{\partial x_j}\left(\rho\bar{u}_i\bar{u}_j + \rho\overline{u_i'u_j'}\right) = -\frac{\partial\bar{p}}{\partial x_i} + \frac{\partial\bar{\tau}_{ij}}{\partial x_j} \tag{3.9}$$

where:

u_i are another writing form of the components of velocity u, v, w;

$\bar{u}_i$ is the time-averaged of u_i;

$\bar{\tau}_{ij}$ are the mean viscous stress tensor components.

$$\bar{\tau}_{ij} = \mu\left(\frac{\partial\bar{u}_i}{\partial x_j} + \frac{\partial\bar{u}_j}{\partial x_i}\right) \tag{3.10}$$

In Equation (3.9), the arising terms $\rho\overline{u_i'u_j'}$ are named the Reynolds stresses, which are the correlation between the fluctuations of velocity components. An unclosed equation system is the consequence of the existence of the Reynolds stresses. Hence, the approximations of turbulence models need to be carried out to close the RANS equations.

In RANS approach, two models $k-\varepsilon$ and $k-\omega$ basing on the Boussinesq hypothesis have been widely used to tackle the turbulence. These models reach the solution by

considering the effect of the transport of turbulence quantities as the transfer of energy in the flow. Furthermore, a second transport equation is also proposed to support the energy transport equation. Therefore, the $k-\varepsilon$ and $k-\omega$ models are termed by another name which is the two equations models.

a) $k-\varepsilon$ turbulence model

- The principle used to derive the $k-\varepsilon$ model is that the rates of production and destruction of turbulence are in near-balance. The dissipation ε, the kinetic energy k, the length scale L and the eddy viscosity μ_t have the relationships as follows:

$$\varepsilon = \frac{k^{3/2}}{L} \tag{3.11}$$

$$\mu_t = \rho C_\mu \sqrt{k} L = \rho C_\mu \frac{k^2}{\varepsilon} \tag{3.12}$$

where C_μ is an empirical constant.

- By using the above relationships, the transport equation for turbulence kinetic energy k is depicted as following:

$$\frac{\partial(\rho k)}{\partial t} + \frac{\partial(\rho \bar{u}_j k)}{\partial x_j} = P_k - \rho\varepsilon + \frac{\partial}{\partial x_j}\left(\frac{\mu_t}{\sigma_k}\frac{\partial k}{\partial x_j}\right) \tag{3.13}$$

- Similarly, the transport equation for dissipation of turbulence kinetic energy ε is written as following:

$$\frac{\partial(\rho\varepsilon)}{\partial t} + \frac{\partial(\rho \bar{u}_j \varepsilon)}{\partial x_j} = C_{\varepsilon 1} P_k \frac{\varepsilon}{k} - \rho C_{\varepsilon 2} \frac{\varepsilon^2}{k} + \frac{\partial}{\partial x_j}\left(\frac{\mu_t}{\sigma_\varepsilon}\frac{\partial \varepsilon}{\partial x_j}\right) \tag{3.14}$$

- P_k is the production term of turbulence kinetic energy and can be given by:

$$P_k = C_\mu \frac{k^2}{\varepsilon}\frac{1}{2}\left(\frac{\partial \bar{u}_i}{\partial x_j} + \frac{\partial \bar{u}_j}{\partial x_i}\right)^2 \tag{3.15}$$

- The other empirical constants are taken as follows:

$$C_\mu = 0.09;\ C_{\varepsilon 1} = 1.44;\ C_{\varepsilon 2} = 1.92;\ \sigma_k = 1.00;\ \sigma_\varepsilon = 1.30 \tag{3.16}$$

- The $\mathrm{k}-\varepsilon$ model is one of the earliest two-equation models. In the free stream, it can give the high accuracy with the small computational time. However, the $\mathrm{k}-\varepsilon$ model often leads to the over-prediction of turbulence near at stagnation region and the length scale is too large in adverse pressure gradient flow.

b) $k-\omega$ turbulence model

- The $\mathrm{k}-\omega$ model was developed by Wilcox (1993) [46] to overcome the disadvantages of the $\mathrm{k}-\varepsilon$ model at the boundary layer area. In this model, the turbulence frequency $\omega = {}^{\varepsilon}/_{\mathrm{k}}$ is used as the variable of equations. The length scale L and the eddy viscosity μ_t are given as follows:

$$L = \frac{\sqrt{k}}{\omega} \tag{3.17}$$

$$\mu_t = \rho \frac{k}{\omega} \tag{3.18}$$

- The transport equation for turbulence kinetic energy k is written as:

$$\frac{\partial(\rho k)}{\partial t} + \frac{\partial(\rho \bar{u}_j k)}{\partial x_j} = P_k - \rho\beta^* k\omega + \frac{\partial}{\partial x_j}\left(\frac{\mu_t}{\sigma_k}\frac{\partial k}{\partial x_j}\right) \tag{3.19}$$

- The ω equation is given by Wilcox as:

$$\frac{\partial(\rho\omega)}{\partial t} + \frac{\partial(\rho \bar{u}_j \omega)}{\partial x_j} = \alpha\frac{\omega}{k}P_k - \rho\beta\omega^2 + \frac{\partial}{\partial x_j}\left(\frac{\mu_t}{\sigma_\omega}\frac{\partial \omega}{\partial x_j}\right) \tag{3.20}$$

- The other empirical constants in this model are chosen as follows:

$$\alpha = \frac{5}{9};\ \beta = 0.075;\ \beta^* = 0.09;\ \sigma_k = \sigma_\omega = 2;\ \varepsilon = \beta^* k\omega \tag{3.21}$$

- The $\mathrm{k} - \omega$ model is better than the $\mathrm{k} - \varepsilon$ model in solving the flow near wall. It is directly resolved with the integration of the ω equation. However, it is estimated that the $\mathrm{k} - \omega$ model over predicted the spreading rates at the free shear layer.

On the other hand, the Reynolds Stress model (RMS) is known as an alternative approach. In this model, the anisotropic features of turbulence are concerned to predict more exactly the behavior of turbulence. The known averaged quantities of flow are used to describe the Reynolds stresses in the governing equations. The effects of the dynamics of turbulence are also taken into account during modelling the turbulence. Then, those equations will be combined with the Navier-Stokes equations to figure out the solution. This approach has the high accuracy, but it cost a lot of computational time in comparison to the two equations models.

3.4. New eddy viscosity turbulence model

In terms of solving the turbulence issue in CFD, there are many resorts mentioned above, such as using DNS, LES and RANS. The two first ones are more exact but an intensive memory and an expensive processing time are required. The latter has resulted in the satisfactory outcomes of aerodynamic prediction in various applications. Some previous researches showed that the RANS approach in combination with the conventional standard $k - \varepsilon$ could not lead to the accurate results for rectangular shape cylinders [47], [48]. This is known as a defect of the conventional standard $k - \varepsilon$ model due to the excessive amount of turbulent kinetic energy is generated near the frontal edges of objects [49]. A modified $k - \varepsilon$ model [50] , in which production of turbulent kinetic energy is formulated with a vorticity tensor and a velocity strain tensor, was proposed to eliminate the above disadvantage. Some researches were successful in prediction of aerodynamic characteristics to a variety of side-ratios of rectangular shape with the modified $k - \varepsilon$ model [51], [52].

On the other hand, a new $k - \varepsilon$ eddy viscosity model, which consists of a new model dissipation rate equation and a new realizable eddy viscosity formulation, was proposed to

improve the conventional standard $k-\varepsilon$ model in cases of high Reynolds number [53]. The new dissipation rate equation was derived from the dynamic equation of the mean-square vorticity fluctuation at large turbulent Reynolds number. The new eddy viscosity was calculated on the realizable constraints, the positivity of normal Reynolds stresses and Schwarz inequality for turbulent shear stresses. The new $k-\varepsilon$ eddy viscosity model can perform very well for a variety of flows, such as rotating homogeneous shear flows, boundary-free shear flows, channel flows, flat plate boundary layers flows and backward facing step separated flows [53].

In the new $k-\varepsilon$ eddy viscosity model, the transport equation for turbulent kinetic energy k is not different from Equation (3.13) used in the standard $k-\varepsilon$ model. However, the new dissipation rate equation was derived from the dynamic equation of the mean-square vorticity fluctuation at large turbulence Reynolds number as :

$$\frac{\partial(\rho\varepsilon)}{\partial t}+\frac{\partial(\rho\bar{u}_j\varepsilon)}{\partial x_j}=\rho C_1 S\varepsilon-\rho C_2\frac{\varepsilon^2}{k+\sqrt{\frac{\mu}{\rho}\varepsilon}}+\frac{\partial}{\partial x_j}\left(\frac{\mu_t}{\sigma_\varepsilon}\frac{\partial\varepsilon}{\partial x_j}\right) \tag{3.22}$$

In Equation (3.22),

$$S=\sqrt{2S_{ij}S_{ij}} \tag{3.23}$$

$$S_{ij}=\frac{1}{2}\left(\frac{\partial\bar{u}_i}{\partial x_j}+\frac{\partial\bar{u}_j}{\partial x_i}\right) \tag{3.24}$$

The standard eddy viscosity formulation for incompressible turbulence is calculated as Equation (3.12) with the value of $C_\mu=0.09$. It becomes non-realizable in the case of large mean strain rate. The new eddy viscosity in this model was proposed to ensure the realizability that the model coefficient C_μ must not be a constant and should be based on the mean strain rate:

$$C_\mu=\frac{1}{A_0+A_sU^*\frac{k}{\varepsilon}} \tag{3.25}$$

In Equation (3.25), the parameter U^* is determined by:

$$U^* = \sqrt{S_{ij}S_{ij} + \bar{\Omega}_{ij}\bar{\Omega}_{ij}} \tag{3.26}$$

$$\bar{\Omega}_{ij} = \Omega_{ij} - 2\varepsilon_{ijk}\omega_k \tag{3.27}$$

$$\Omega_{ij} = \frac{1}{2}\left(\frac{\partial \bar{u}_i}{\partial x_j} - \frac{\partial \bar{u}_j}{\partial x_i}\right) \tag{3.28}$$

where:

Ω_{ij} are the averaged vorticities;

$\bar{\Omega}_{ij}$ are the averaged rotation rates;

ε_{ijk} is the Levi-Civita symbol;

ω_k is the angular velocity;

In Equation (3.25), the parameter A_s is determined by:

$$\begin{gathered} A_s = \sqrt{6}cos\theta; \theta = \arccos\left(\sqrt{6}W\right); \\ W = \frac{S_{ij}S_{jk}S_{ki}}{\bar{S}^3}; \bar{S} = \sqrt{S_{ij}S_{ij}} \end{gathered} \tag{3.29}$$

In the new $k-\varepsilon$ eddy viscosity model, the other coefficients are set as follows:

$$\begin{gathered} C_1 = max\left\{0.43, \frac{\eta}{5+\eta}\right\};\ \eta = \frac{Sk}{\varepsilon}; \\ \sigma_k = 1.00;\ \sigma_\varepsilon = 1.30; C_2 = 1.90; A_0 = 4.0 \end{gathered} \tag{3.30}$$

3.5. Summary of Chapter 3

By the purpose of providing basic aspects to comprehensively access the next chapters, Chapter 3 presents the background theory of CFD the mathematic methods used in numerical simulations. The first important content related to the governing equations of fluid flow is

provided in Section 3.1. The fundamental principle used to derive the equations and methods for solving the equations can be referred in this section. The second vital content is carefully composed in Section 3.2 to clarify the significance, function and role of CFD. The basic procedures in CFD simulation such as pre-processor, solver and post processor are outlined as a sub-division of the section. In addition, the discretization from physical field to computational domain is clearly mentioned in another sub-division. Turbulent models applied in CFD simulations are quite crucial to obtain the accurate results. These models are introduced in Section 3.3 and 3.4 as the third important content of the chapter. The concepts of DNS, LES and RANS are defined. Section 3.4 is intentionally divided as a separated section to determine the advantage of the new $k-\varepsilon$ eddy viscosity turbulent model, which is used to examine all simulations in the thesis.

Chapter 4: COLLECTION OF EXPERIMENTAL DATA

4.1. Introduction

The exactly quantitative information of evaluation the impact of wind on bridge structures can be provided by wind tunnel test (WTT). It has been demonstrated that WTT leads to the reliable results in examining the unsteady aerodynamic phenomena such as SEV, VIV and BV. It is considered as a very important procedure in wind resistant design to investigate the wind-induced forces and response of bridges. The static aerodynamic coefficients of objects, the amplitude of vibrations and the critical velocity of vibrations are major quantities obtained from WTT. In the past decades, a variety of experimental works in WTT were devoted by various authors. The precious and significant researches in wind-bridge engineering have been made by that way. In many cases, however, WTT only can accommodate us with the characteristics of oscillations without the flow mechanism around the objects. Hence, the combination between CFD and WTT has been expected in supporting each other.

This chapter supplies the next chapters with the confirmation data of the validation of numerical simulations. Firstly, some basic concepts regarding WTT procedure are introduced. Then, the well-known experimental results of aerodynamic characteristics of rectangular cylinders in the study of Nakaguchi et al. [32] are mentioned. Next, the experimental results of the Shin-minato Bridge conducted by Katsuchi et al. [7], [8], directly related to this study, are presented so as to not only ensure the validation of numerical simulations but also illustrate the effect of flap countermeasure.

4.1.1. Wind tunnel test procedure

According to Wind Resistant Design of Bridges in Japan [12], WTT can be divided into two different types. The first type is often implemented to examine the bridge model responses (including section model tests, taut strip model tests and full bridge model tests). The second type is often conducted to inspect the aerodynamic force characteristics acting on the bridge model (including static the three components measurement and the unsteady force measurement). The classification of WTT is manifested in Table 4.1.

Table 4.1. Classification of wind tunnel tests [12]

No	Type	Characteristic		Note
1	Response measurement	Modelling the actual structures:	Full bridge model test	
		Modelling by the modified structures:	Section model test	
			Taut strip model test	
2	Aerodynamic force measurement	3-component measurement test		
		Unsteady aerodynamic force measurement test		

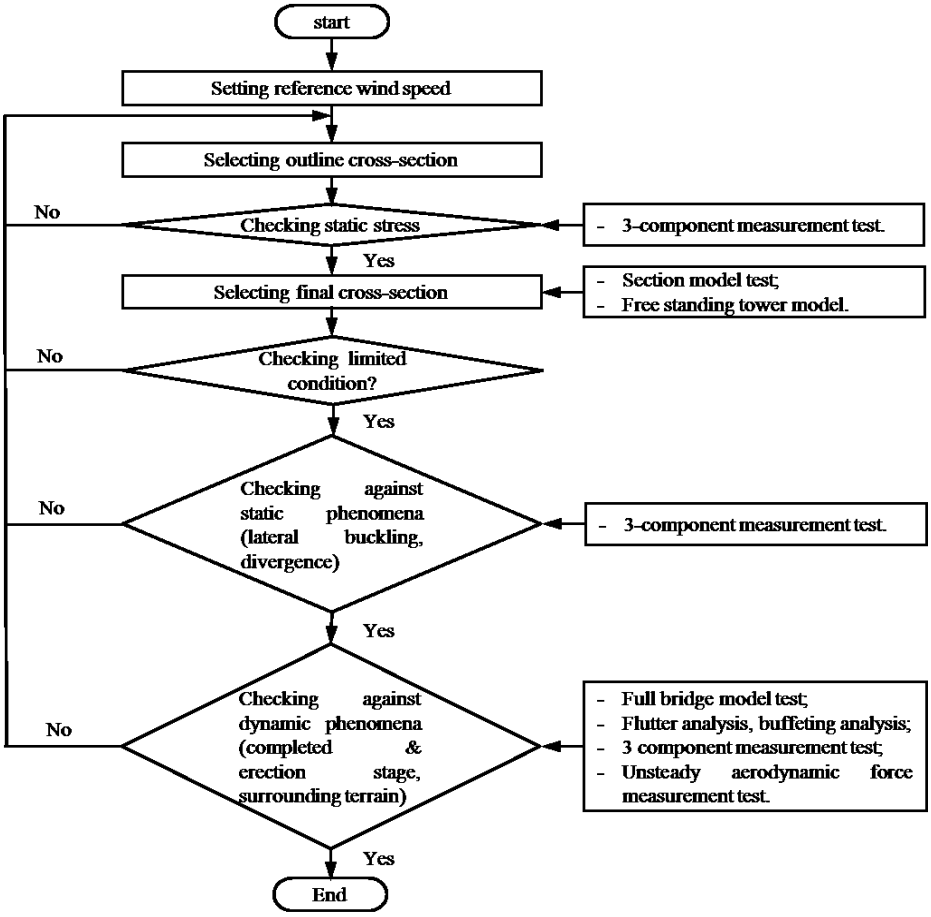

Figure 4.1. Wind tunnel tests in wind resistant design procedure [12]

Depending on the purpose of the investigation and the importance of projects, the relevant type of WTT is decided to carry out. The general procedure can be found in Figure 4.1. The influence of natural turbulence in wind flow with the required turbulence intensity is made by grid system in wind tunnel. Normally, smooth wind with small turbulence is flowed to investigate the common wind-induced vibrations. In cases of static analyses such as stress

and buffeting analysis, the aerodynamic force coefficients measured in three-component tests, such as the drag, lift and moment force coefficients, are used to evaluate the impact of wind action. On the other hand, in cases of flutter analyses or a detailed study, the unsteady aerodynamic force coefficients obtained from WTT with forced vibration tests or free vibration tests, are taken into account in order to derive the flutter derivatives.

4.1.2. Similarity law

The similarity law of the full-scale structure and the model-scale structure must be satisfied in WTT. The wind flow around the model should be similar to the wind flow around the prototype. Generally, there are five crucial dimensionless parameters need to be ensured: viscous parameter (Reynolds' model law), gravity parameter (Froude's model law), elastic parameter, damping parameter and wind velocity parameter.

a) Viscous parameter

The viscous parameter is the Reynolds number which is defined as the ration between the inertia forces and viscous forces acting on the flow.

$$Re = UL/\vartheta \tag{4.1}$$

where U is the wind velocity, L is the characteristic length and $\vartheta = \mu/\rho$ is the kinematic viscosity.

The drag force coefficient, C_D, depends on the Reynolds number so much in case of the body having a curved surface. However, it is not repeated in case of the body having sharp edges. Therefore, the Reynolds' law has no meaning when examining the sharp edge bodies. Normally, the atmospheric pressure and the kinematic viscosity in wind tunnel have the same value as in the actual conditions of the prototype. In curved surface bodies, the Reynolds number is satisfied by modifying the velocity scale.

b) Gravity parameter

The gravity parameter is the Froude number which is defined as the ration between the inertia forces and the gravity forces on the structure.

$$Fr = U^2/gL \tag{4.2}$$

where g is the acceleration of gravity.

If the gravity forces control the wind-induced vibrations, then the Froude's law has to be satisfied. It is necessary to set up the same Froude number in the model and the prototype. This condition can be is expressed by the Equation (4.3):

$$\frac{U_m}{U_p} = \sqrt{\frac{L_m}{L_p}} = \sqrt{\frac{1}{n}} \tag{4.3}$$

where the sub-indexes m, p indicate the relevant properties in the model and the prototype, $n = L_p/L_m$ is the ration between the representative length of full-scale and model-scale.

c) Elastic parameter

The elastic parameter can be determined from the ratio $E/\rho U^2$. In this ratio, E is the modulus of structure immerged in the wind flow. The similarity law needs to be fulfilled in this parameter and this condition can be expressed as followings:

$$\begin{aligned} &\frac{E_m}{\rho U_m^2} = \frac{E_p}{\rho U_p^2}; \\ &\frac{E_m}{E_p} = \frac{U_m^2}{U_p^2} = \frac{1}{n} \end{aligned} \tag{4.4}$$

where E_m, E_p are the elastic modules for model-scale structure and full-scale structure.

d) Damping parameter

It is important to set up the similarity law in the damping parameter of the model-scale structure and the full-scale structure.

e) Wind velocity parameter

The reduced velocity U_{re} needs to be satisfied in the similarity law as the Equation (4.5) or (4.6). This scaling also follows from the similarity requirement of Strouhal number in the model of WTT and the full-scale structure.

$$(U_{re})_m = (U_{re})_p;$$
$$\frac{U_m}{f_m L_m} = \frac{U_p}{f_p L_p} \tag{4.5}$$

This condition can be expressed by the frequency relationship:

$$\frac{f_m}{f_p} = \frac{U_m L_p}{U_p L_m} = \sqrt{n} \tag{4.6}$$

where f_m, f_p are the vibration frequency of model-scale structure and full-scale structure.

4.2. Rectangular cylinders

In order to ensure the validation of numerical simulations in this study, the comparison between the results obtained from numerical simulations and the results obtained from experiments in WTT need to be made sense. Rectangular cylinders, with the width-to-depth ratios that is close to the width-to-depth ratios of box girder sections used in long span bridges, are basic benchmark cases should be taken into account to confirm the main numerical schemes and analysis parameters. The most well-known experimental study on aerodynamic characteristics of rectangular cross-section series devoted by Nakaguchi et al. in 1968 should be considered.

This section introduces Nakaguchi et al.'s study conducted so as to investigate the drag force coefficient and the Strouhal number of rectangular cylinders in the Reynolds number ranges up to 6.10^4 [32]. It was implemented in smooth flow to examine the flow pattern around the objects. The results are mentioned in Figure 4.2, Figure 4.3 and Figure 4.4.

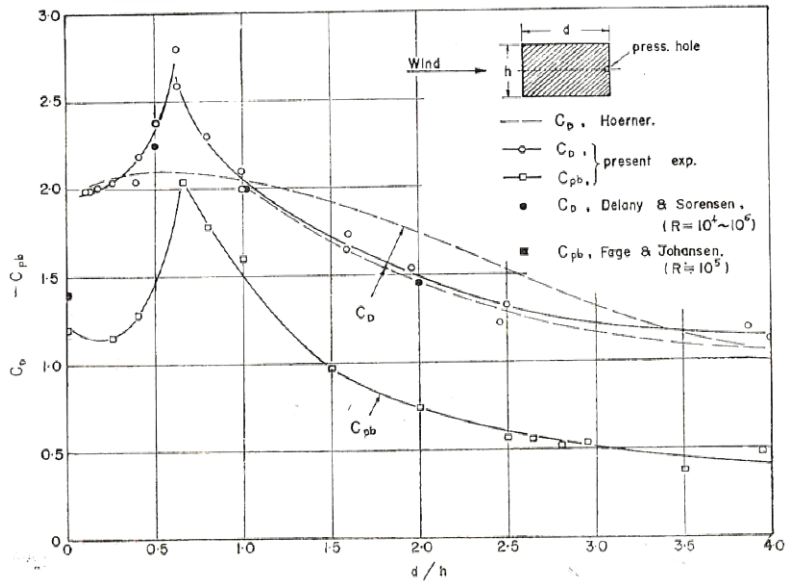

Figure 4.2. Drag force coefficient of rectangular cylinders [32]

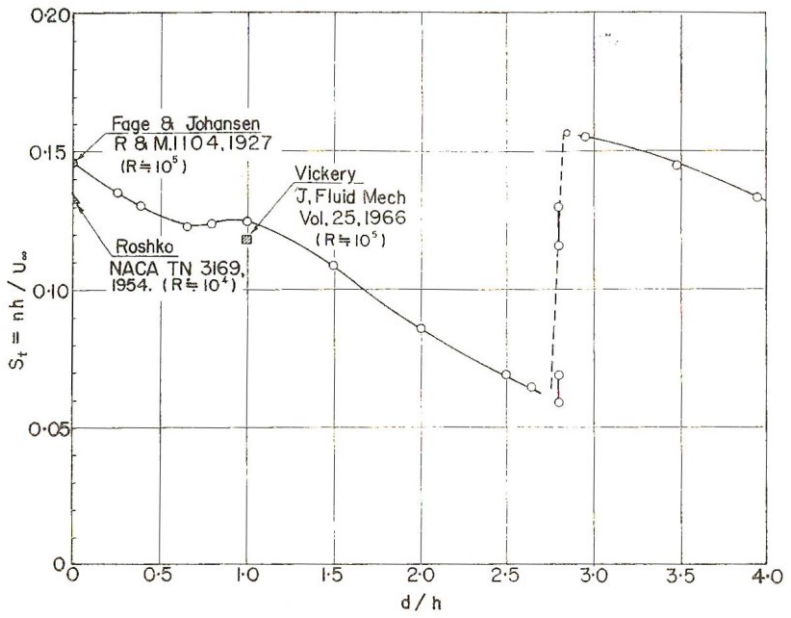

Figure 4.3. Strouhal number of rectangular cylinders [32]

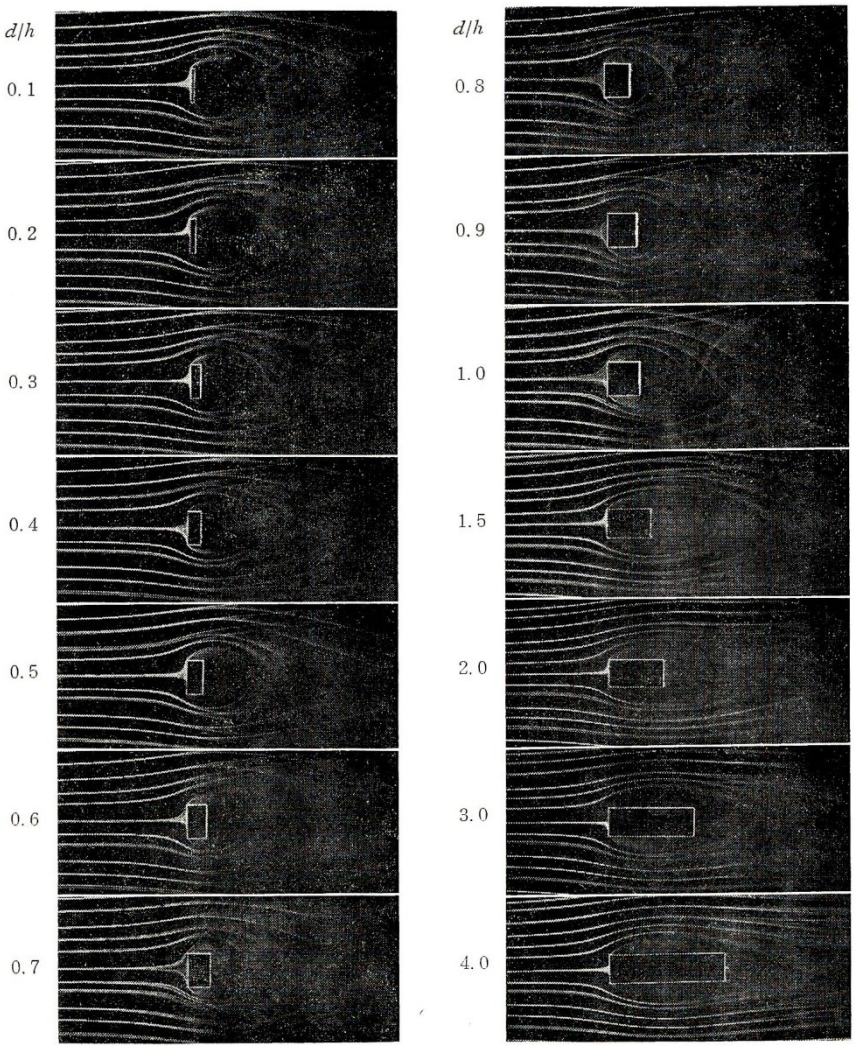

Figure 4.4. Flow pattern around rectangular cylinders [32]

It is revealed that there has been the existence of a peak in the drag coefficient C_D at the ratio of 0.6 and the maximum value C_D around 2.0 occurred at the ratio of flat plate and the square cylinder. In terms of the Strouhal number of the shedding vortices at the leeward, on the contrary, the study showed that it approximately remains constant with every ratio, but it dramatically rises at the ratio of 2.8. At the ratio of 2.8, it also found that the flow reattaches on the lateral surfaces of the cylinder. In flow pattern, the study clarified the aerodynamic behavior of the bodies through the absence or presence of reattachment phenomenon at the shear layer (with three categories: separated, intermittently reattached and fully reattached flow).

4.3. Box girder of the Shin-minato Bridge

The main object of the thesis is concentrated on the effect of flap countermeasure attached to box girder. The significance of flap used to suppress VIV of the Shin-minato bridge was experimentally reported by Katsuchi et al. in 2013 [7]. Therefore, it is concerned as the essential evidence to estimating the results achieved from numerical study. However, its meaning does not cease at the confirmation of the validation of numerical simulations. It can effectively support to the numerical investigation to figure out the mechanism of the wind flow around box section in the presence of flap countermeasure. By that purposes, this section is organized as a kernel part to provide the necessary information related to the investigation in WTT. It is noted that all the information is cited from Katsuchi et al. [7].

4.3.1. Overview

The shin-minato Bridge located near Toyama port is a cable-stayed bridge with 5 continuous spans (60+60+360+60+60) m, Figure 4.5. A steel box girder was selected at the center span of 360 m and a PC box girder was chosen at each side span of 120 m. The width and the depth of girder section are 15 m and 4.5 m, respectively, Figure 4.6 . At design stage, the WTT was conducted to decide the geometry of the box girder in considering VIV as well as SEVs with/without side barrier blockade. A deep box girder section with triangular-shape faring and without installing aerodynamic countermeasure was final solution used. After the competition of the center span, however, VIV with large vibration amplitude was observed at the mean wind speed of 10-15 m/s normal to the direction of the bridge axis. The large vibration amplitude reached 35 cm with the natural frequency of 0.45 Hz corresponding to the vertical direction, Figure 4.7. Hence, it was necessary to reproduce a WTT at that time to find countermeasure for suppressing the oscillation. The WTT was implemented at Yokohama National University by Katsuchi et al. in 2013 [7].

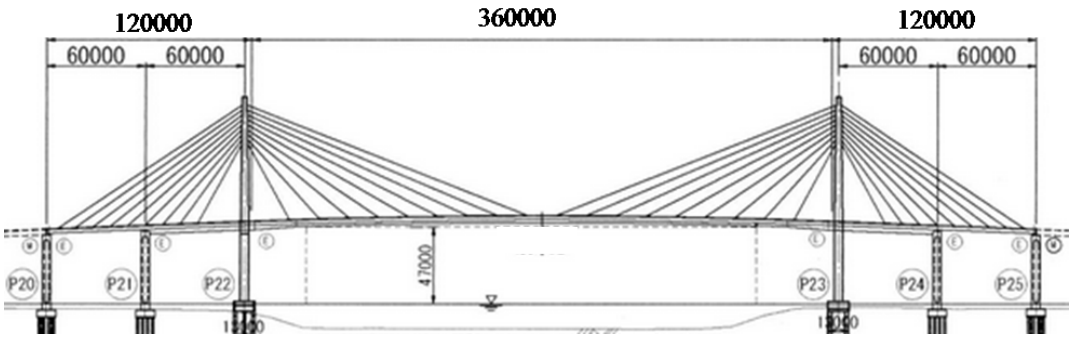

Figure 4.5. General view of the Shin-minato Bridge [7]

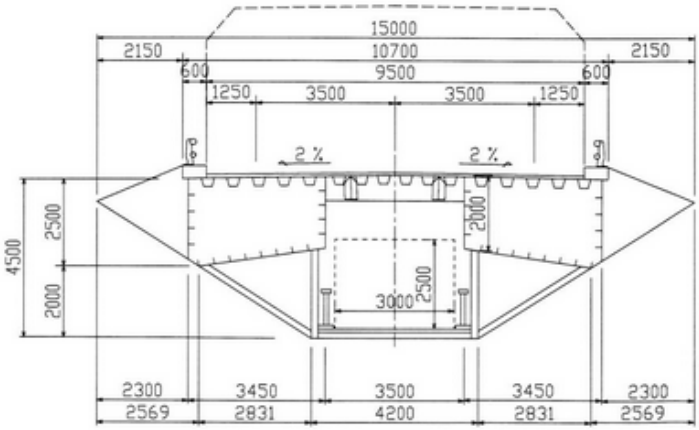

Figure 4.6. Cross-section of the center span of the Shin-minato Bridge [7]

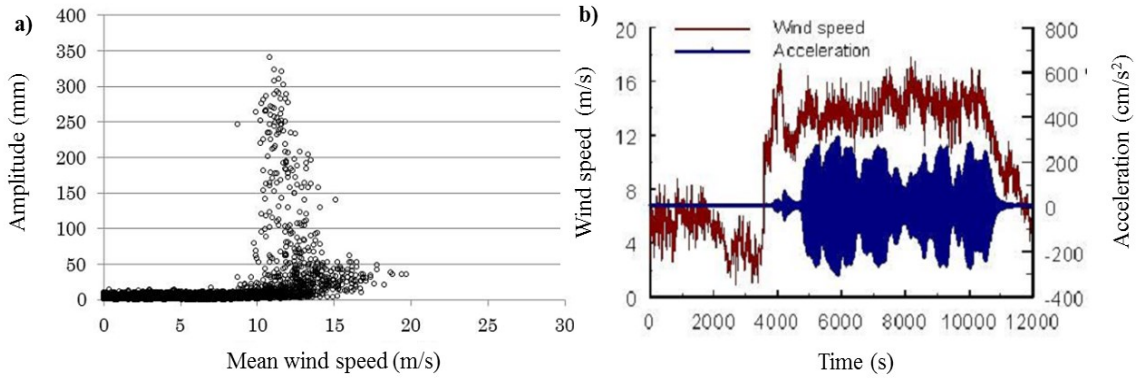

Figure 4.7. VIV vibration: a) amplitude vibration and b) time history of deck acceleration [7]

4.3.2. Wind tunnel test

The test was carried out in a smooth flow with the scale of 1/50 in a wind tunnel 1.8x1.8 m. The same scale was chosen in order to resemble with the previous test at the design stage, in the sense that a spring supported section model was examined, Figure 4.8 . The test conditions are summarized in Table 4.2. The basic girder without aerodynamic countermeasure was inspected to confirm the occurrence of VIV which is observed at the full-scale bridge. Then, many kinds of flap and bottom plate were installed in the test to examine the solutions for suppressing the oscillations.

Table 4.2. Test conditions in WTT [7]

Quantity		Full Scale	Model requirement	Model measurement	Note
Girder width B (m)		15	0.3	0.3	
Girder height D (m)		4.5	0.09	0.09	
Mass m (kg/m)		12.15×10^3	4.881 (6.076 kg)	(6.076 kg)	
Polar moment of inertia (kgm^2/m)		188.98×10^3	0.03024 ($0.0378\ kgm^2$)	($0.0378\ kgm^2$)	
Frequency (Hz)	Vertical	0.464	–	2.718	
	Torsion	1.208	–	6.255	
Structural Damping in log. Derement	Vertical	–	0.014	0.0139	
	Torsion	–	0.023	0.0164	

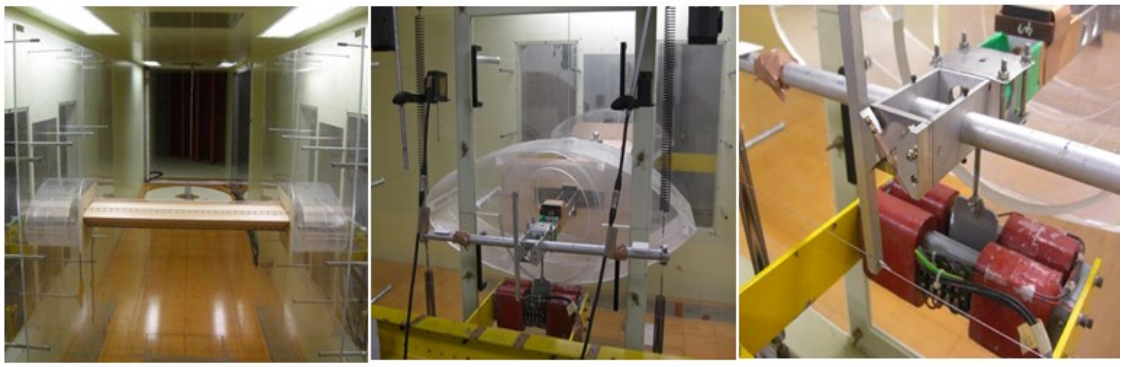

1) Model Installation 2) Support Spring 3) Electro-magnetic Damper

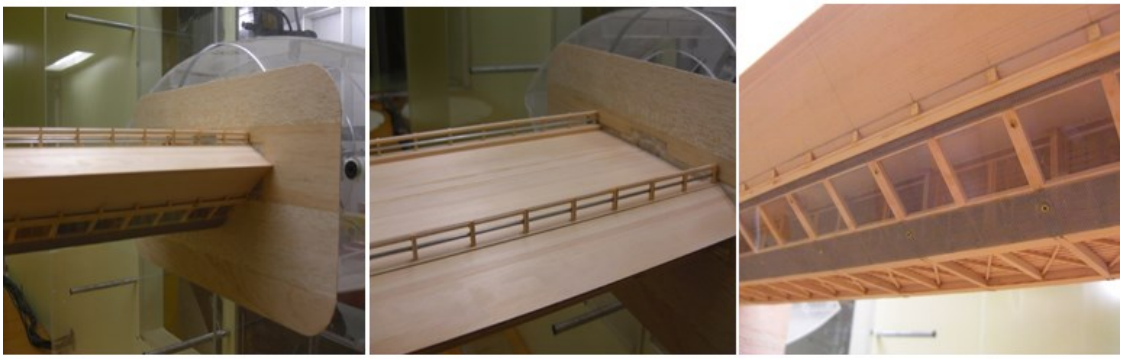

4) Lateral side 5) Upper Surface 6) Lower surface

Figure 4.8. String supported model of the Shin-minato Bridge in WTT [7]

4.3.3. Experimental results

This sub-section only presents some basic results obtained from WTT which are related to the next chapters, especially focusing on the effect of flaps. The geometric configurations of flaps (a, b, θ) include length a, gap b and angle θ degrees, as Figure 4.9. In order to generalize the dimensions of those configurations, the length a and the gap b are expressed by dimensionless values corresponding to the height D of the girder. Firstly, three force coefficients measured in case of the girder having a flap (0.22D, 0.29D, 30) attached are showed as Figure 4.10. Then, the VIV amplitudes captured with some different flaps are indicated as Figure 4.11. The Reynolds number was round 10^4. There were two flaps leaded to good solutions for suppressing the VIV vibration: flap (0.33D, 0.18D, 30) and flap (0.22D, 0.29D, 30). Finally, the flap (0.22D, 0.29D, 30) was decided to install in the Shin-minato Bridge, Figure 4.12. By monitoring in the site of the bridge, the VIV vibration has not occurred any more after finishing installing the flap (0.22D, 0.29D, 30) on one side.

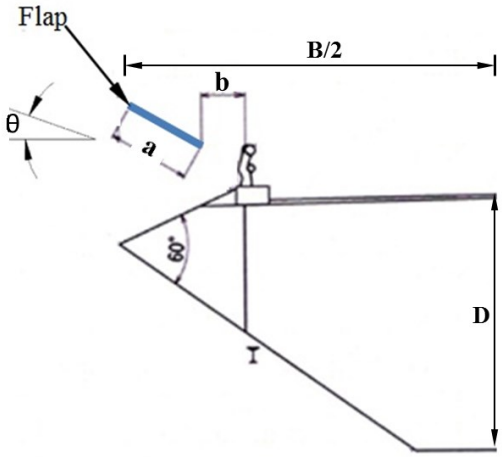

Figure 4.9. Geometric configurations of flap(s)

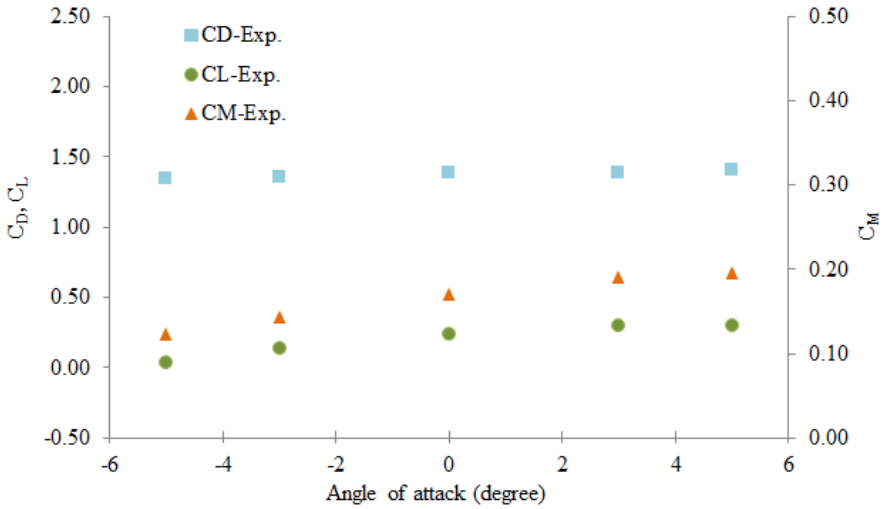

Figure 4.10. Three-components force coefficients measured in WTT [8]

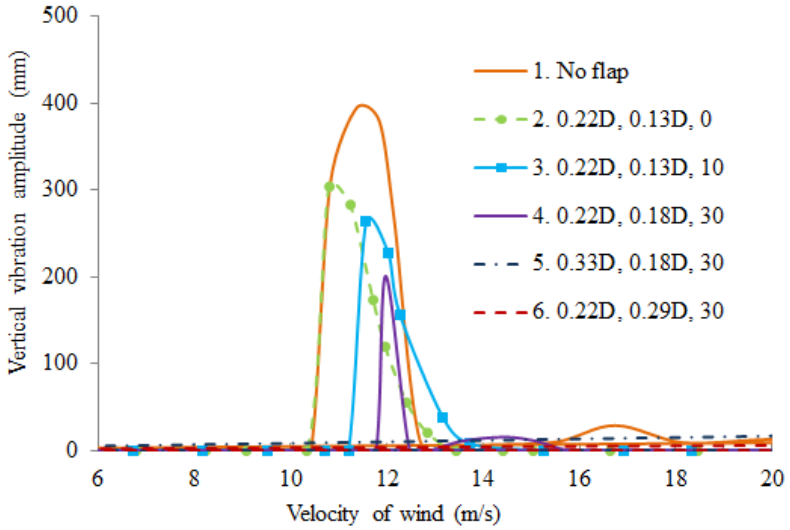

Figure 4.11. VIV amplitude measured in WTT [7]

Figure 4.12. Flap (0.22D, 0.29D, 30) installed in the Shin-minato Bridge [7]

4.4. Summary of Chapter 4

WTT has been the key word in the present chapter. How to comprehend the procedures in WTT and how to set up the model with the similarity laws are firstly presented in Section 4.1 as the introduction part of the chapter. By the purposes of providing vital experimental data for ensuring the validation of numerical simulations in the next chapters, two researches are then introduced in Section 4.2 and 4.3. In there, the popular experimental results regarding aerodynamic characteristics of rectangular cross-sections with various width-to-depth ratios, which were conducted by Nakaguchi et al. [32], are mentioned in Section 4.2. Next, the WTT of investigating flap countermeasures in eliminating the VIV oscillation

observed at the Shin-minato Bridge, which was implemented by Katsuchi et al. [7], is provided in Section 4.3. The later one is used not only to confirm the validation of numerical schemes, but also to clarify the role of flap in reducing the VIV of the box girder.

5.1. Introduction

Static numerical analysis used in the thesis can be defined as numerical simulations in which the concerned sections are fixed at a computational domain. The numerical investigation is started on studying the aerodynamic characteristics of the wind flow. In static simulations, the box girder of the Shin-minato Bridge and the rectangular cross-section with many the width-to-depth ratios are investigated in the presence of flap. In there, the impact of flap is emphatically inspected in order to figure out the controlling behavior for the wind flow, as well as to explain its effect in VIV mitigation. One after another, the PSD of lift force, the RMS of pressure coefficient along the sectional perimeter, the RMS of force coefficients, the flow pattern and the flow field are presented to illustrate the influence of the different configurations of flap. In addition, how flap disturbs the wind speed profile above the section is considered as its side effect to automobile steering.

5.2. Numerical simulations

5.2.1. Governing equations

Numerical simulations are performed in the RANS equations. In this approach, all of the unsteadiness is averaged out to deal with the turbulence. In addition, the new $k-\varepsilon$ eddy viscosity model is utilized to close the governing equations. All numerical analyses are run on the commercial software STAR-CCM+, and the finite volume method is used for discretization.

The theory of the governing equations was presented in Chapter 3: at Section 3.1. Hence, those equations are not repeated in this section. It is noted that the governing equations for incompressible flows and without body forces are utilized. In Section 3.3.3, those ones can be written again as Table 5.1.

Table 5.1. Governing equations

N0	Equation Name	Description	Note
1	Continuity	$\frac{\partial(\rho\bar{u}_i)}{\partial x_i} = 0$	(3.8)
2	Momentum	$\frac{\partial(\rho\bar{u}_i)}{\partial t} + \frac{\partial}{\partial x_j}\left(\rho\bar{u}_i\bar{u}_j + \rho\overline{u_i'u_j'}\right) = -\frac{\partial\bar{p}}{\partial x_i} + \frac{\partial\bar{\tau}_{ij}}{\partial x_j}$	(3.9)

In terms of tackling the turbulence, the new $k-\varepsilon$ eddy viscosity model is used to close the above equations. The theory of this turbulence model was carefully presented in Section 3.4. This section only summarizes the main equations of the model in Table 5.2.

Table 5.2. New $k-\varepsilon$ eddy viscosity model

N0	Equation Name	Description	Note
1	The transport equation for turbulent kinetic energy k	$\frac{\partial(\rho k)}{\partial t} + \frac{\partial(\rho\bar{u}_j k)}{\partial x_j} = P_k - \rho\varepsilon + \frac{\partial}{\partial x_j}(\frac{\mu_t}{\sigma_k}\frac{\partial k}{\partial x_j})$	(3.13)
2	The new dissipation rate equation ε	$\frac{\partial(\rho\varepsilon)}{\partial t} + \frac{\partial(\rho\bar{u}_j\varepsilon)}{\partial x_j} = \rho C_1 S\varepsilon - \rho C_2\frac{\varepsilon^2}{k+\sqrt{\frac{\mu}{\rho}\varepsilon}} + \frac{\partial}{\partial x_j}(\frac{\mu_t}{\sigma_\varepsilon}\frac{\partial\varepsilon}{\partial x_j})$	(3.22)

5.2.2. Model near solid boundary

Numerical results are considerably influenced by the type of treatment model near solid boundary. A precise treatment is always important to a simulation of flow field around bluff bodies, especially around rectangular/box sections involved with separation and reattachment. The log-law is not a proper resort for rectangular/box sections. Therefore, the present study employs a two-layer model which was first suggested by Rodi [54]. It is an approach that allows the k-ε model to be applied in the viscous sub-layer, dividing the computation into two layers. In this study, the two-layer formulations of the Wolfstein model [55] are used.

5.2.3. Geometry and analysis parameters

Numerical simulations are performed on the consistent analysis conditions with the experimental ones in wind tunnel. Particularly, the geometrical configurations of the rectangular sections and the box section are shown in Figure 5.1. The other analytical parameters are summarized in Table 5.3 and Table 5.4.

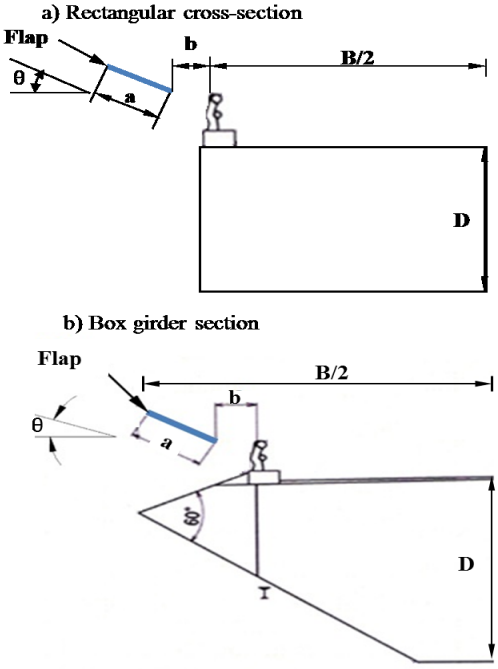

Figure 5.1. Geometry of rectangular and box girder sections with flap attached

The representative dimensions of the rectangular sections and the box section, which are used in analyses, are the width B between two extreme edges of the section and the depth D between the higher and the lower points at the vertical center line. The geometric configurations of flaps are symbolized (a, b, θ) including the length a, the gap b and the angle θ degrees. In order to generalize the dimensions of those configurations, these ones are expressed by dimensionless values corresponding to the height D of the section. In simulations, the ones are also varied case by case. The length a is changed from 0.2D to 0.3D (1000 mm to 1500 mm), the gap b is examined from 0.12D to 0.43D (600 mm to 2150 mm) and the angle θ is analyzed from 0° to 70°. The barrier of the girder is set up in simulations to consider its impingement to the flow pattern.

Table 5.3. Analysis parameters of rectangular sections

Parameter	Units	Model Scale	Note
Width (B)	(m)	0.2, 0.3, 0.35, 0.4, 0.8	
Height (D)	(m)	0.1	
Aspect Ratio (B/D)		2, 3, 3.5, 4, 8	
Number of elements		200000	
Reynolds number		10,000	
Scale		1/50	
Time step (Δt)	(s)	0.0005	

Table 5.4. Analysis parameters of the box girder in the Shin-minato Bridge

Parameter	Units	Model Scale	Full Scale	Note
Width (B)	(m)	0.3	15	
Height (D)	(m)	0.094	4.7	
Aspect Ratio (B/D)		3.2	3.2	
Number of elements		140,000-150,000		
Reynolds number		10,000		
Scale		1/50		
Time step (Δt)	(s)	0.0005		

5.2.4. Computational domain, boundary conditions and mesh

In numerical analysis, the dimension of computational domain and the boundary conditions decide the accuracy of the outcomes. Many previous researchers such as Kelkar and Patankar (1992) [56], Sohankar et al. (1995) [57] and Behr et al. (1995) [58] showed the relationship between the upstream distance (distance from the inlet to the object), the downstream distance (distance from the object to the outlet), the height of the domain and the

height of object in order to get independent results. As far as above references and tested work for some examples, to examine the influential domain of flow, the section is placed into a computational domain having width and depth equal to 40D and 20D, respectively.

In terms of boundary conditions, a no-slip boundary is assigned not only at the perimeter of the section but also at the top and bottom wall of the computational domain to resemble the conditions of WTT in case of the box section, because the height of the computational domain and the height of the wind tunnel are nearly the same. However, a slip boundary is set up at the perimeter of the rectangular sections. In addition, a velocity inlet and a pressure outlet boundary condition are imposed at the inlet and outlet, respectively. Figure 5.2 describes in detail about the analysis domain, the boundary conditions and the mesh.

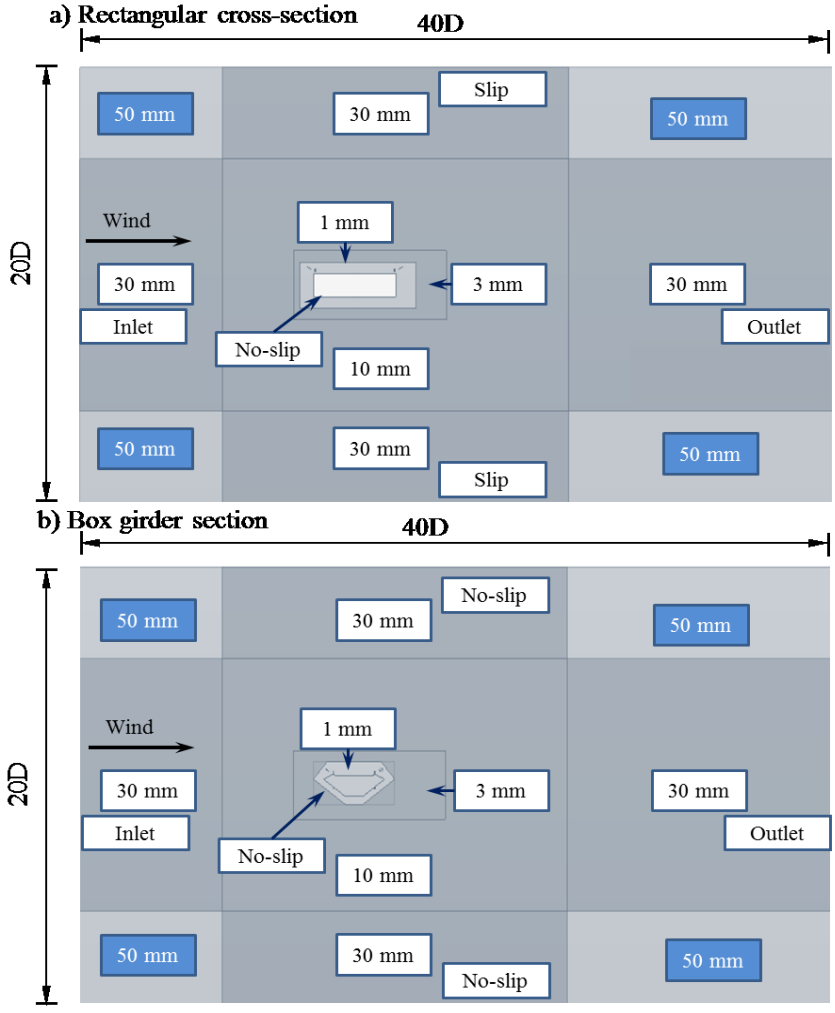

Figure 5.2. Computational domain, boundary conditions and mesh

The domain is discretized by a structured mesh system with around 140,000-200,000 hexahedral/tetrahedral cells. The whole domain is divided into five blocks with many different mesh sizes. The mesh system approximately 2.5 $x10^{-3}$ - $3.3x10^{-3}$B is applied in the vicinity of the sections, gradually becoming coarser to 1.25 $x10^{-1}$ - $1.6x10^{-1}$B at the inlet and outlet boundaries. Figure 5.3 shows the fine mesh at the vicinity of the sections.

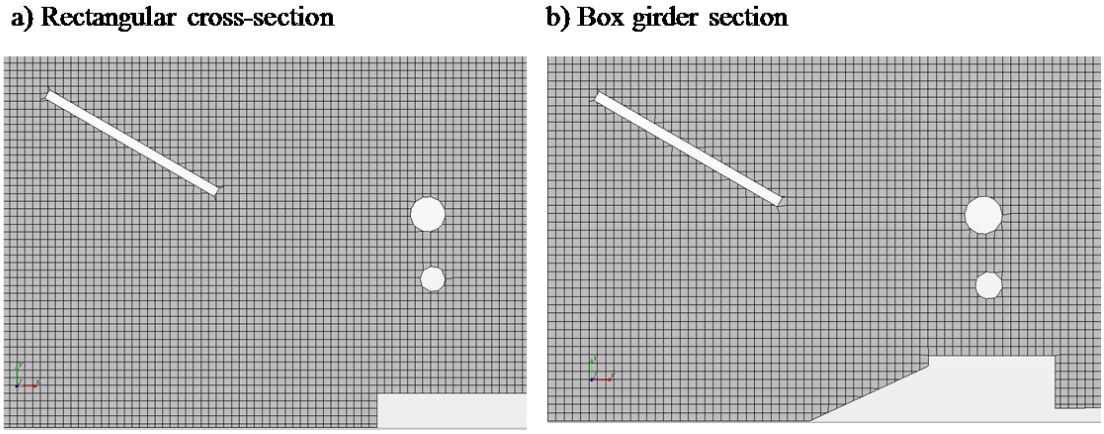

Figure 5.3. Mesh size at the vicinity of the sections

5.3. Validation

The validation of all numerical simulations is confirmed in this section. In order to ensure the reliability, the outcomes obtained from the numerical simulations are compared to the outcomes measured in WTT. Firstly, in some benchmark cases of the rectangular cross-sections having the width-to-depth ratios which are closed to the box girder sections of the Shin-minato Bridge, the comparison is done through the static force coefficients, the Strouhal number and the RMS of lift coefficient. Secondly, the collation is carried out in case of the box girder section of the Shin-minato Bridge. In there, it is conducted by means of the static force coefficients and the behavior of the VIV measured in WTT.

The concepts of the static force coefficient and the Strouhal number can be found in Chapter 2:. The drag force F_D, lift force F_L and pitching moment M on the sections (per unit of span) can be rendered dimensionless in terms of the drag coefficient C_D, lift coefficient C_L and moment coefficient C_M. The along-flow direction of F_D, the upward direction of F_L and the clockwise direction of M are conventionally positive directions, as Figure 5.4.

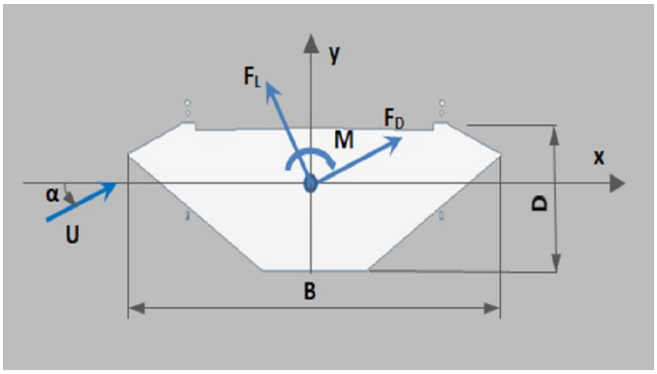

Figure 5.4. Definition of direction of forced and angle of attack

$$C_D = \frac{F_D}{\frac{1}{2}\rho U^2 D} \tag{5.1}$$

$$C_L = \frac{F_L}{\frac{1}{2}\rho U^2 B} \tag{5.2}$$

$$C_M = \frac{M}{\frac{1}{2}\rho U^2 B^2} \tag{5.3}$$

5.3.1. Rectangular sections

It is necessary to confirm the reliability of numerical scheme used in the study through some benchmark cases of rectangular sections. Hence, there are three cases of rectangular sections, having the width-to-depth ratio closed to the box girder section of the Shin-minato Bridge: 3.0, 3.5, 4.0, are studied to set up the main numerical schemes and analysis parameters.

Regarding the comparison between numerical and experimental results, a good agreement between them can be found at the mean drag coefficient, the stroulhal number and the RMS of lift coefficient, as indicated in Table 5.5, Table 5.6 and Table 5.7 (or Figure 5.5, Figure 5.6 and Figure 5.7). Apart from the experimental results cited from Nakaguchi et al. (1968) [32] and Mizota et al. (1988) [59], the comparison comprises the numerical results studied previously by Sohankar [60]. In Figure 5.8, the resemblance between the present study and Sohankar's study about the flow pattern around the rectangular section with ratio 4.0 can be observed. Therefore, it is reasonable to ensure the main numerical scheme and analysis parameters used in this study.

Table 5.5. Comparison table - Mean drag of some rectangular sections

N0	Side ratio	Present	Nakaguchi	Mizota	Sohankar
1	3.0	1.55	1.26	1.40	1.21
2	3.5	1.59			1.20
3	4.0	1.32	1.18	1.40	1.20

Table 5.6. Comparison table - Strouhal number of some rectangular sections

N0	Side ratio	Present	Nakaguchi	Sohankar
1	3.0	0.14	0.16	0.17
2	3.5	0.12	0.15	0.15
3	4.0	0.12	0.13	0.14

Table 5.7. Comparison table - RMS of lift coefficient of some rectangular sections

N0	Side ratio	Present	Sohankar
1	3.00	0.53	0.60
2	3.50	0.51	0.53
3	4.00	0.42	0.50

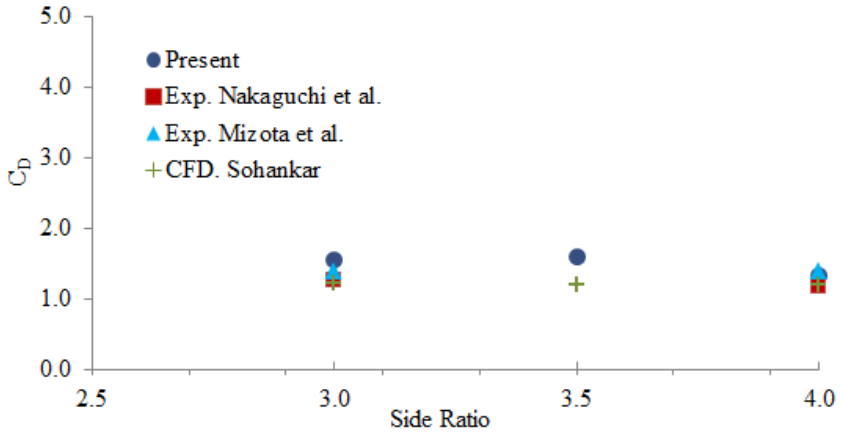

Figure 5.5. Mean drag coefficient of some rectangular sections

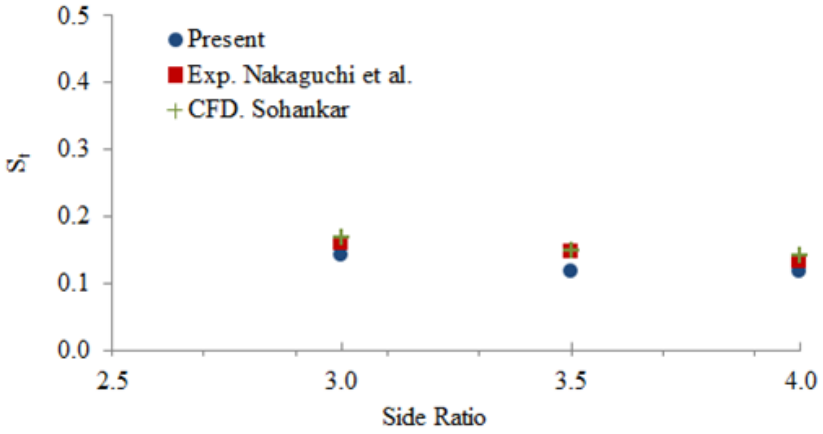

Figure 5.6. Strouhal number of some rectangular sections

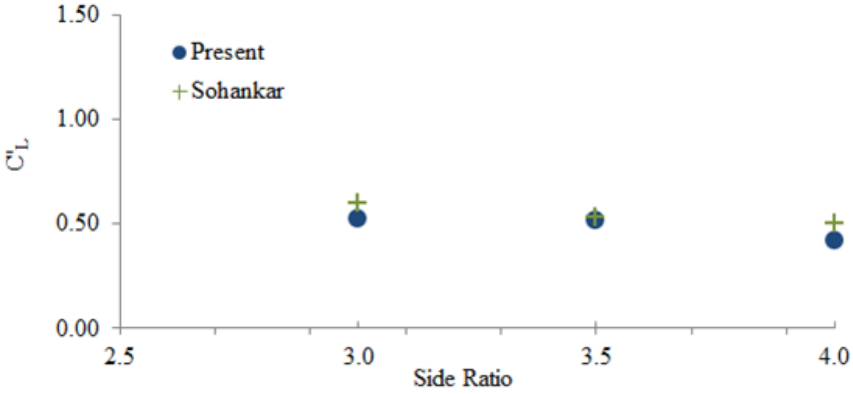

Figure 5.7. RMS of lift coefficient of some rectangular sections

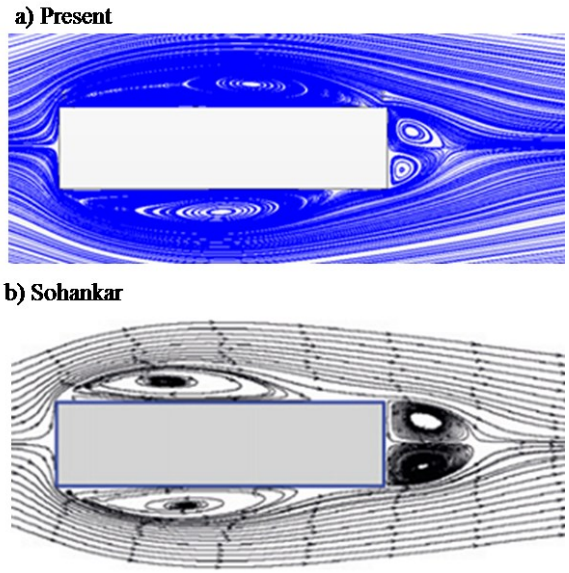

Figure 5.8. Resemblance about flow patter at rectangular section ratio 4

5.3.2. Box girder section

The mean values of C_D, C_L and C_M compared with the experimental ones for the box girder section with flap of the Shin-minato Bridge are indicated in Table 5.8, Table 5.9 and Table 5.10 (or Figure 5.9), at the angles of attack from -5° to +5°. In this case, the length, gap and angle of flap are 1000 mm, 1300 mm and 30° (0.22D, 0.29D, 30), respectively. It illustrates that the use of the RANS approach coupled with the new $k-\varepsilon$ eddy viscosity turbulent model in this study leads to the agreement with the experimental results in the negative range of angles of attack (-5° to 0°). However, the numerical results of these coefficients are underestimated in the positive ones.

Table 5.8. Comparison table - Drag coefficient with some attack of angles

N0	Attack of angle (degree)	C_D		Note
		Experimental	Numerical	
1	-5	1.35	1.32	
2	-3	1.36	1.30	
3	0	1.38	1.23	
4	3	1.38	1.21	
5	5	1.41	1.16	

Table 5.9. Comparison table - Lift coefficient with some attack of angles

N0	Attack of angle (degree)	C_L		Note
		Experimental	Numerical	
1	-5	0.04	-0.03	
2	-3	0.14	0.12	
3	0	0.24	0.20	
4	3	0.29	0.22	
5	5	0.30	0.21	

Table 5.10. Comparison table - Moment coefficient with some attack of angles

N0	Attack of angle (degree)	C_M		Note
		Experimental	Numerical	
1	-5	0.12	0.11	
2	-3	0.14	0.14	
3	0	0.17	0.16	
4	3	0.19	0.16	
5	5	0.20	0.17	

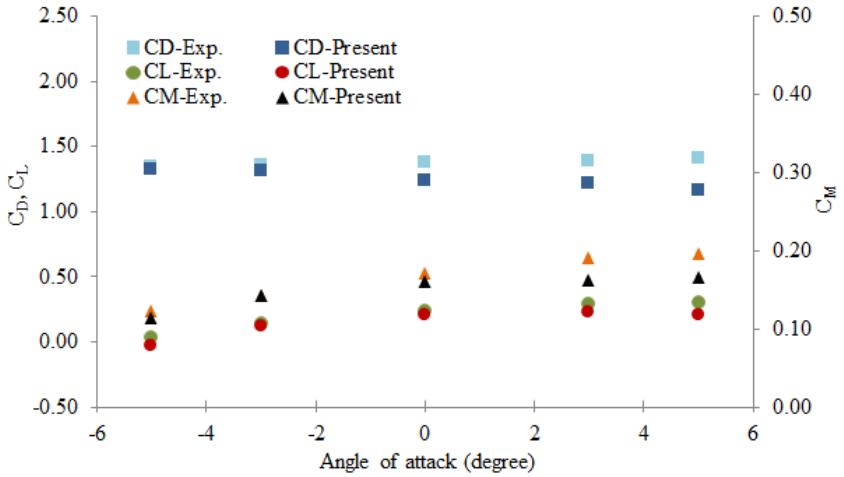

Figure 5.9. Comparison in mean force coefficients

At the windward, the flow in the positive range of angles of attack approaches the section less smoothly than the flow in the negative ones and in the zero one. This unsmooth interaction and the complicated geometry of section produce flow severe separation, creating a more intensive turbulent area at the surface and the leeward region. At that time, the RANS approach coupled with the new $k-\varepsilon$ model cannot result in high accuracy. In addition, the gap between the experimental and numerical results is partly due to the inexact calibration of the experimental apparatus. In this study, however, the numerical investigation on the effect of flap is performed with the zero angle of attack, leading to the outcomes that are good enough for the validation.

On the other hand, it is noted that there is a correlation between the VIV amplitude measured in WTT and the PSD of lift force obtained in the present study, Figure 5.10.

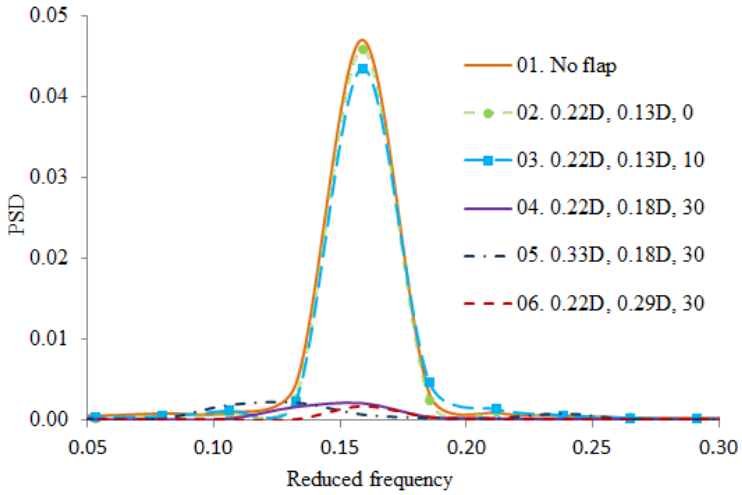

Figure 5.10. PSD of lift force from CFD

5.4. Box girder section with flap attached

5.4.1. Aerodynamic characteristics

In numerical analysis, the simulations similar to the experimental ones are conducted. It is indicated that the obtained results have the good correlation with the experimental ones, and the unsteady lift force is one of those. The PSD of lift force is determined through the time history obtained (Figure 5.11).Turning to details, the PSD of lift force has the same behavior with the VIV amplitude measured in the WTT. The peak of the PSD attains the maximum value at the section without flap and drops off at the section with flap attached, as is shown in Figure 5.12. When the angle, the gap and the length of flap are increased, the peak gradually lessens, especially in the cases of 30^{o} angle, such as (0.22D, 0.18D, 30), (0.33D, 0.18D, 30) and (0.22D, 0.29D, 30).

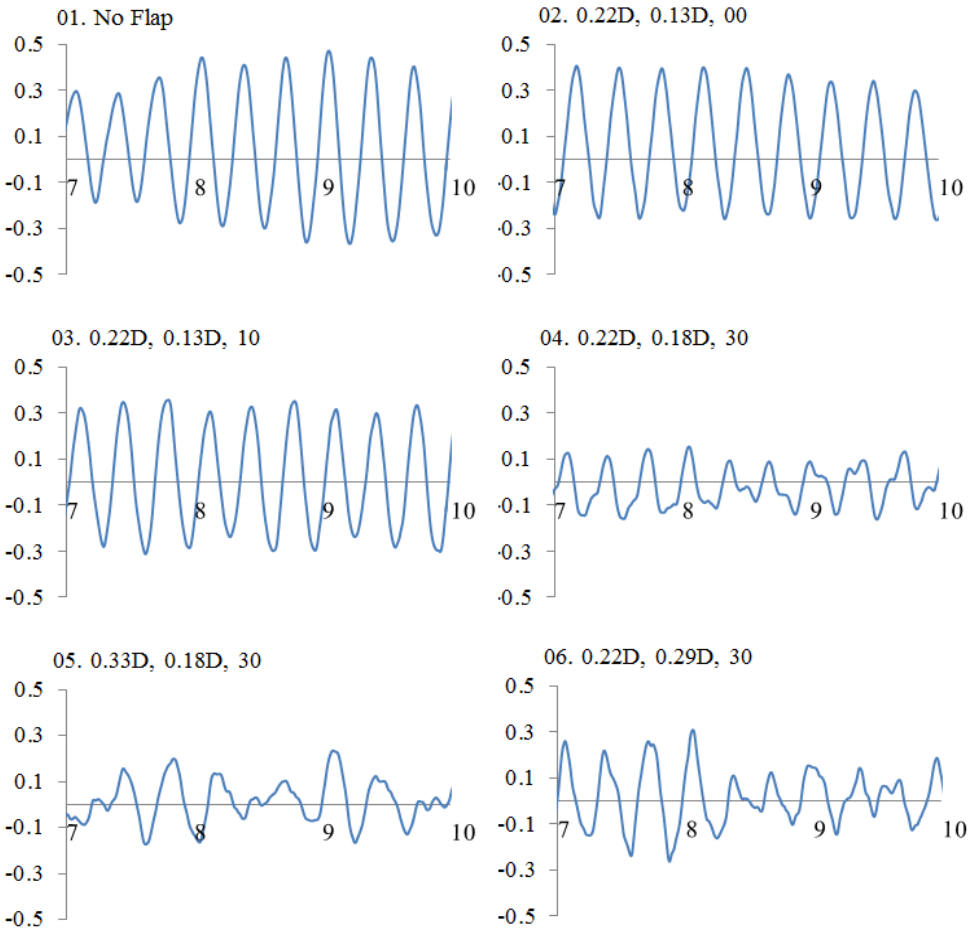

Figure 5.11. Time history of lift force on box girder section during 3 seconds period

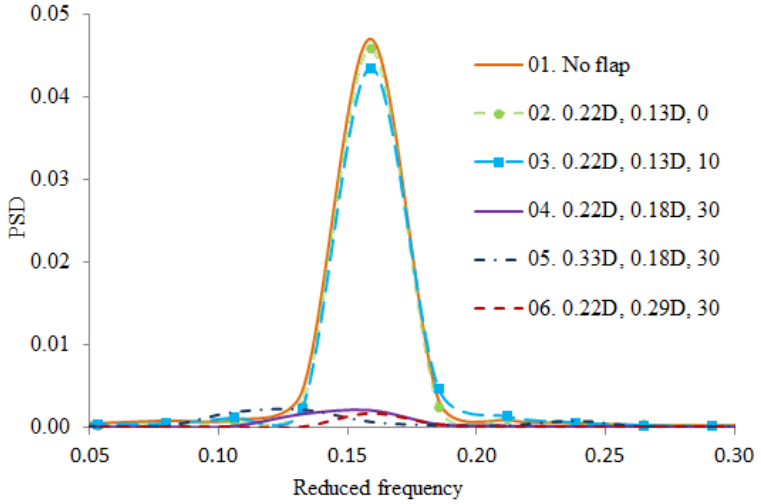

Figure 5.12. PSD of lift force impacting on the box girder section with flap attached

The correlation between the PSD of lift force and the thickness of wake layer can be found in Figure 5.13 and Figure 5.14. The thickness of wake layer can be defined as the distance between the surface of object (where it is assumed that the velocity of wind equals to zero) and the boundary position of wake (where the velocity of wind equals to the currently oncoming one). The prominent influence occurs at the point 6 of the leeward (Karman vortex shedding). In the angle 30°, the thickness directly impacting on the section at leeward is lessened significantly.

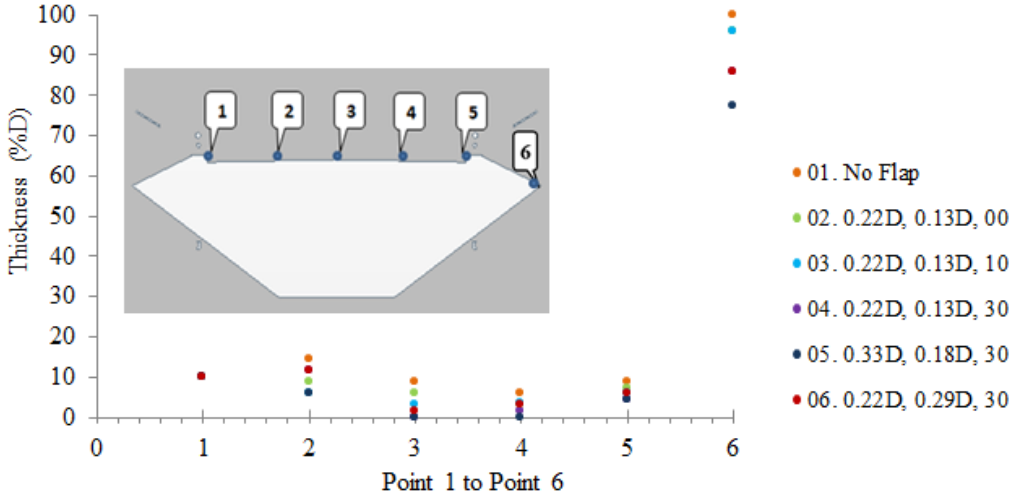

Figure 5.13. Thickness of wake layer at some points

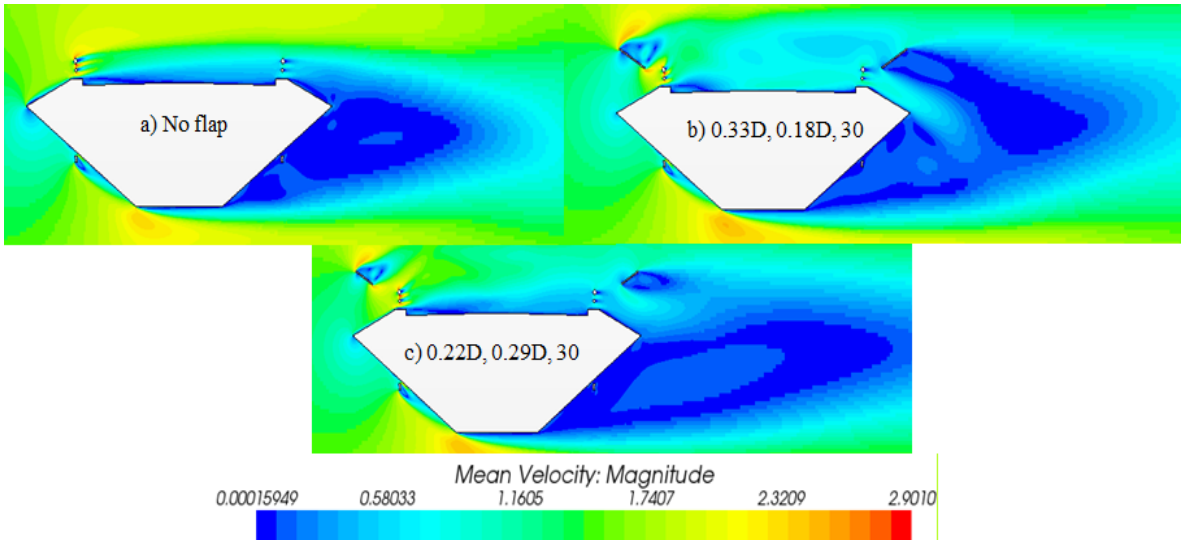

Figure 5.14. Flow field around the section in some typical cases

Considering the surface pressure coefficient on the surface of girder, the mean value of surface pressure coefficient has not changed so much with/without flap attached, as Figure 5.15. However, the same performance like the PSD of lift force can be observed in the RMS of surface pressure coefficient. It is defined as the square root of the arithmetic average of fluctuating pressure coefficient squares. In the numerical simulations, the time history of pressure coefficient is obtained at the points along the perimeter of the section to calculate the RMS. Its distribution around the section is drawn in Figure 5.16 and Figure 5.17 for some typical cases. It shows that the RMS gets the largest value for the section without flap. Next, the RMS has the high value when the angle of flap approaches to 0^{o}, whereas it has the smaller one when the angle equals to 30^{o}. Consequently, the presence of suitable flap plays an important role to reduce the fluctuation of pressure coefficient.

To comprehend the characteristics of the flow around the section, the flow visualization is given. Figure 5.18 depicts the flow pattern around the section in the previous cases. As can be seen, the flap and the faring at the windward and leeward regions play very important roles in the vortex formation at the upper surface of section and at the downstream, respectively. At the windward, if the angle of flap has sufficiently large value, then the flow will be oriented moving strongly forward the upper surface of the section. As a result, it can suppress the vortices generated from the leading edge. Therefore, it is considered that the windward flap can contribute the effect of suppressing the MIV. At the leeward, if the angle and the gap of flap have sufficiently large value, then the flow will be intercepted and it goes

down stronger to the upper surface of the faring. As a result of the combination between the fairing and the appropriate flap at the leeward, it accelerates the wind flow to deliver a high performance on controlling the wind flow to be smoother at the wake region and the vortex formation (KV shedding) is weakened. It can adjust the vortex formation more regular, reducing the amplitude of KV oscillation, whereas this phenomenon will not occur with the horizontal flap/the insufficient large gap and angle ones. Hence, the presence of flap with appropriate configurations will redistribute the flow pattern and control the flow towards reducing the sources which can cause the VIV.

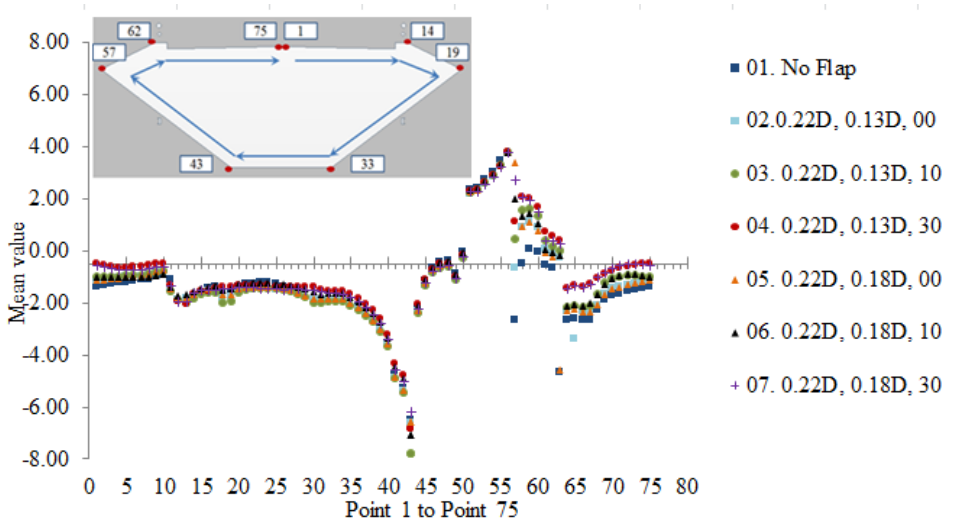

Figure 5.15. Mean surface pressure coefficient in some typical cases

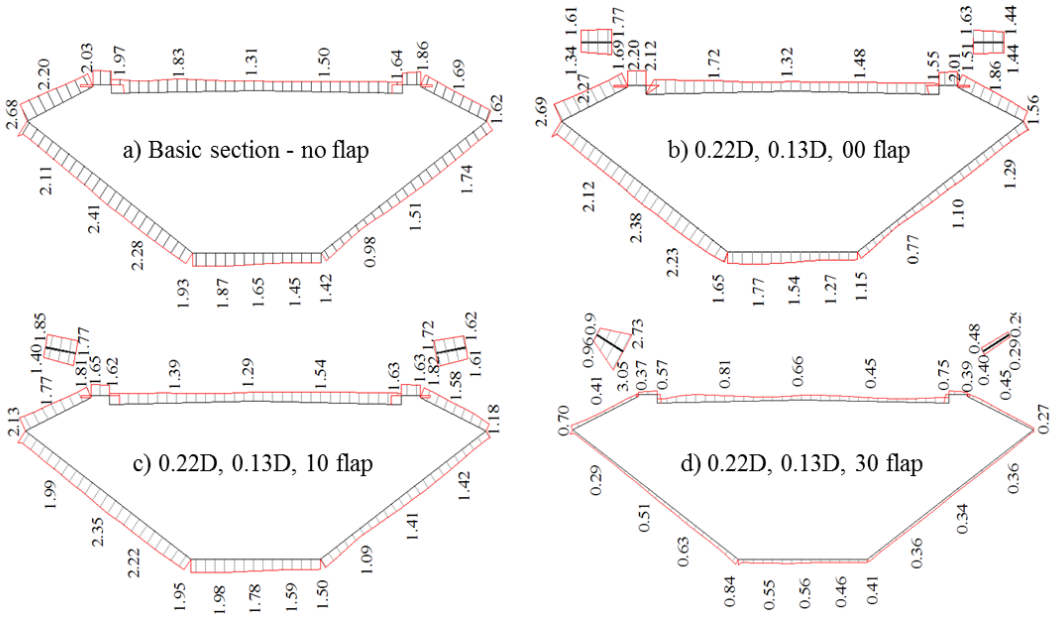

Figure 5.16. RMS of surface pressure coefficient in some typical cases (1)

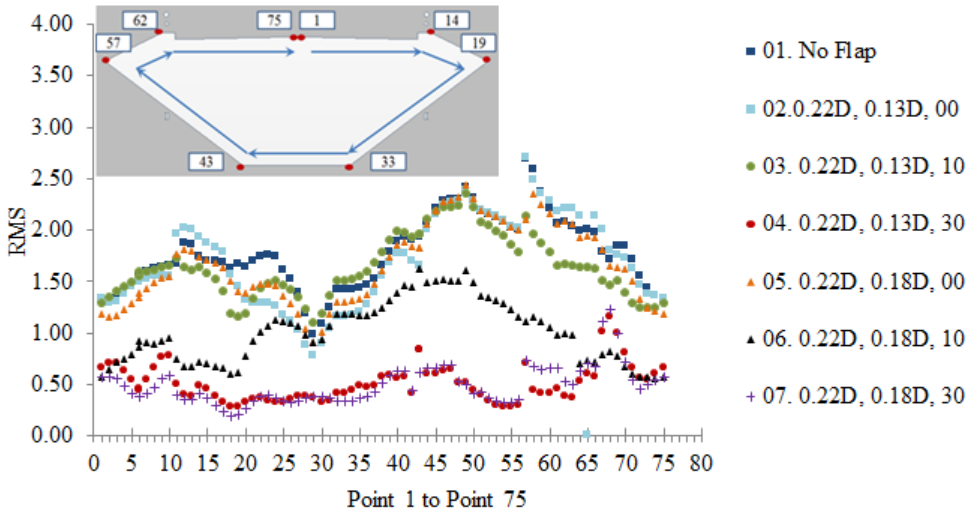

Figure 5.17. RMS of surface pressure coefficient in some typical cases (2)

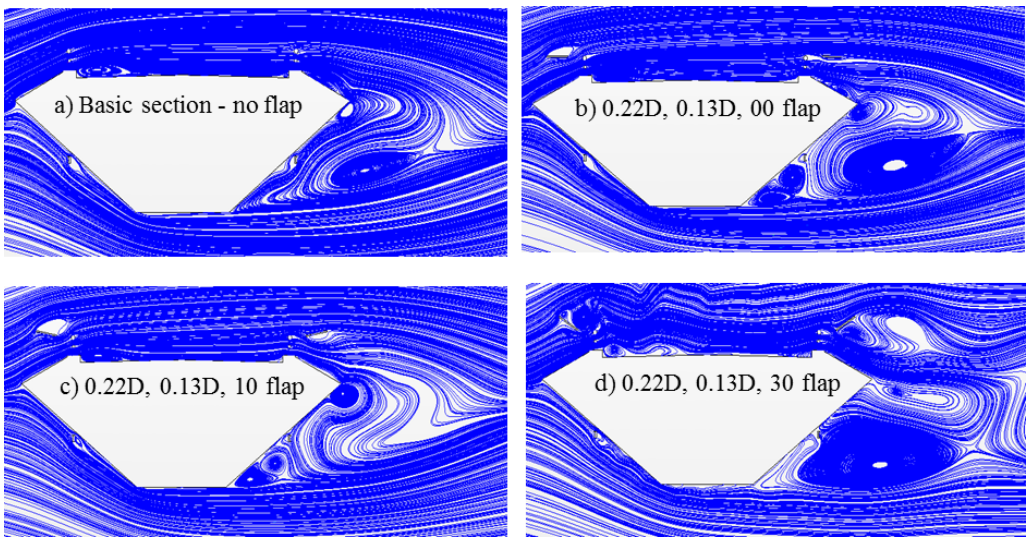

Figure 5.18. Flow pattern around the box section in some typical cases

5.4.2. Cases of large angle and gap flap

In this part, numerical simulations are carried out with the cases in where the angle and gap of flap are changed to larger values.

a) Large angle

The angle of flap is changed to 70^0 with the intervals of 10^0, while its gap is kept constant. According to the results, the cases of large angles are unsure to achieve the efficiency to the vibration reduction. It is demonstrated through the time history, the PSD and RMS of

lift force in Figure 5.19, Figure 5.20 and Figure 5.21. These results also have the agreement with the thickness of wake layer, as Figure 5.22.

As can be seen in Figure 5.20, there has been a notable fall of the peak of PSD of lift force when the angle reaches 30^0, but it only continues decreasing at the cases of 40^0 and 50^0 angles slightly. On the other hand, the peak develops at the different frequency in the cases of 60^0 and 70^0 angles. In Figure 5.21, the RMS of lift force has the same performance. It is obvious that the fluctuation of lift force significantly drops about 83%, from the 0^0 angle case to the 50^0 angle one. However, if the angle is continuously enhanced, then the fluctuation starts to rise. This point can be explained by the thickness of wake layer increases on the upper surface of the section due to the bluff-body of the high angle flap at the windward region, as shown in Figure 5.22.

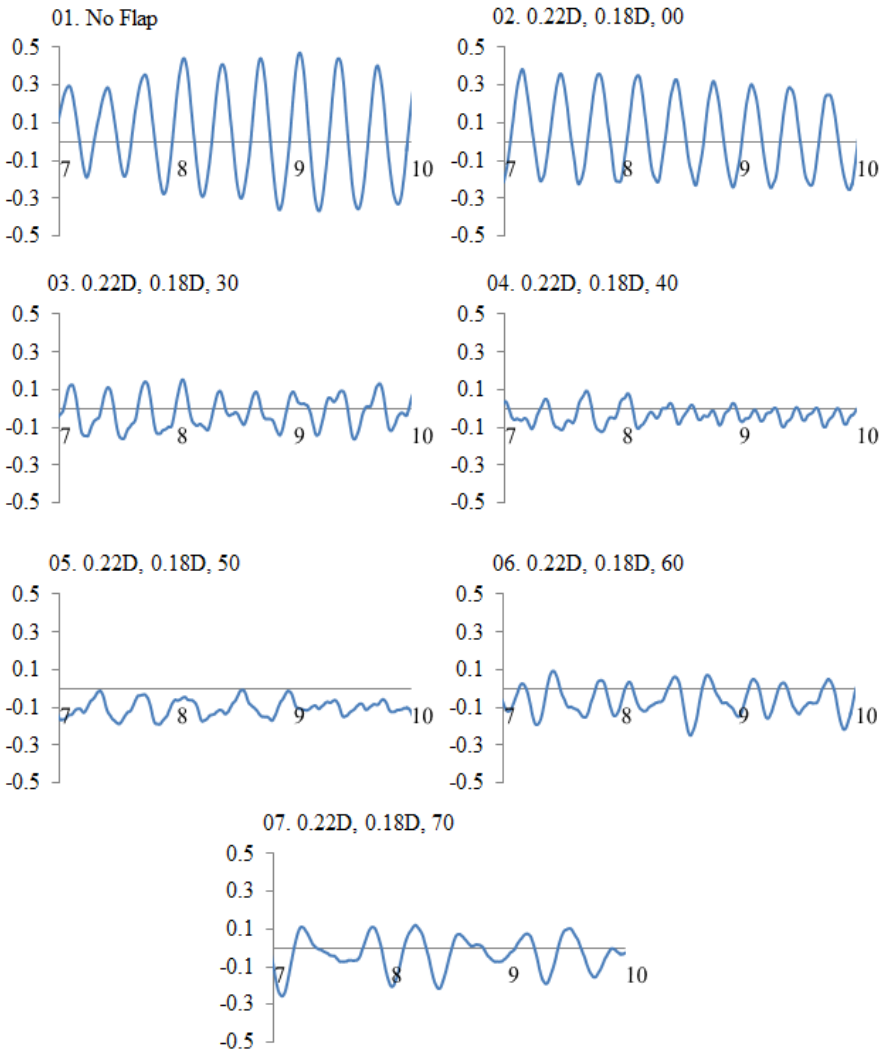

Figure 5.19. Time history of lift force in cases of large angle flap

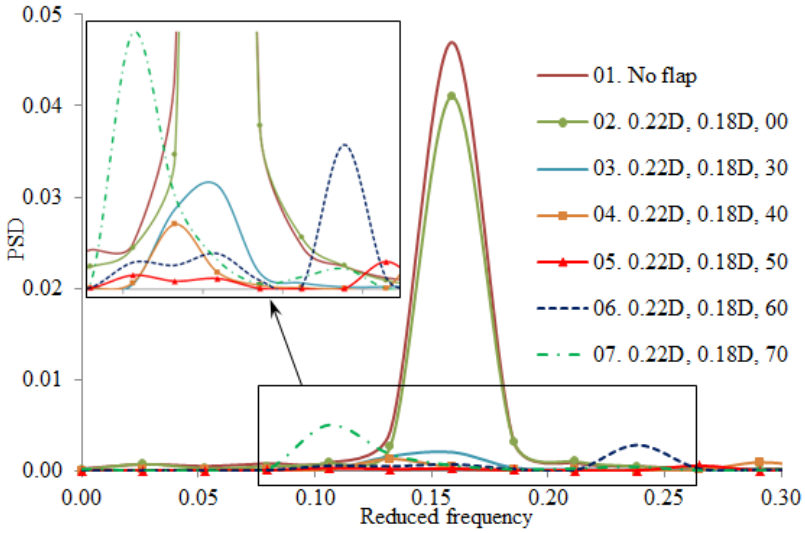

Figure 5.20. PSD of lift force in cases of large angle flap

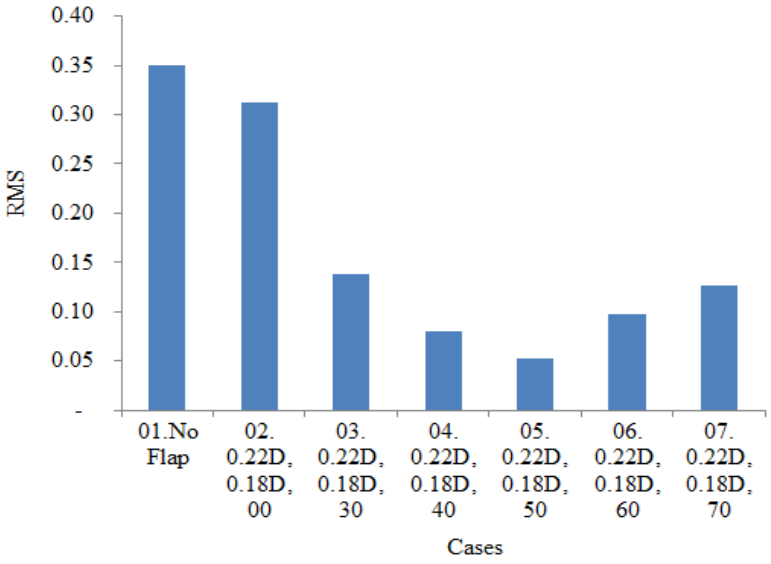

Figure 5.21. RMS of lift force in cases of large angle flap

In addition, the use of the large angle of flap also causes the enhancement of mean drag coefficient C_D as shown in Figure 5.23. For example, the approximately 77% growth of C_D is the consequence of the increase of the angle from 0^0 to 50^0, which is an effective solution in the fluctuation mitigation. Moreover, the flap with the large angle leads to the difficulty in installation at construction site.

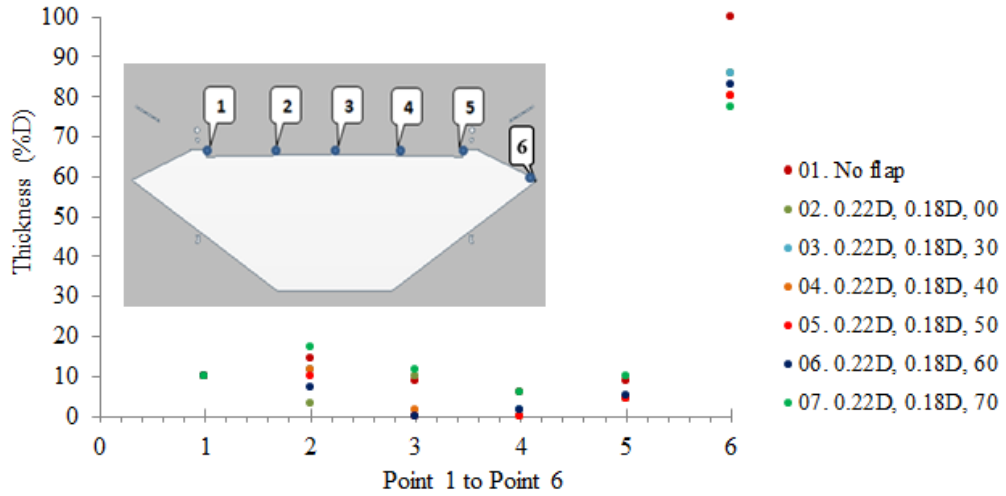

Figure 5.22. Thickness of wake layer in cases of large angle flap

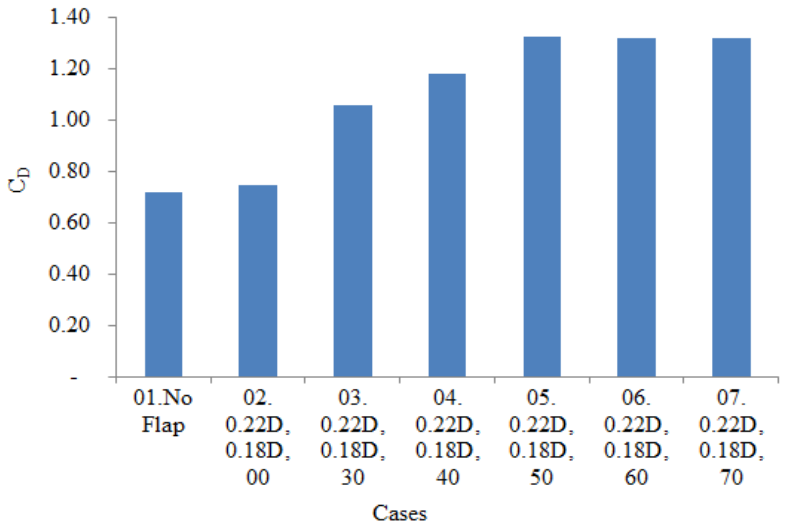

Figure 5.23. Mean drag coefficient in cases of large angle flap

b) Large gap

The gap of flap is changed from 0.13D (600 mm) to 0.48D (2150 mm) to investigate the effect of the horizontal flap. From the time history of lift force in Figure 5.24, the PSD of lift force given in Figure 5.25 shows that its peak insignificantly lessens when the gap is not large enough, such as the case of (0.22D, 0.13D, 00) flap and the case of (0.22D, 0.18D, 00) flap. Yet, the dramatic decrease occurs in the cases of 0.39D (1750 mm) and 0.48D (2150 mm) gaps. The larger the gap is, the smaller the lift force can be generated.

It is easy to identify the effect of the large gap in oscillation suppression by means of the RMS of lift force. In Figure 5.26, the unsteady lift force only is lightened about 2% to 10% when the gap lies in the range from 0.13D (600 mm) to 0.18D (800 mm), comparing with its value in the section without flap. However, the fluctuation of lift force strongly drops in the cases of 0.39D (1750 mm) and 0.48D (2150 mm) gaps, around 85% to 90%. On the other hand, the same behavior can be observed by the thickness of wake layer in Figure 5.27.

As shown in Figure 5.28, contrasting with the large angle flaps, the mean drag coefficient C_D is not remarkably varied when the gap is changed. Nevertheless, it is also necessary to adequately pay attention in the selection process, because of the feasibility of the flap installation at construction site.

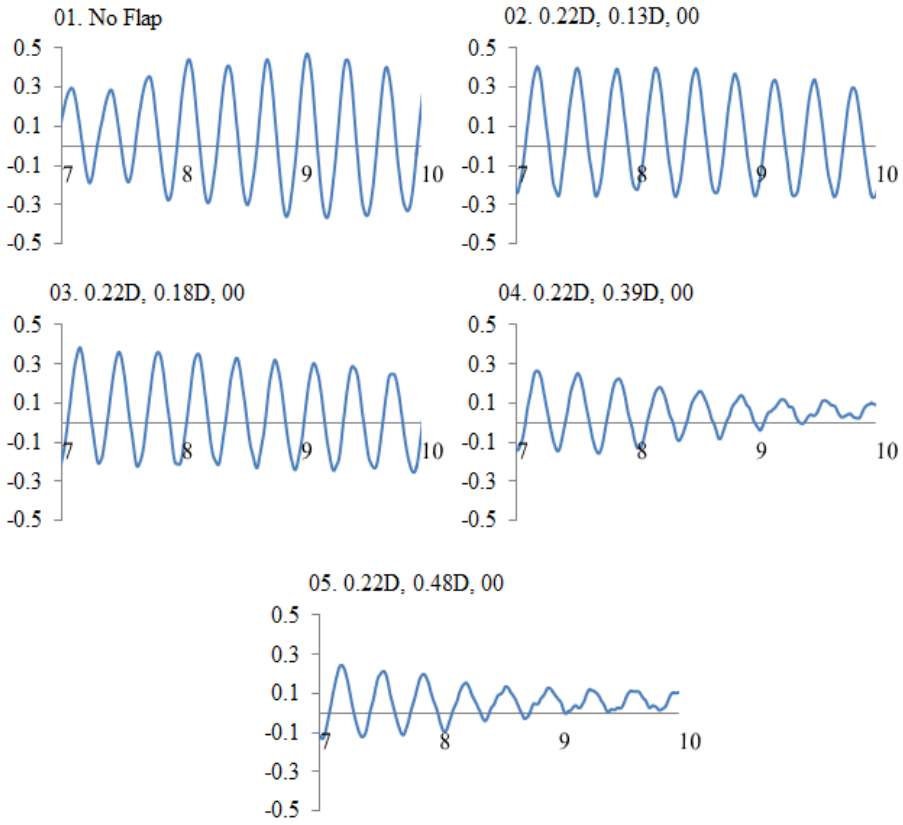

Figure 5.24. Time history of lift force in cases of large gap flap

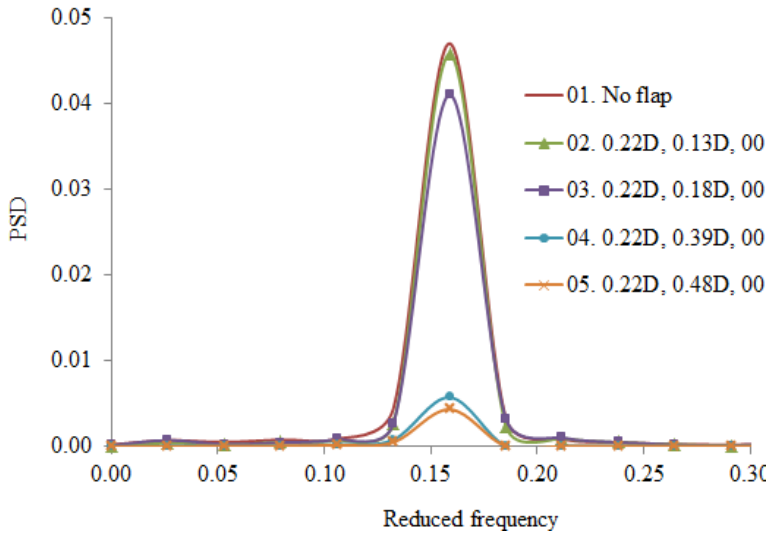

Figure 5.25. PSD of lift force in cases of large gap flap

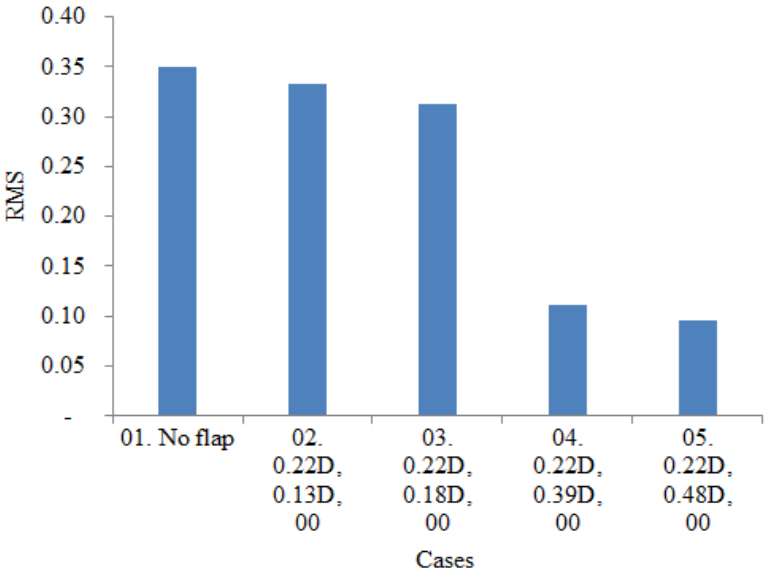

Figure 5.26. RMS of lift force in cases of large gap flap

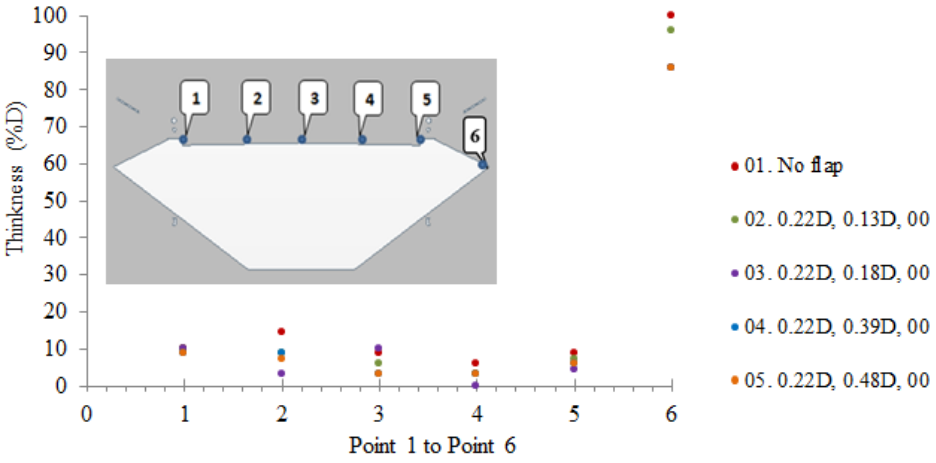

Figure 5.27. Thickness of wake layer in cases of large gap flap

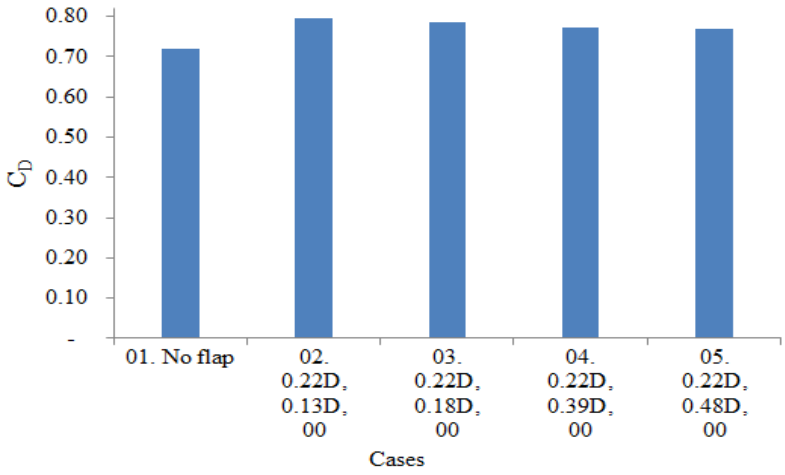

Figure 5.28. Mean drag coefficient in cases of large gap flap

5.4.3. Single flap at leeward region

As the suppression mechanism in VIV explained in Sub-section 5.4.1, the flap in leeward region plays a key role in reducing the wake vortices (KV). In order to prove that role, some numerical simulations with just single flap at the leeward region are set up. Again, the essential effect of flap at leeward region is confirmed. In addition, this result is consistent with the result observed in WTT at where the single flap is just only installed.

The time history and the PSD of lift force in some cases are indicated in Figure 5.29, Figure 5.30. In there, it remarkably decreases with the only single flap. The same mechanism with the flap at both sides can be found in the flow pattern as Figure 5.31. It is obvious that the flow is intercepted by the flap to accelerate the velocity. The combination between the flap

and the faring delivers the good controlling in the vortex formation at the leeward. It can reduce the wake zone which directly imposed the box girder. One good solution will be achieved if the flap has a large enough angle and gap, such as 30° angle gap and 0.18D gap.

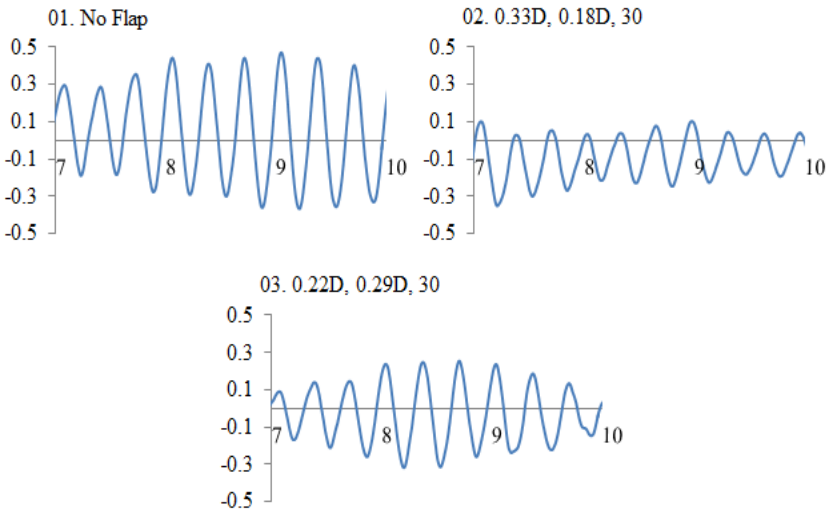

Figure 5.29. Time history of lift force in cases of single flap at leeward region

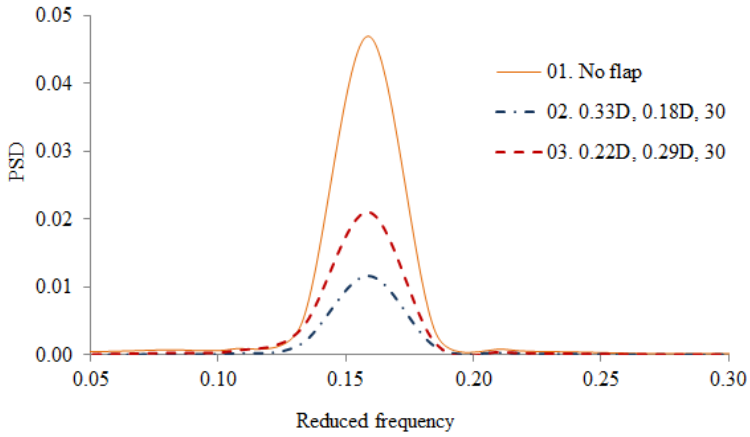

Figure 5.30. PSD of lift force in cases of using single flap at leeward region

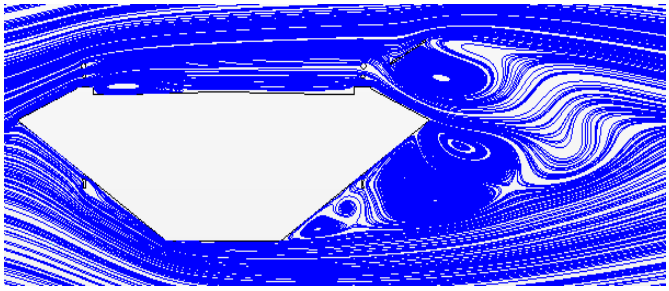

Figure 5.31. Flow pattern around the section in case of single flap 0.33D, 0.18D, 30

5.4.4. Influence of flap on wind velocity profile

Although the use of flap brings a significant diminution in VIV, it is necessary to take into account some side-effects that designers can encounter. One of those is the disturbance to the wind profile above the section. This section discusses about how flap disturbs the wind profile for some effective cases, including (0.33D, 0.18D, 30) flap and (0.22D, 0.29D, 30) flap.

The examination is based on the ratio of wind speed $R(z)$, defined as the ratio of the wind speed on the deck $U'(z)$ at the points with elevation z against the oncoming one U, and the turbulent in-tensity $I(z)$ at the points with elevation z, defined as the ratio of the RMS of the fluctuating component of the longitudinal wind velocity to its time-averaged value $U(z)$:

$$R(z) = \frac{U'(z)}{U} \tag{5.4}$$

$$I(z) = \frac{\sqrt{\overline{u^2(z)}}}{U(z)} \tag{5.5}$$

The $R(z)$ and $I(z)$ values of all points, from the deck surface to the elevation of 5.25 m, at 5 positions on the girder, are drawn in Figure 5.32. It is generally obvious that the height of the influential zone by flap attached is less than 4.00 m. The $R(z)$ value progressively goes up from the surface to the elevation 4.00 m at all 5 positions, but it no longer virtually changes from 4.00 m to 5.25 m. Though there is not the noticeable difference in the $R(z)$ values between the section with and without flap at the height of 0.50 m or less than 0.50 m, the R(z) values become considerably small from 0.50 m to 4.00 m in case of no flap. Similarly, the turbulent intensity of all cases does not vary from the elevation more than 4.00 m, but it strongly fluctuates at the lower locations. When the flap is attached, the turbulence intensity is much larger than in the section without flap at position 1 and 2, but there is not the remarkable difference at position 3, 4 and 5.

In short, the use of flap will create the disturbance to the wind profile in a specific region, and the strong turbulent intensity is found at the upper zone of the section surface in the windward. Hence, it is important to carefully consider in the flap selection.

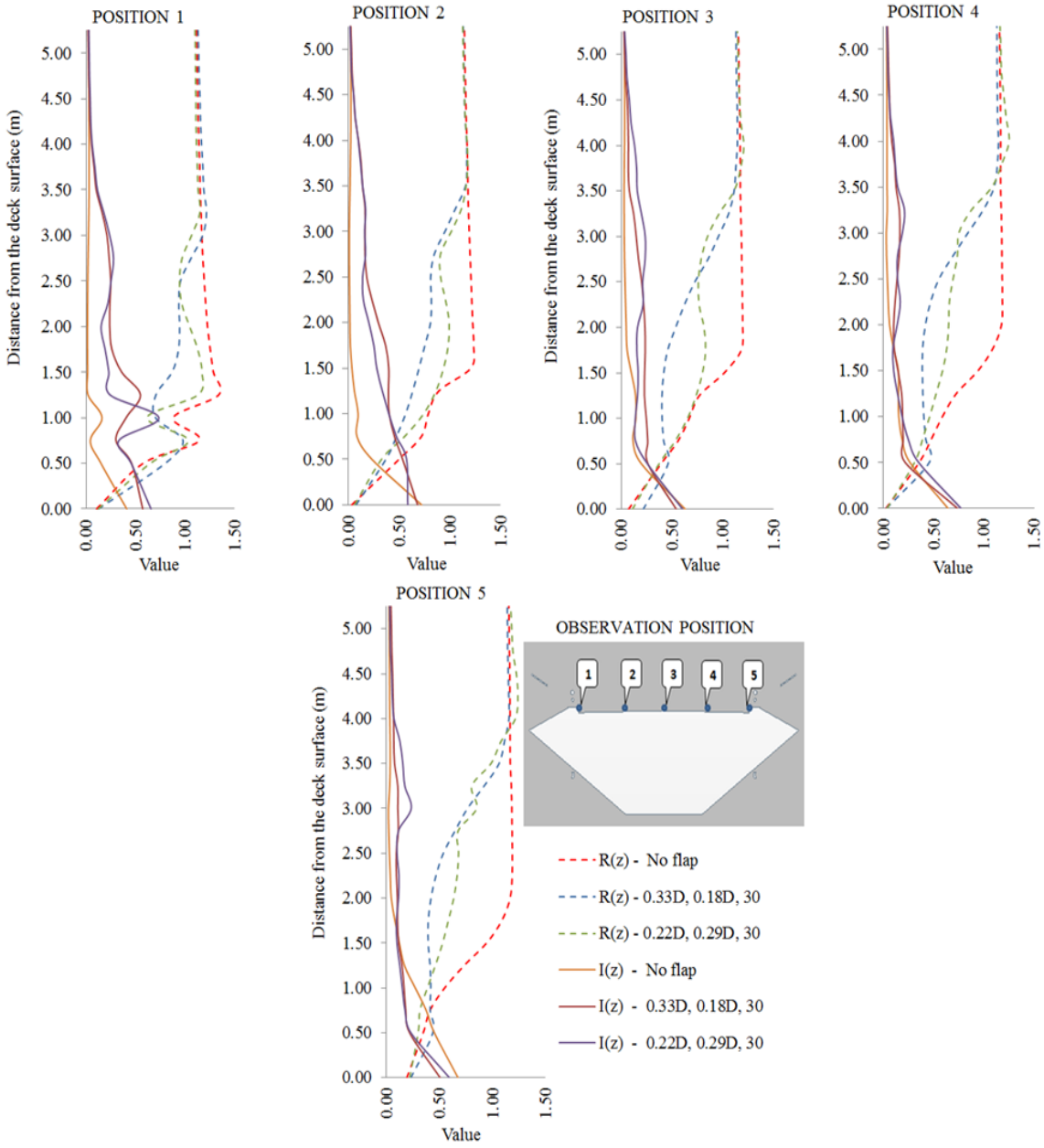

Figure 5.32. R(z) and I(z) above the section with and without flap

5.5. Rectangular section with flap attached

Numerical investigation into many rectangular sections with different side ratios are implemented in the presence of flap with two main reasons:

- Fortifying the effect and the VIV suppression mechanism of flap which are explained in case of the box girder section.

- Providing a general view of the significance of flap in mitigating the aerodynamic instability oscillations.

In this study, the rectangular sections with the width-to-depth ratio of 2, 4, 8 are taken into account. The aerodynamic instability is analyzed through the PSD of lift force, the RMS of surface pressure coefficient and the flow pattern.

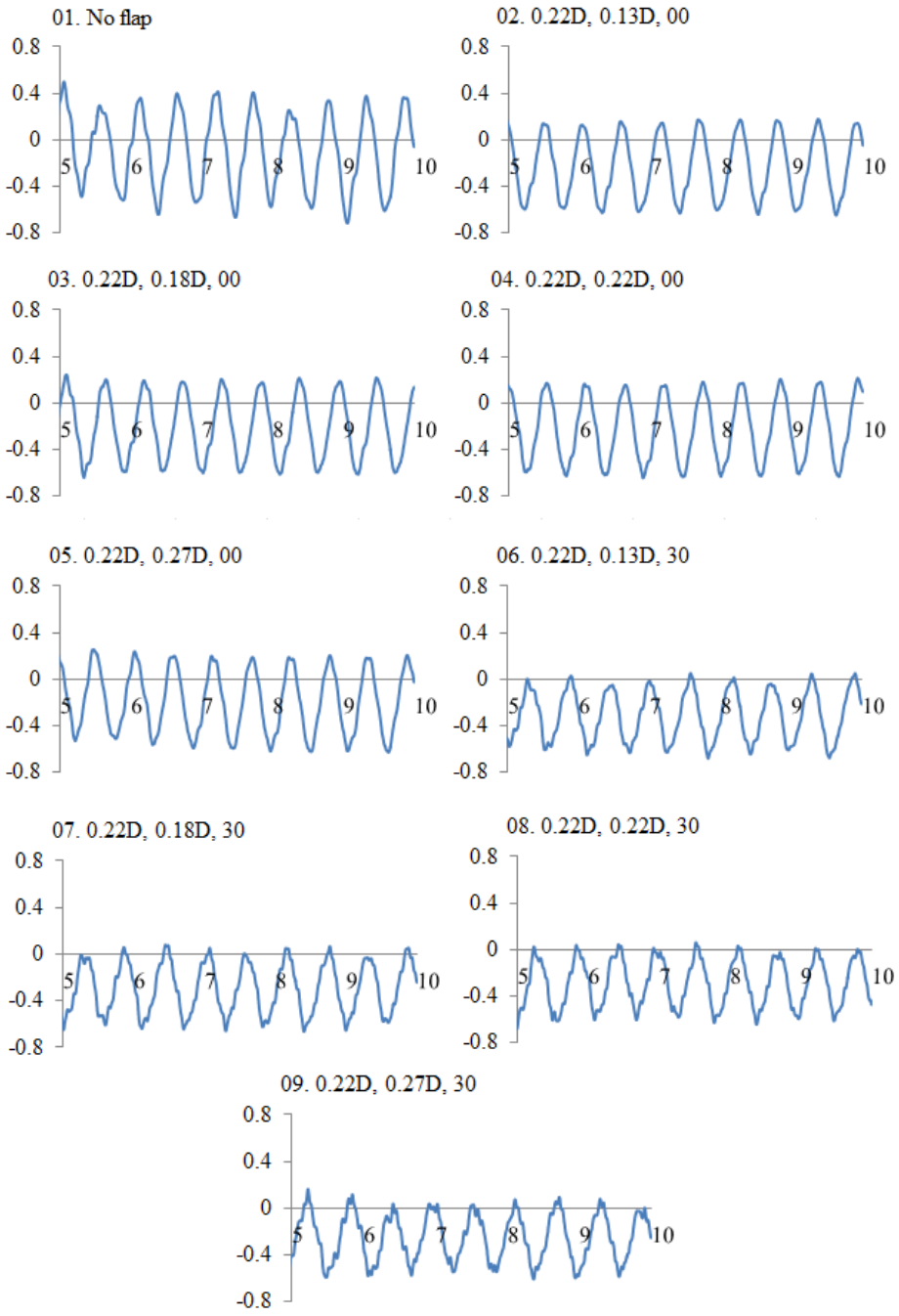

Figure 5.33. Time history of lift force – Rectangular section with ratio 4

Firstly, the rectangular section with side ratio 4 is examined. Figure 5.33, Figure 5.34, Figure 5.35 and Figure 5.36 show the time history, the PSD of lift force, the mean value and the RMS surface pressure coefficient, respectively. The high values are found in case of the section having no flap attached and the smaller values are discovered in the presence of flap. These ones deeply decrease when the flaps have large gaps and angles, especially in case of the angle 30^0. How the wind flow across the section is indicated in Figure 5.37 and Figure 5.38. It proves that the presence of flap has resulted in the change of wind flow behavior and has significantly impacted on the reduction of aerodynamic instability characteristics involved in the VIV. It can be concluded that the angle of flap plays a vital role in controlling the suppression mechanism of the section. The flaps with large gaps and angle 30^0 are recommended to improve aerodynamic instability. On the other hand, the above investigation reinforces the significance of flap using in the box girder section, in the sense that the large gaps and the angle 30^o of flap can decide its effectiveness in mitigating the oscillation if any.

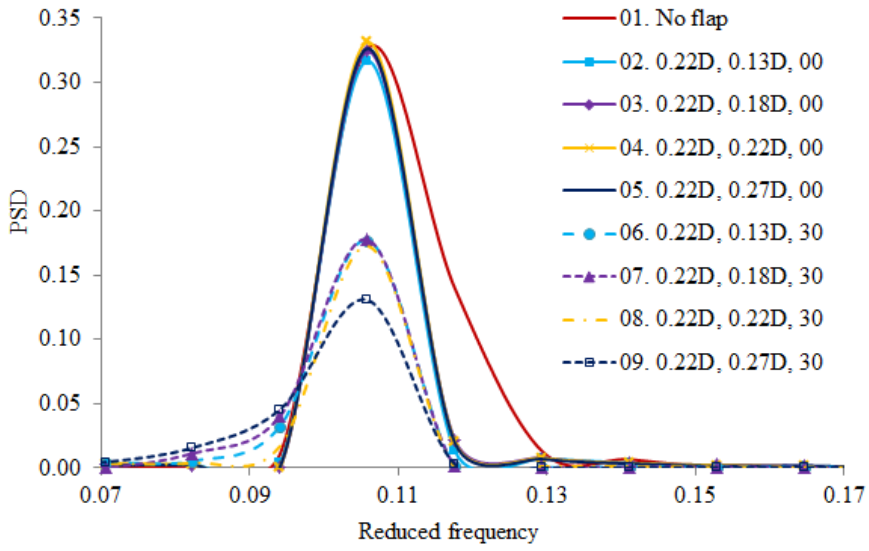

Figure 5.34. PSD of lift force – Rectangular section with ratio 4

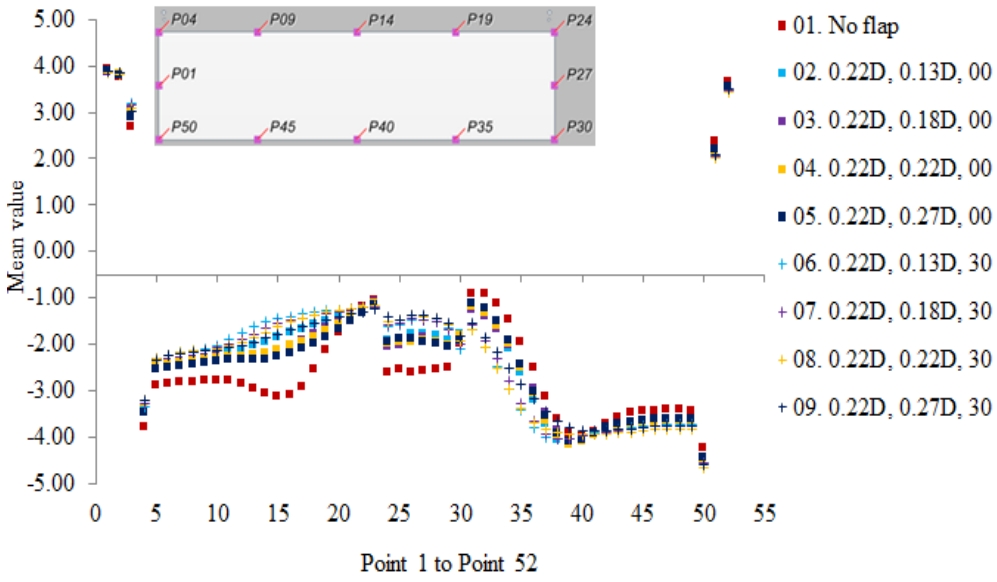

Figure 5.35. Mean surface pressure coefficient – Rectangular section with ratio 4

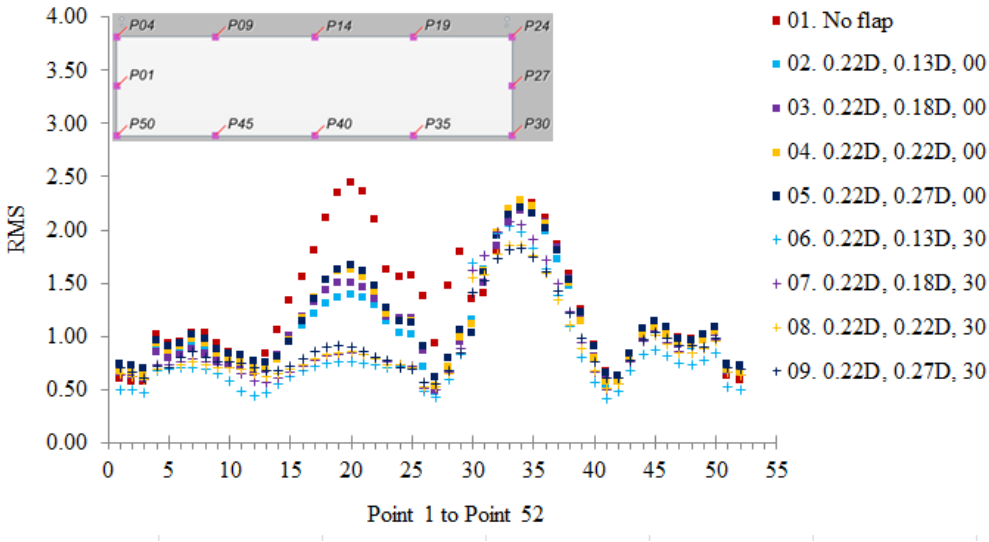

Figure 5.36. RMS of surface pressure coefficient – Rectangular section with ratio 4

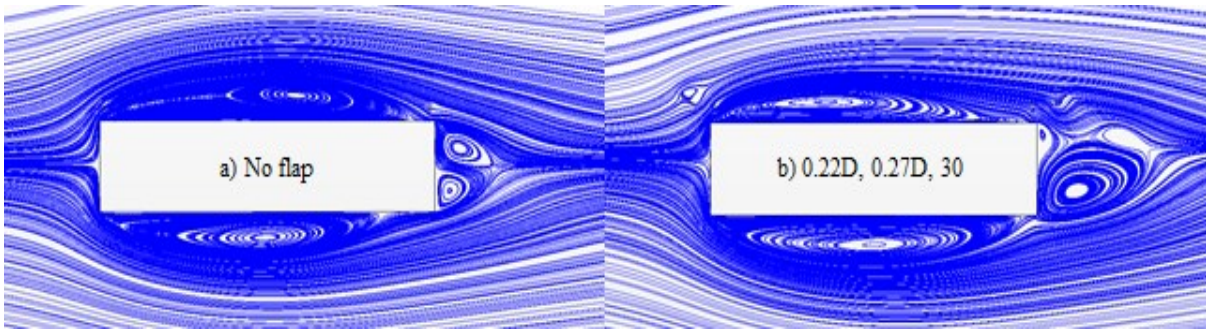

Figure 5.37. Flow pattern - Rectangular section with ratio 4

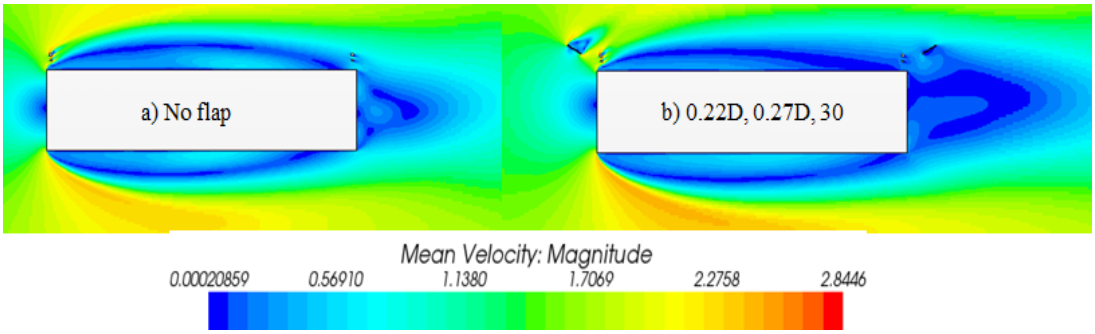

Figure 5.38. Mean velocity field – Rectangular section with ratio 4

Secondly, the rectangular sections with side ratio 2 and 8 are taken into account in order to represent not only for the bluff-body sections but also for the flat-body sections. Similarly, the time history, the PSD of lift force, the mean value, the RMS of surface pressure coefficient, the mean velocity field and the flow pattern are indicated from Figure 5.39 to Figure 5.50, respectively. With or without flap installed, there is no significant difference in the mean values of surface pressure coefficient, as Figure 5.41 and Figure 5.47. However, this one is not found in the PSD of lift force and the RMS of surface pressure coefficient, as shown in Figure 5.40, Figure 5.42, Figure 5.46, and Figure 5.48.

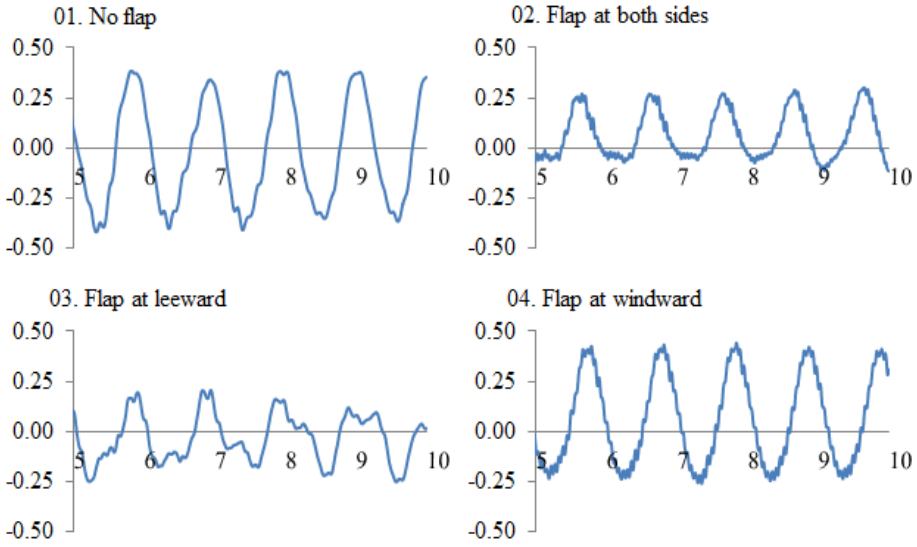

Figure 5.39. Time history of lift force – Rectangular section with ratio 2

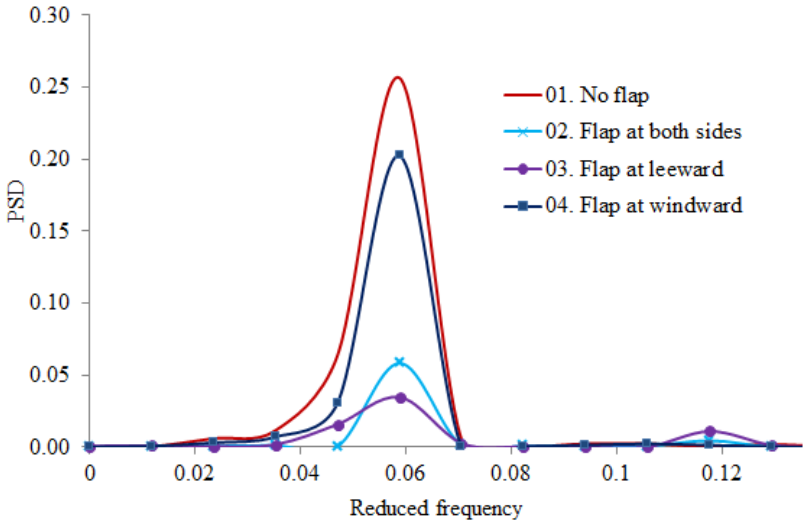

Figure 5.40. PSD of lift force - Rectangular section with ratio 2

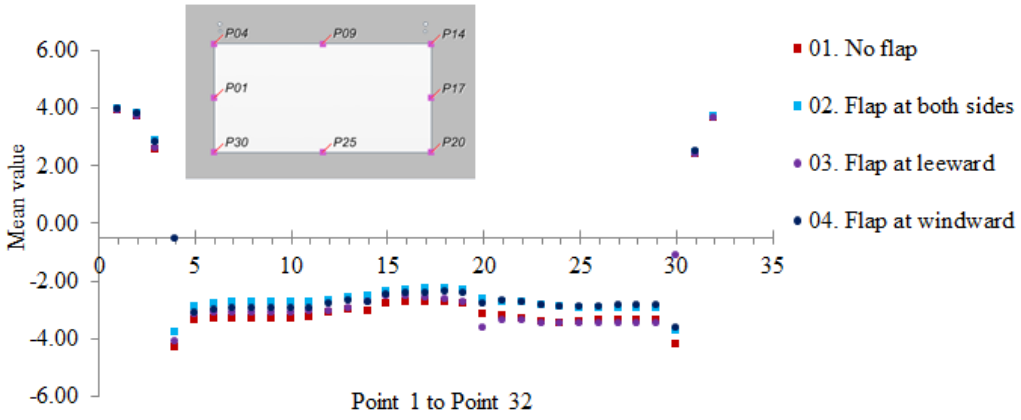

Figure 5.41. Mean surface pressure coefficient – Rectangular section with ratio 2

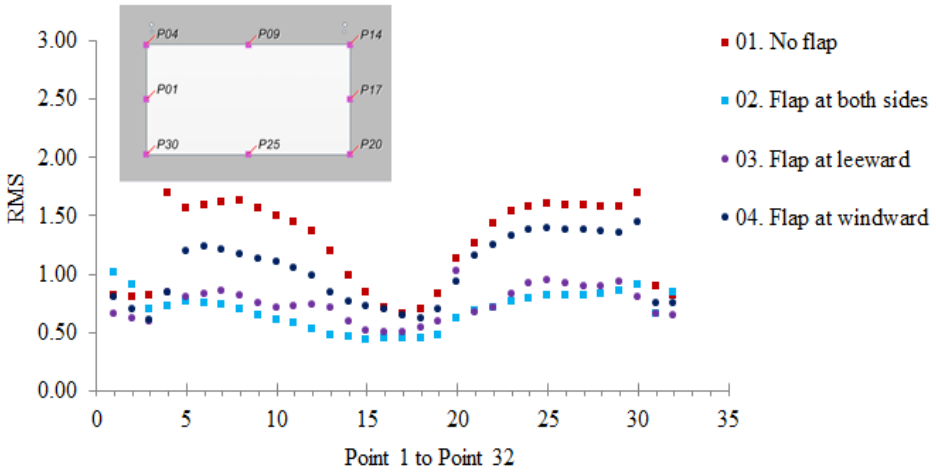

Figure 5.42. RMS of surface pressure coefficient – Rectangular section with ratio 2

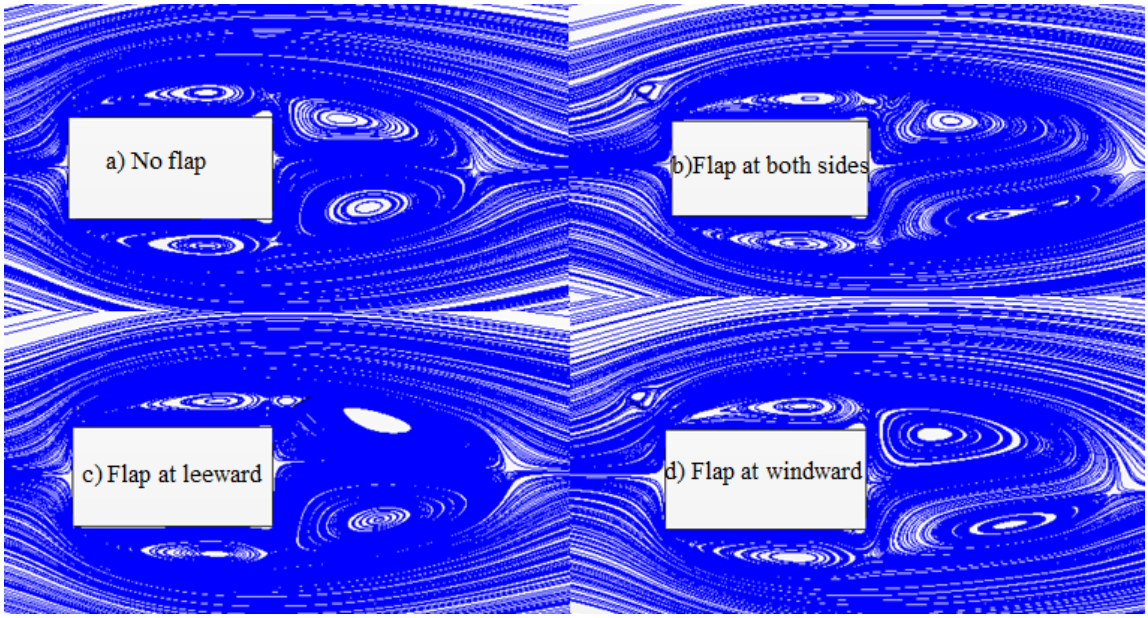

Figure 5.43. Flow pattern - Rectangular section with ratio 2

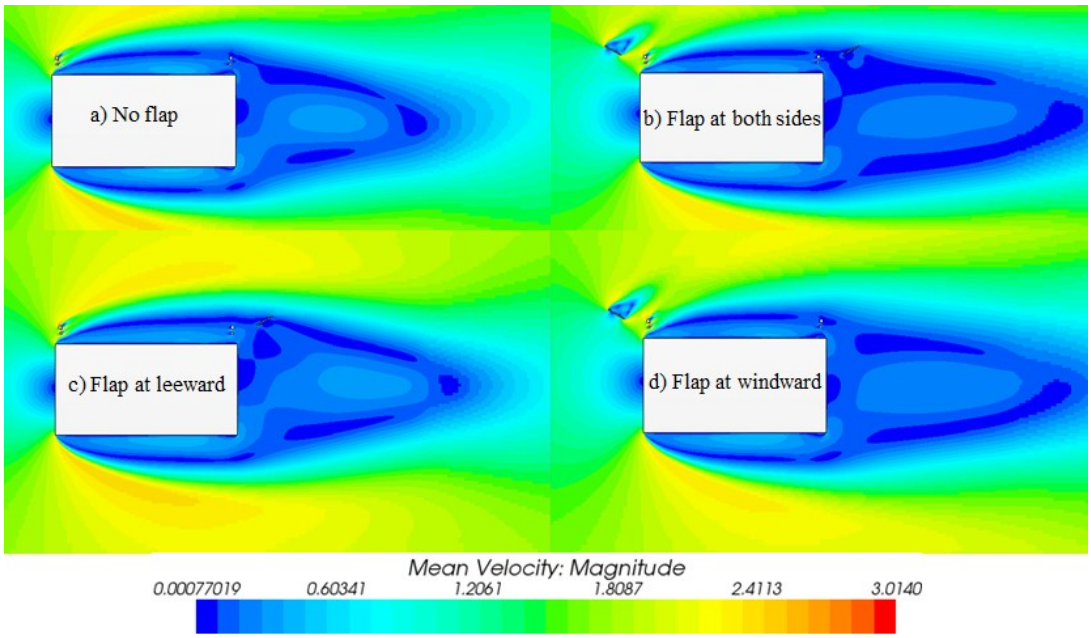

Figure 5.44. Mean velocity field – Rectangular section with ratio 2

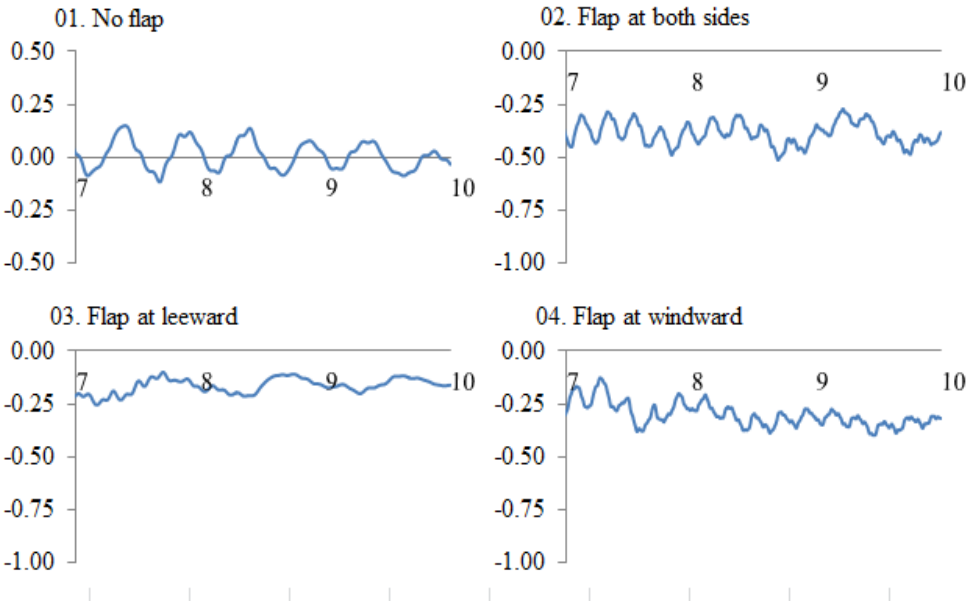

Figure 5.45. Time history of lift force – Rectangular section with ratio 8

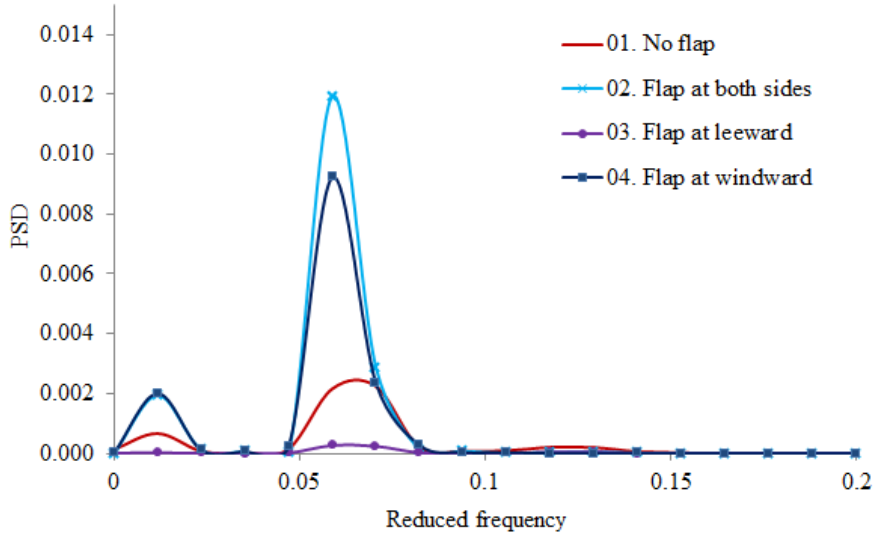

Figure 5.46. PSD of lift force - Rectangular section with ratio 8

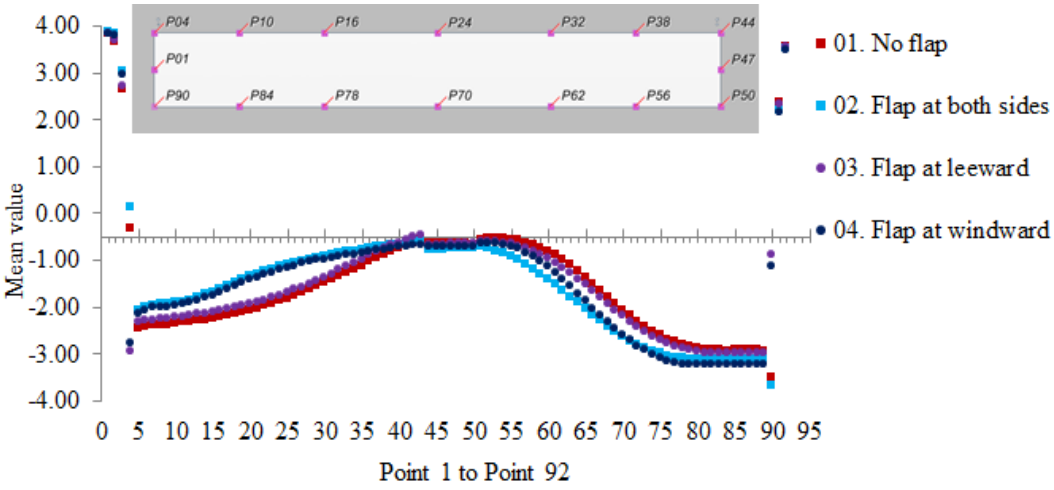

Figure 5.47. Mean surface pressure coefficient – Rectangular section with ratio 8

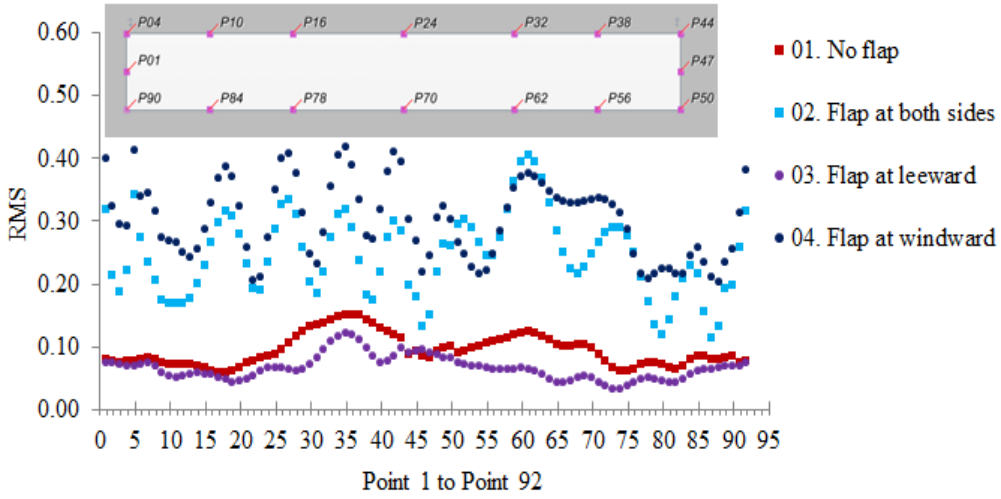

Figure 5.48. RMS of surface pressure coefficient – Rectangular section with ratio 8

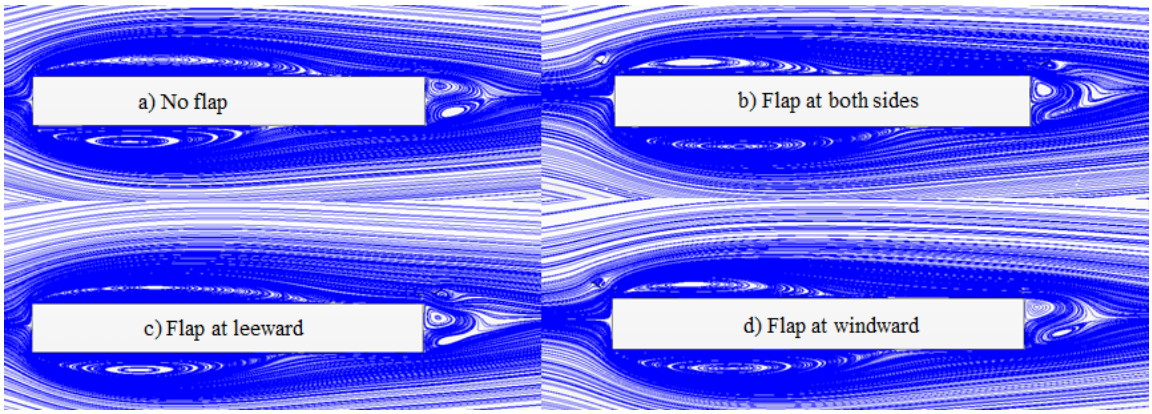

Figure 5.49. Flow pattern - Rectangular section with ratio 8

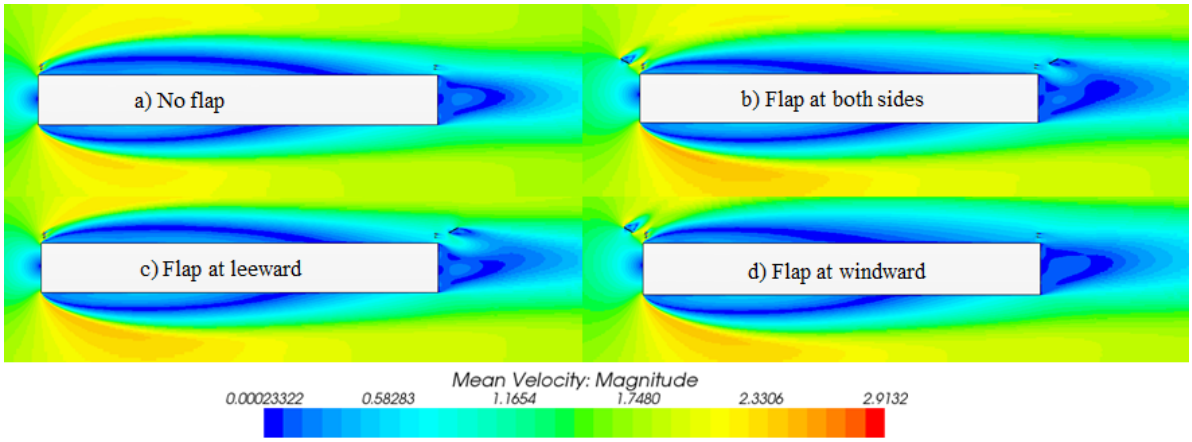

Figure 5.50. Mean velocity field – Rectangular section with ratio 8

It is noted that the critical role of the flap at leeward is illustrated again. The presence of it leads to the mitigation of wake formation at downstream (KV shedding). Therefore, the PSD of lift force and the RMS of pressure coefficient on the surface have small values. The going down flow made by the prevention of the flap at leeward is source in producing performance that controls the wake formation, reducing the KV shedding. At the ratio 2, because of the occurrence of the fully separated phenomenon, the flap at windward does not work well. On the other hand, in case of flat-body section, the flap with high angle at windward can cause stronger vortices on the upper surface. Hence, the aerodynamic instability in this case should be attached much importance.

5.6. Summary of Chapter 5

In this chapter, the significance of flap attached on the box girder section in suppressing the VIV is presented through the numerical investigation using the RANS equations coupled with the new $k-\varepsilon$ eddy viscosity turbulent model. Firstly, the concept of the static numerical analysis and the study object are introduced in Section 5.1. Then, the details of numerical simulations in this study, such as the governing equations with the RANS approach and the new $k-\varepsilon$ eddy viscosity turbulent model, the geometries of the sections and the analysis parameters, the computational domain, the boundary conditions and the mesh used, are carefully discussed in Section 5.2. Next, Section 5.3 presents the reasonable approximation of the numerical results to the experimental ones in case of the box girder section of the Shin-minato Bridge, as well as some rectangular sections. Hence, Section 5.3 is

concerned as the validation of this study. Finally, the effect of flap is particularly presented in Section 5.4 and 5.5 by the numerical investigation results in case of the box girder and some rectangular sections, respectively. It is illustrated that the presence of flap has resulted in the change of the wind flow distribution. On the one hand, the flap at windward can suppress the vortices generated from the leading edge of the section, eliminating the MIV. On the other hand, the flap at leeward can control the KV shedding at the downstream, reducing the KV oscillation. This study also showed that the combination of fairing of a box section and large enough angle of flaps plays an important role in controlling the wind flow to be smoother at the leeward region. In there, flaps at leeward have a dominant function in weakening the wake formation at downstream. Based on numerical results, the peak of the lift force PSD and the RMS of pressure coefficient on the section significantly decreased in the case of the flap angle of 30^{o}. However, in the case of using flaps with very large angle, it is not always ensure to achieve the effective performance, and the increase of drag force is necessary to be considered. The chapter proves that the use of horizontal flap and insufficient gap does not lessen the disordering flow at the leeward area remarkably. As far as this study concerned, the angle and the gap of flap should be 30^{o} and larger than 0.13D, respectively. In addition, it suggests that the disturbance to the wind profile and the turbulence intensity on the deck need to be carefully inspected in the process of flap selection.

6.1. Introduction

Dynamic numerical analysis used in the thesis can be defined as numerical simulations in which the concerned sections can be moved with a forced excitation at a computational domain. These simulations are carried out to investigate deeper the dynamic properties of the sections through flutter derivatives. In this study, the box girder of the Shin-minato Bridge is examined in dynamic simulations under vertically harmonic excitations in order to calculate the flutter derivative H_1^*. Then, it is used to clarify the aerodynamic damping in each case of the flap attached. Numerical results are compared with the amplitude of VIV measured in WTT, as a confirmation for validation.

The concept of the flutter derivatives was introduced at Section 2.1.1 of Chapter 2:. In quantitative analysis, these ones are parameters that can be calculated from the results measured in WTT or obtained in dynamic numerical study. If a vertical or a torsional harmonic oscillation is imposed on the object, then the flutter derivatives are extracted by means of the correlation between the fluid forces acting on the object and the forced excitation, as the formulation (6.1) for the vertical forced motion or the formulation (6.2) for the torsional forced one.

$$H_1^* = \frac{L_h \sin(\emptyset_{L_h})}{\frac{1}{2}\rho B^2 \Omega_h^2 h_0}, H_4^* = \frac{L_h \cos(\emptyset_{L_h})}{\frac{1}{2}\rho B^2 \Omega_h^2 h_0},$$
$$A_1^* = \frac{M_h \sin(\emptyset_{M_h})}{\frac{1}{2}\rho B^3 \Omega_h^2 h_0}, A_4^* = \frac{M_h \cos(\emptyset_{M_h})}{\frac{1}{2}\rho B^3 \Omega_h^2 h_0} \quad (6.1)$$

$$H_2^* = \frac{L_\alpha \sin(\emptyset_{L_\alpha})}{\frac{1}{2}\rho B^3 \Omega_\alpha^2 \alpha_0}, H_3^* = \frac{L_\alpha \cos(\emptyset_{L_\alpha})}{\frac{1}{2}\rho B^3 \Omega_\alpha^2 \alpha_0},$$
$$A_2^* = \frac{M_\alpha \sin(\emptyset_{M_\alpha})}{\frac{1}{2}\rho B^4 \Omega_\alpha^2 \alpha_0}, A_3^* = \frac{M_\alpha \cos(\emptyset_{M_\alpha})}{\frac{1}{2}\rho B^4 \Omega_\alpha^2 \alpha_0} \quad (6.2)$$

where:

Ω_h or Ω_α is the frequency of forced oscillation;

h_0 or α_0 is the amplitude of harmonic forced oscillation;

L_h, M_h *or* L_α, M_α are the amplitudes of the relevant lift force, moment profiles;

$\emptyset_{L_h}, \emptyset_{M_h}$ *or* $\emptyset_{L_\alpha}, \emptyset_{M_\alpha}$ are the lag phases of the lift force, moment in respect to the imposed motion;

6.2. Numerical simulation

6.2.1. Numerical scheme

The numerical scheme and analysis parameters used in the dynamic simulations are not different from in the static ones presented in Chapter 5:. The box girder of Shin-minato Bridge is examined in the presence of flaps and its geometries were described in Figure 5.1. The governing equations with the RANS approach coupled with the new $k-\varepsilon$ eddy viscosity turbulence model are discretized in calculation. In addition, the simulations remain the computational domain and boundary conditions unchanged like the static simulations. To set up the forced excitations, however, the mesh is divided into two separated zones: moving zone and static zone as Figure 6.1.

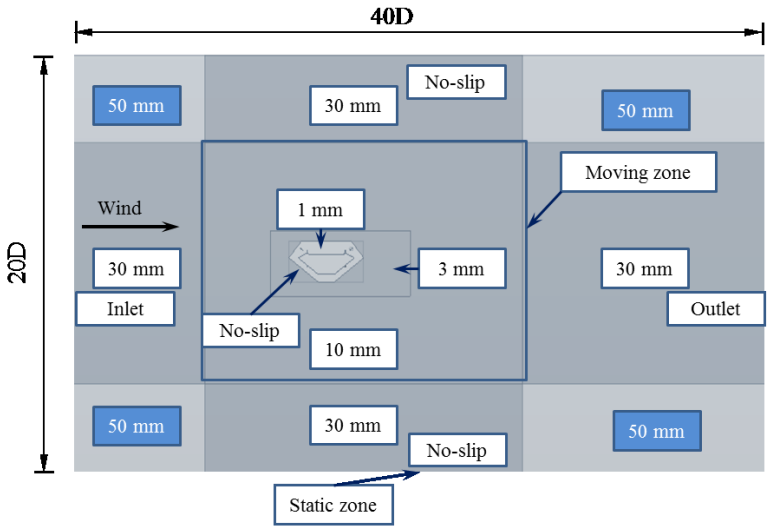

Figure 6.1. Computational domain, boundary conditions, mesh zone in dynamic simulations

6.2.2. Mesh in dynamic simulation

In the dynamic simulations, the computational domain is split into two parts including moving zone and static zone. How to tackle the interaction between those zones is an important strategy in numerical method. In here, the relative motion between moving zone and static zone is simulated by using overset grids method in STAR-CCM+ version 7.04 [61]. The moving one is set up as an overset region which can be overlapped the static one considered as background region. The main idea is found that the cells of these regions are classified of active, inactive or acceptor cells. The discretized governing equations are solved at the active cells and no equation is solved at the inactive ones. Acceptor cells separate active and inactive cells in the background region and are attached to the overset boundary in the overset region, being used to couple solutions on the two overlapping grids. To estimate the flux across the interface, variable values at acceptor ones are determined by a certain number of donor cells, which are nearest active cells from the other mesh, through interpolation.

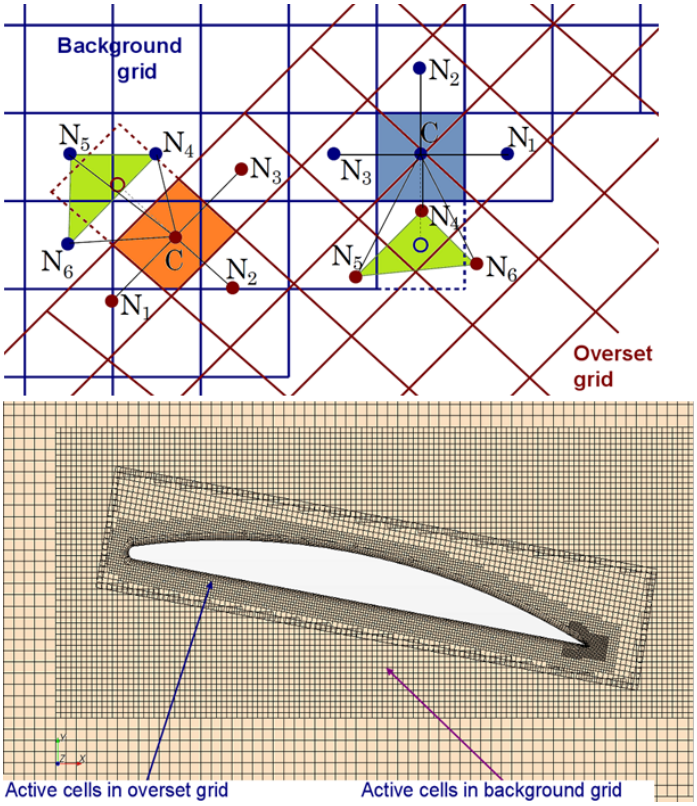

Figure 6.2. Overset methodology in STAR-CCM+ version 7.04 [61]

6.2.3. Harmonic excitation

In the dynamic simulations, a vertically harmonic forced oscillation $y = y_0 \sin(2\pi f_0 t)$ is imposed to the section. More detail, the amplitude $y_0 = 0.08\mathrm{D}$ is kept constant to set up the forced motion. The value y_0 is selected basing on the maximum amplitude of VIV observed. In order to compute the flutter derivative H_1^* at some different velocities, the excited frequency f_0 is changed according to a variety of the reduced velocities, instead of directly varying the reduced velocity to avoid any phenomenon arising due to the change of Re number.

6.3. Flutter derivative $\mathbf{H_1^*}$

Flutter derivatives are used to estimate the properties of aerodynamic oscillation of the bridge deck under the flow action. In quantitative analysis, these ones are parameters that can be calculated from the results measured in wind tunnel or the results obtained in numerical study. If a vertical or a torsional harmonic oscillation is imposed on an object, then flutter derivatives are extracted by means of the correlation between the fluid forces acting on the object and the forced excitation, as the formulation (6.1) for the vertical forced motion or the formulation (6.2) for the torsional forced one.

As known, the flutter derivative H_1^* represents an aeroelastic transfer function between the wind force and the object displacement, in the sense that it is directly related to the aerodynamic damping coefficient. The positive value H_1^* leads to a negative aerodynamic damping and vice versa. Therefore, it is able to judge the property of VIV through the aerodynamic damping coefficient.

In this study, the dynamic numerical simulations take into account many different configurations of the flap attached on the box girder section. In order to explain the vertical VIV, the time history of lift force is firstly obtained in each case, as Figure 6.3 . The flutter derivative H_1^* is then calculated following to the formulation (6.1). For each harmonic motion, four reduced velocities, defined as $2\pi U/(\Omega B)$, are considered: 1, 2, 3 and 5. In there, it is noted that the VIV occurred at the reduced velocity $U_{re} = 2$ in the WTT.

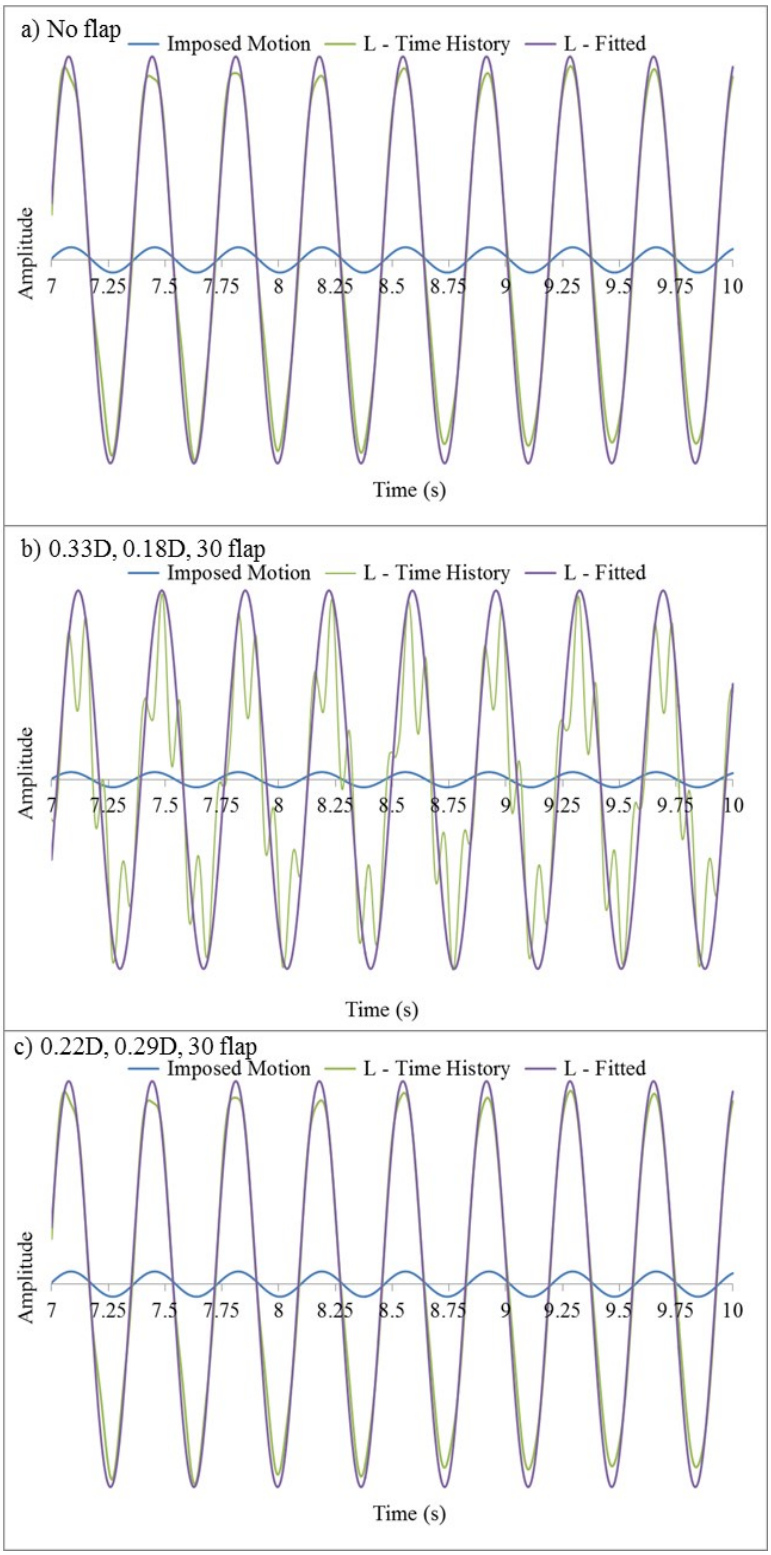

Figure 6.3. Time history of lift force from numerical results in dynamic simulations

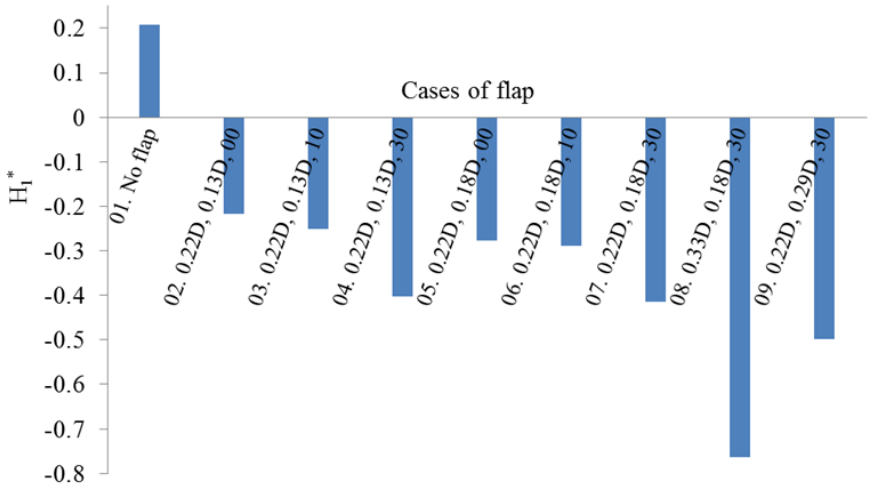

Figure 6.4. Flutter derivative H_1^* at the reduced velocity $U_{re} = 2$

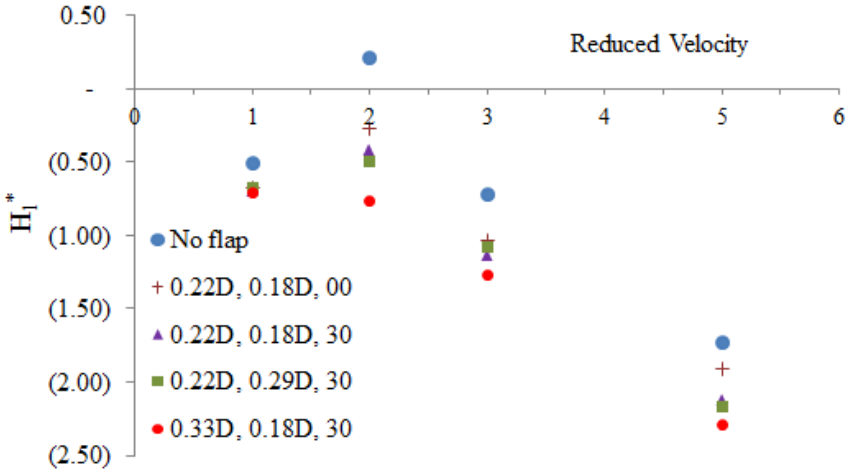

Figure 6.5. Flutter derivative H_1^* at several reduced velocities

At reduced velocity $U_{re} = 2$, as depicted in Figure 6.4, it is obvious that flutter derivative H_1^* has the positive value in case of the section without flap, where the highest VIV amplitude was observed in the WTT. On the other hand, it has the different negative values in cases of various shapes of flap installed on the section. It can be easily seen that the value of H_1^* remarkably decreases if the angle of flap is 30^0 and the gap is larger than 0.13D (800 mm). The section without flap installed has the severe VIV corresponding to the increase of negative aerodynamic damping. Furthermore, the same performance is repeated at several reduced velocities, as shown in Figure 6.5. Hence, it can be concluded that the flap 30^0 with the gap extended 0.13D (800 mm) always surpass the other ones in VIV suppression. Once

again, the significance of flap with suitable geometric configurations in VIV reduction is confirmed in the dynamic simulations.

6.4. Summary of Chapter 6

The Chapter 6 presents the numerical investigation through dynamic simulations. It is considered as another approach to estimate the effect of flap in suppressing the oscillation due to the wind load. The flutter derivative H_1^* , which is calculated from dynamic simulations with vertically harmonic excitations, is the main quantity used to clarify the significance of flap in mitigating the vertical vibration. In Section 6.1, it is mentioned about the concept of the dynamic simulations and the method of determining the flutter derivatives by means of the excitation imposed on the section. Then, the information related to the numerical scheme, the mesh technology in the dynamic simulations and the forced excitations are elucidated in Section 6.2. In there, it is noted that the overset methodology in STAR-CCM+ Version 7.04 utilized to simulate the static and moving zones. Next, the flutter derivative H_1^* in case of the box girder section of the Shin-minato Bridge with and without flap is particularly discussed in Section 6.3. There has been a good correlation between the numerical results in the dynamic simulations and the experimental ones in WTT. It shows that the presence of flap leads to the effectiveness in the VIV suppression. It is easily seen that the flutter derivative H_1^* has the negative value in the case of flap attached, and H_1^* gradually decreases along with the increase of the angle and gap of flap. Subsequently, as far as the chapter concerned, a large angle around 30^0 and gap more than 0.13D of flap are recommended to the box girder sections having the similar shapes with the one used in the study.

Chapter 7: CONCLUSIONS AND FUTURE RESEARCH

7.1. Conclusions

The effect of flap countermeasure attached to the box girder section is numerically grasped in details by this thesis. The numerical investigation into the suppression mechanism of the VIV, for the box girder in the presence of flap, is performed by the RANS approach, coupled with the new $k-\varepsilon$ eddy viscosity turbulence model. As an important part, it is carefully considered the validation of numerical simulations by comparing to the experimental results in WTT. When it comes to the main contents, the static and dynamic analysis simulations are conducted to examine the aerodynamic characteristics of the wind flow. In there, many different changes of the geometric configurations of flap are taken into account by the analyses. In addition, the rectangular sections are examined as auxiliary cases to clarify the significance of flap, as well as fortifying the main scheme and analysis parameters used in all numerical simulations. The works of the study are devoted towards achieving the aim and the objectives of the thesis, in the sense that a useful reference or a basic guideline of the flap application to suppress the VIV is concentrated as the major purpose. The followings conclude the achievements and the findings on the study:

- In terms of dealing with the signature turbulence around the bluff-body in the smooth wind flow, the works done has successfully validated the application of the RANS approach coupled with the new k-ε eddy viscosity turbulence model by comparison with experimental investigation in WTT. The validation, the reliability of numerical scheme and analysis parameters are confirmed through not only the static numerical analysis, but also the dynamic one.

- In setting up the simulations, adequately simulating the small attachment members on the girder, the boundary conditions and the mesh size is one of vital factors to get the results having the high reliability, approaching the good agreement with the ones in WTT.

- It is necessary to confirm that CFD analysis in this study can afford provide variety of extreme useful information in investigating the behavior of the wind flow, significantly supporting to WTT in comprehending the suppression mechanism of wind-induced vibrations.

- In the static numerical analysis, it is illustrated that the PSD of lift force and the RMS of surface pressure coefficient remarkably decrease in case of the flap having large enough gap and angle. These ones are in accordance with the box girder section having the bluff-body shape and the relevant rectangular section as well.

- The suppression mechanism of VIV has the sources from the flow controlling capability of flap at windward and leeward. At windward, flap can orient the flow at the upper surface of the section to suppress the vortices generated from the leading edge, eliminating the MIV. At leeward, because of the results of intercepting the wind flow, it accelerates the wind flow going down to weaken the wake formation, reducing the KV oscillation. It is noted that the above mechanism leads to the effectiveness of oscillation reduction in case of using the flap having large enough gap and angle.

- The flap with very high angle can increase the PSD of lift force and the mean drag coefficient. It produces the high thickness of wake layer at the upper surface of the section due to the bluff-body form of flap at windward. On the other hand, the flap with very large gap does not result in the dramatic significance in controlling the wake region. Furthermore, it should be carefully considered the difficulty of installation at construction site with the flaps having large angle and gap.

- In the dynamic numerical analysis, it shows that the presence of flap leads to the effectiveness in the VIV suppression. It is clarified that the flutter derivative H_1^* has the negative value in the case of flap attached, and H_1^* gradually decreases along with the increase of the angle and gap of flap. It does mean that the presence of suitable flap contributes the positive aerodynamic damping, enhancing the aerodynamic stability of the girder.

- As far as the study concerned in both static and dynamic analysis, a large angle around 30^0 and a gap more than 0.13D of flap are recommended to the box girder sections having the similar shapes. This recommendation is consider as a useful reference or a basic guideline in flap application to suppress the VIV.

- When all is said and done, regarding to the influence of flap countermeasure on the wind profile above the section, as a side effect to vehicles, is one vital aspect in flap selection. It can give the best solution from a various promising flap to ensure the safety of passengers.

7.2. Future research

As stated in the background, the interaction between bridge girder and wind flow is very complicated. From the past decades, a plenty of experimental tests in WTT have been done to investigate its aerodynamic and aeroelastic behavior. It is one open and promising area for CFD in the combination with those experimental results to deeply comprehend the inside operation. The numerical results presented herein shed some light on several other issues be involved. Hence, it is believed that this thesis provides the fundamental findings which could be extended. The followings are feasible direction of future works:

- Examining the flow controlling mechanism of other aerodynamic countermeasures corresponding to various wind-induced vibrations by means of CFD approach.

- Using CFD to investigate the effect of turbulence content of the oncoming flow on aeroelastic stability of usual girder section in long span bridges.

- Studying minutely the other turbulence models in CFD to deal with the signature turbulence around girder sections, adequately assisting in the selection of ones.

7.3. Summary of Chapter 7

As the name of this chapter, conclusions and future research trends are main contents in Chapter 7:. The background of the study is summarized at the first part in Section 7.1. In there, the major information, related to the aim of the research, the objectives, the numerical approach and analysis models, is mentioned. Then, the second part of Section 7.1 provides some crucial conclusions of the thesis. A useful reference like a basic guideline in flap application for VIV reduction is recommended in this part. Beside that, some minor conclusions are also given. Last but not the least, several prospects of future research are drawn in Section 7.2.

Bibliography

[1] *http://www.nssmc.com/en/product/use/case/bridge/akashi.html.*

[2] *http://rusbridge.net/2012/07/russian-prime-minister-dmitry-medvedev-opens-trial-traffic-over-russky-bridge.*

[3] S. Holger, "Cable-Stayed Bridges," *Lecture, Wilhelm Ernst & Sohn, Berlin, Germany,* 2012.

[4] J. D. Holmes, "Wind Loading of Structures," *Book, 2nd edition, Abingdon: CRC Press,* 2007.

[5] *http://en.wikipedia.org/wiki/Tacoma_Narrows_Bridge_(1940).*

[6] Fujino, Y., Yosida, Y., "Wind-induced vibration and control of Trans-Tokyo Bay Crossing Bridge," *Journal of Structural Engineering,* vol. 128, pp. 1012-1025, 2002.

[7] Katsuchi, H., Yamada, H., Etoh, K., Nagai, S., Sekiguchi, T., Morikawa, Y., Nakagaki, T. and Yui, R., "Vortex-induced vibration and its countermeasures ob-served at long-span cable-stayed bridge," *Proc. of 12th America Conference on Wind Engineering,* 2013.

[8] Hitomi, J., Katsuchi, H., Yamada, H. and Nishio, M., "Analysis of Vibration Characteristics of Shinminato Bridge based on Field Measurement Data," *Proc. of 68th Annual Conference of Japan Society for Civil Engi-neers JSCE,* pp. 983-984, 2013.

[9] H. S. B. Authority, "Wind Resistant Design Code for Honshu Shikoku Bridges," 2001.

[10] J. R. Association, "Specifications for highway birdges," *in Japanese, Maruzen, Tokyo,* 2002.

[11] J. R. Association, "Wind resistant design manual for highway bridges," *in Japanese, Maruzen, Tokyo,* 1991.

[12] Fujino Y., Kimura K., Tanaka H., "Wind resistant design of bridges in Japan developments and practices," *Springer,* 2012.

[13] Toyama, N., Hata, K., Kusuhara, S., "The Re-evaluation of the Aerodynamic Stability of the Tozaki Viaduct," *Proceedings of 18th National Symposium on Wind Engineering, (in Japanese),* pp. 491-495, 2004.

[14] Hjorth-Hansen, "Fluctuating drag, lift and overturning moment for a line-like structure predicted (primarily) from static, mean loads," *Department of Structural Engineering, University of Trondheim, Norway,* 1993.

[15] Santo, H. P. and Branco, F. B., "Wind forces on bridges numerical vs experimental methods," *Journal of Wind Engineering and Industrial Aerodynamics,* vol. 32, pp. 145-159, 1989.

[16] Tamura, T., Ohta, I. and Kuwahara, K., "On the reliability of two-dimensional simulation for unsteady flows around a cylinder-type structure," *Journal of Wind Engineering and Industrial Aerodynamics,* vol. 35, pp. 275-298, 1990.

[17] Kuroda, S., "Numerical simulation of flow around a box girder of a long span suspension bridge," *Journal of Wind Engineering and Industrial Aerodynamics,* Vols. 67-68, pp. 239-252, 1997.

[18] Larsen, A. and Walther, J. H., "Aeroelastic analysis of bridge girder sections based on discrete vortex simulations," *Journal of Wind Engineering and Industrial Aerodynamics,* Vols. 67-68, pp. 253-265, 1997.

[19] Larsen, A., "Advances in aeroelastic analysis of supension and cable-stayed bridges," *Journal of Wind Engineering and Industrial Aerodynamics,* Vols. 74-76, pp. 73-90, 1998.

[20] Buno, L., Khris, S. and Marcillat, J., "Contribuition of numerical simulation tp evaluating the effect of section details on the aerodynamic behavior of a long span bridge deck," *Wind engineering into the 21st Century, Larsen, Larose & Livesse, Balkema,* pp. 1229-1236, 1998.

[21] Shimada, K. and Ishihara, T., "Applicability of modified k-ε model on the prediction of aerodynamic properties of rectangular cylinders with various elongated cross section," *Journal Structure Construction Engineering, AIJ,* vol. 514, pp. 73-80, 1998.

[22] Tamura Tetsuro, "Reliability on CFD estimation for wind-structure interaction problems," *Journal of Wind Engineering and Industrial Aerodynamics,* vol. 81, pp. 117-143, 1999.

[23] Frandsen, J. B., "Computational fluid-structure interaction applied to long span bridges," *Ph.D Thesis, University of Cambridge,* 1999.

[24] Taylor, I., and Vezza, M., "Prediction of unsteady flow around square and rectangular cylinders using a discrete vortex method," *Journal of Wind Engineering and Industrial Aerodynamics,* vol. 82, pp. 247-269, 1999.

[25] Taylor, I., and Vezza, M., "Analysis of wind loading on bridge deck sections using a discrete vortex method," *Wind Engineering into the 21st Century, Larsen, Larose & Livesey, Eds, Balkema,* 1999.

[26] Morgentha, G., "Comparison of numerical methods for bridge deck aerodynamics," *M. Phil. Thesis,* 2000.

[27] Morgentha, G., "Aerodynamic analysis of structures using high resolution vortex particle methods," *PhD Thesis, University of Cambridge,* 2002.

[28] Shimada, K., Ishihara, T. and Wakahara, T., "Prediction of flutter characteristics of rectangular cross-section by k-ε model," *The Second International Symposium on Wind and Structures, Busan, Korea,* pp. 211-218, 2002.

[29] Ishihara, T., Oka, S. and Fujino, Y., "Numerical prediction of aerodynamic characteristics of rectangular prism under uniform flow," *Journal of Structural and Earthquake Engineering,* vol. 62, pp. 78-90, 2006.

[30] Sarwar, M. W. et al., "Prediction of aerodynamic characteristics of a box girder bridge section using the LES turbulence model," *Journal of Wind Engineering and Industrial Aerodynamics,* vol. 96, pp. 1895-1911, 2008.

[31] Sarwar, M. W. and Ishihara, T. , "Numerical study on suppression of vortex-induced vibrations of box girder bridge section by aerodynamic countermeasures," *Journal of Wind Engineering and Industrial Aerodynamics,* vol. 98, pp. 701-711, 2010.

[32] Nakaguchi H., Hashimoto K. and Muto S., "An experimental study on aerodynamics drag of rectangular cylinders," *Journal of Japan Society of Aeronautical and Space Science,* vol. 16, pp. 1-5, 1968.

[33] Mizota T. and Okajima A., "Experimental studies of unsteady flows around rectangular prisms," *Japan Society of Civil Engineering,* vol. 312, pp. 39-47, 1981.

[34] Simiu E. and Scanlan R., "Wind effects on structures," *Book, Third Edition, A Wiley-interscience Publication,* 1996.

[35] Nakamura Y., "Video flow visualization of bluff-body flutter," *Kyushu University, Research Institute of Applied Mechanics,* 1985.

[36] JSCE, "Video the Century of Civil Engineering," *Data of NHK Techno-Power Series, Long Span Bridges,* vol. 1, no. 3, 1994.

[37] Miyata T., "Historical view of long span bridge areodynamics," *Journal of Wind Engineering and Industrial Aerodynamics,* vol. 91, pp. 1393-1410, 2003.

[38] Brusiani F., Miranda S., Patruno L., Ubertini F. and Vaona P., "On the evaluation of bridge deck flutter derivatives using RANS turbulence models," *Journal of Wind Engineering and Industrial Aerodynamics,* vol. 119, pp. 39-47, 2013.

[39] Shiraishi N. and Matsumoto M., "On vertex-induced oscillations of bluff cross sections

used for bridge structures," *Proceedings of the JSCE,* vol. 322, pp. 37-50, 1982.

[40] *http://en.wikipedia.org/wiki/File:Vortex-street-animation.gif.*

[41] Larsen, A., Esdhal, S., Andersen, J.E. and Verjum, T., "Vortex shedding excitation of the Great Belt suspension bridge," *Proceeding 10th International Conference on Wind Engineering, Denmark,* pp. 947-954, 1999.

[42] Kusuhara, S., Yamada, I. and Toyama, N., "Reevaluation on Aerodynamic Stability of Steel Box Girder," *The 7th Asian-Pacific Conference on Wind Engineering, Taiwan,* 2009.

[43] John D. Anderson, Jr., "Computational fluid dynamics, The basics with applications," *International Editions, McGraw-Hill Book Co.,* 1995.

[44] Ferziger H. and Peric M., "Computational Methods for Fluid Dynamics," *Book, Thrid Edition, Springer,* 2002.

[45] Versteeg H. K. and Malalasekera W., "An Introduction to Computational Fluid Dynamics," *Book, Second Edition, Pearson Prentice Hall,* 2007.

[46] Wilcox D.C., "Turbulence modelling for CFD," *DCW Industries Inc., California,* 1993.

[47] Franke, R. and Rodi, W., "Calculation of Vortex Shedding past a Square Cylinder with Various Turbulence Models," *Proc. of 8th Symposium on Turbulent Shear Flows, Technical Univ. of Munich, Germany,* pp. 1-20, 1991.

[48] Okajima, A. and Sakai, H., "Numerical Simulation of Flows around Rectangular Bodies using Direct Method and Model," *Journal of Wind Engineering ,* 1991.

[49] Murakami, S., Mochida, A. and Hayashi, Y., "Examining the Model by means of a Wind Tunnel Test and Large-Eddy Simulation of the Turbulence Structure around a Cube," *Journal of Wind Engineering and In-dustrial Aerodynamics 35,* pp. 87-100, 1990.

[50] Kato, M. and Lauder, B. E., "The Modeling of Turbulent Flow around Stationary and Vibrating Square Cylin-ders," *Proc. of 9th Symposium on Turbulent Shear Flows, Kyoto, Japan,* pp. 4-10, 1993.

[51] Kato, M., "2-D Turbulent Flow Analysis with Modi-fied Model around a Stationary Square Cylinders and Vibrating One in the along and across Wind Direction," *Journal of Structural Mechanics and Earthquake Engineering I-41,* pp. 217-230, 1997.

[52] Shimada, K. and Ishihara, T., "Application of a Modi-fied model to the Prediction of Aerodynamic Characteristics of Rectangular Cross-Section Cylin-ders," *Journal of Fluids and*

Structures 16, pp. 465-485, 2002.

[53] Shih, T.-H., Liou, W.W., Shabbir, A., Yang, Z. and Zhu, J., "A New Eddy Viscosity Model for High Reynolds Number Turbulent Flows – Model Development and Validation," *NASA Technical Memorandum 106721,* pp. 1-30, 1994.

[54] Rodi, W., "Experience with Two-Layer Models Com-bining the Model with a One-Equation Model Near the Wall," *29th Aerospace Sciences Meeting,* pp. 91-216, 1991.

[55] Wolfstein, M. , "The Velocity and Temperature Dis-tribution in One-Dimensional Flow with Turbulence Augmentation and Pressure Gradient," *International Journal of Heat and Mass Transfer,* vol. 12, pp. 301-318, 1969.

[56] Kelkar, K.M., "Numerical prediction of vortex shedding behind a square cylinder.," *International Journal Numerical Methods in Fluids,* 1992.

[57] Sohankar, A., Davidson, L., Norberg, C., "Numerical simulation of unsteady flow around a square two-dimensional cylinder," *Proc. Twelfth Australian Fluid Mechanics Conf, Sydney, Australia,* pp. 517-520, 1995.

[58] Behr, M., Hastretier, D., Mittal, S. and Tezduyar, T.E., " Incompressible flow past a circular cylinder: dependence of the computed flow field on the location of the lateral boundaries: Comput.," *Meth. Appl. Mech. Engng.,* pp. 309-316, 1995.

[59] Mizota, T., Yamada, H., Kubo, Y., Okajima, A., Knisely, C.W. and Shirato, H., "Aerodynamic characteristics of fundamental structures, part 1, section 2," *Journal of Wind Engineering, in Japanese,* vol. 36, pp. 50-52, 1988.

[60] Sohankar A., "Large eddy simulation of flow past rectangular section cyliders: side ratio effects," *Journal of Wind Engineering and Industrial Aerodynamics,* vol. 96, pp. 640-655, 2008.

[61] CD-adapco, "User Guide - STAR-CCM+ Version 7.04".